UNIVERSIDADE FEDERAL DE PERNAMBUCO
CENTRO DE CIÊNCIAS DA SAÚDE
PROGRAMA DE PÓS-GRADUAÇÃO EM ODONTOLOGIA

CECÍLIA MARIA DE SÁ BARRETO CRUZ FALCÃO

ATIVIDADE DE NANOPARTÍCULAS DE PRATA EM CEPAS DE *CANDIDA ALBICANS* E APLICABILIDADE DA TOMOGRAFIA POR COERÊNCIA ÓPTICA NA AVALIAÇÃO DE MATERIAIS DENTÁRIOS

Recife
2022

CECÍLIA MARIA DE SÁ BARRETO CRUZ FALCÃO

ATIVIDADE DE NANOPARTÍCULAS DE PRATA EM CEPAS DE *CANDIDA ALBICANS* E APLICABILIDADE DA TOMOGRAFIA POR COERÊNCIA ÓPTICA NA AVALIAÇÃO DE MATERIAIS DENTÁRIOS

Tese apresentada ao Programa de Pós-Graduação em Odontologia da Universidade Federal de Pernambuco, como requisito parcial para obtenção do título de doutor em Odontologia. Área de concentração em Clínica Integrada.

Orientador: Anderson Stevens Leonidas Gomes

Recife

2022

Catalogação na fonte:
Bibliotecária: Elaine Freitas, CRB4:1790

F178a Falcão, Cecília Maria de Sá Barreto Cruz
Atividade de nanopartículas de prata em cepas de C*andida albicans* e aplicabilidade da tomografia por coerência óptica na avaliação de materiais dentários / Cecília Maria de Sá Barreto Cruz Falcão. – 2022.
93 f.

Orientador: Anderson Stevens Leônidas Gomes.
Tese (Doutorado) – Universidade Federal de Pernambuco, Centro de Ciências da Saúde. Programa de Pós-graduação em Odontologia. Recife, 2022.
Inclui referências e apêndices.

1. Nanopartículas metálicas. 2. Prata. 3. Candida albicans. 4. Tomografia de coerência óptica. 5. Lasers. 6. Falha de restauração dentária. I. Gomes, Anderson Stevens Leônidas (orientador). II. Título.

617.6 CDD (23.ed.) UFPE (CCS 2022 - 256)

CECÍLIA MARIA DE SÁ BARRETO CRUZ FALCÃO

ATIVIDADE DE NANOPARTÍCULAS DE PRATA EM CEPAS DE *CANDIDA ALBICANS* E APLICABILIDADE DA TOMOGRAFIA POR COERÊNCIA ÓPTICA NA AVALIAÇÃO DE MATERIAIS DENTÁRIOS

Tese apresentada ao Programa de Pós-Graduação em Odontologia da Universidade Federal de Pernambuco, como requisito parcial para obtenção do título de doutor em Odontologia. Área de concentração em Clínica Integrada.

Aprovado em: 17/08/2022.

Orientador:

Prof. Dr. Anderson Stevens Leônidas Gomes

BANCA EXAMINADORA

Prof.ª Dr.ª Denise Maria Zezell (Examinadora Externa)
Instituto de Pesquisas Energéticas e Nucleares – USP

Prof.ª Dr.ª Vanda Sanderana Macêdo Carneiro (Examinadora Externa)
Universidade de Pernambuco

Prof.ª Dr.ª Juliana Raposo Souto Maior (Examinadora Interna)
Universidade Federal de Pernambuco

Prof.ª Dr.ª Maria Luiza Dos Anjos Pontual (Examinadora Interna)
Universidade Federal de Pernambuco

Prof.ª Dr.ª Flavia Maria De Moraes Ramos Perez (Presidente)
Universidade Federal de Pernambuco

Aos meus pais, Antonio Cruz (*in memorian*) e Antonia Filgueira
Numa época na qual nos faltava quase tudo, vocês não deixaram que nos faltasse educação, livros e amor.

A Glauber, Larissa e a neném. Tudo por vocês. Minha vida!

AGRADECIMENTOS

A Deus e à Nossa Senhora, pelo sentido, luz e força nessa e em todas as minhas caminhadas.

À Universidade Federal de Pernambuco, pela formação e pelas incontáveis oportunidades que tem me proporcionado ao longo desses anos.

Agradeço em especial ao Professor Anderson Gomes. Muito mais do que docente, pesquisador admirável e orientador ímpar, o professor é exemplo e inspiração por sua conduta ética, seu olhar visionário, seu respeito ao próximo, sua habilidade nas relações humanas, seu empenho e comprometimento com a educação. Meus eternos respeito e gratidão!

Ao Corpo Docente do Programa de Pós-Graduação em Odontologia, pois tive o privilégio de conviver com professores que transformaram meu senso crítico e minha percepção de ciência e trabalho.

Aos servidores, técnicos administrativos e trabalhadores terceirizados que viabilizaram que tudo isso fosse possível, em especial à Antônio Gomes, Oziclere Sena, Tamiris Cibelly e D. Tânia.

À Daene Tenório pelo imenso aprendizado e crescimento no estágio em docência e pelas oportunidades de ensino, orientação e pesquisa.

À Professora Eulália Ximenes por todos os ensinamentos “de bancada” e de vida. Pela parceria, confiança e desafios. Obrigada, professora!

À Professora Regina Bressan, pela oportunidade de desfrutar de seu conhecimento. Por sua dedicação, apoio e incentivo. Obrigada, professora!

Às professoras Gabriela Monteiro e Renata Almeida pelas sugestões, orientações e suporte.

Às professoras Maria Luiza Pontual, Denise Zezell e Juliana Souto Maior que contribuíram com recomendações preciosas para o texto dessa tese.

Aos colegas pesquisadores e colaboradores, vocês foram imprescindíveis nos trabalhos produzidos: Audrey Nunes, Vanderlan Nogueira, Patrícia Cassimiro, Luana Osório e Sirley Veloso.

À Priscilla Chaves, pela leveza, determinação e empenho. No caminho da pesquisa, cresci imensamente com você. Obrigada!

À Kamylla Silva, por partilhar comigo essa estrada da pesquisa odontológica.

À minha querida equipe do Labfoton, o melhor grupo de pesquisa! Em especial, à Pollyana Alencar, Cláudia Mota, Evair Josino, Vanda Carneiro, Daniela Siqueira e Tereza Dias.

Aos meus queridos amigos de pós-graduação, com vocês dividi felicidades, crescimento e desafios: Izabel Ribeiro, Fabiana Menezes, Izabela Xavier, Fernanda Benevides, Elizabeth Louisy, Mayra Aquino e Augusto César. Obrigada por serem parte de minha vida, de minha história.

À Universidade Federal Rural de Pernambuco pela viabilização para que eu realizasse essa pós-graduação. Em especial, à ex-Reitora Professora Maria José de Sena, ao Reitor Professor Marcelo Carneiro Leão, à Pró-Reitora de Gestão de Pessoas Patrícia Gadelha, à ex-Diretora Rivonylda Araújo, ao ex-Diretor José Luiz Malheiros, à Diretora Luana Amaral e à Coordenadora Marina Mendes.

Agradeço às colegas de trabalho da Seção de Saúde Bucal Ayonara Silva, Maria Ângela Mota, Mariana Andrade e Tatiana Zovka que incentivaram e estiveram comigo nessa jornada.

Às queridas amigas Carolina Ribeiro e Taciana Black por serem conforto, palavra de força, compreensão e incentivo em tantos momentos de minha vida! Amo vocês!

À Raquel Balaban, mesmo longe, sempre tão próxima. Minha eterna gratidão.

À Luara Carneiro, minha amiga há quase 30 anos, que a vida me presentou com suas contribuições nesse trabalho.

À Talita Graziano e Clara Formiga, ainda que de forma exclusivamente virtual, vocês influenciaram meu crescimento, aguçaram meu olhar e minha sede pelo conhecimento. Vocês são inspiração!

Aos familiares e amigos queridos, que torceram por esse trabalho. Apesar de minhas ausências, não tenho dúvidas dos sentimentos que nos unem: Érica e Armando Cruz, Zilda e Wandelson Rangel, Amanda Filgueira, Rita Acioli, Tarcísio Falcão, Rodrigo e Cecília Silva, Zhoraia Barros. Amo vocês!

Ao Sr. Edilson Falcão e à D. Teresinha Falcão. Nunca terei como lhes agradecer pela família que vocês me deram! Amo vocês! Meu respeito, carinho e gratidão!

Às crianças de minha vida, sobrinhos e afilhadas amadas: Ana Louise Filgueira, Maria Clara Rangel, Maria Alice Rangel, Isabelle Filgueira, Clara Falcão, Benjamin Falcão, Álvaro Leonardo e Daphne Sá. Que vocês continuem sendo sinal de esperança, luz no mundo e sal da terra. Amo vocês!

Agradeço principalmente aos meus pais... pois todos os caminhos que trilhei e que me trouxeram aqui devo a vocês... Devo tudo a vocês! Não tenho palavras! Vocês sabem do meu eterno respeito, admiração e amor.

E ainda, meu profundo agradecimento à Glauber, meu amado marido, companheiro da vida, indelével de meus passos e minhas conquistas... Essa vitória também é sua! E às minhas filhas: Larissa e a neném que hoje cresce em meu ventre. Vocês são minha vida. Meu sentimento. Minha força motriz. Minha razão. Tudo por vocês. Hoje e sempre! Para sempre.

RESUMO

A nanotecnologia e a fotônica tem trazido novas perspectivas para a odontologia: nanopartículas de prata (AgNPs) tem se destacado por suas propriedades antimicrobianas e a Tomografia por Coerência Óptica (OCT) tem sido empregada como promissora ferramenta diagnóstica. O principal objetivo do presente trabalho foi avaliar os efeitos de AgNPs em cepas de *Candida albicans* e seu potencial de citotoxicidade em células de mamíferos. Ainda como parte desta tese, OCT foi utilizada como ferramenta de diagnóstico em áreas de interesse na dentística restauradora: 1) para avaliação de materiais restauradores submetidos a experimentos de resistência de união ao microcisalhamento; 2) e, realização de uma revisão sistemática investigando a OCT como método de imagem para a detecção de falha restauradora. Para isso, primeiramente foram realizados testes de suscetibilidade fúngica às AgNPs, ensaio do *checkerboard*, teste do tubo germinativo, e testes de citotoxicidade. Para os experimentos com OCT, imagens foram obtidas de espécimes de dentina (saudável e desmineralizada) expostas a diferentes parâmetros do laser femtosegundo (11 and 18 J/cm^2), restauradas e submetidas a teste de microcisalhamento. Por fim, foi realizada uma revisão sistemática da literatura e meta-análise quantitativa para investigar o uso da OCT como ferramenta de diagnóstico para detecção de falha restauradora em restaurações em resina composta. Os resultados dos experimentos indicaram atividade das AgNPs sobre cepas resistentes de *C. albicans* com menor citotoxicidade nas células de mamíferos do que nas células fúngicas. OCT foi ferramenta útil na identificação do padrão de resistência de união de materiais restauradores e na detecção precoce de falhas restauradoras.

Palavras-chave**:** nanopartículas metálicas; prata; Candida albicans; tomografia de coerência óptica; lasers; falha de restauração dentária.

ABSTRACT

Nanotechnology and photonics have brought new perspectives to dentistry: silver nanoparticles (AgNPs)have stood out for their antimicrobial properties and Optical Coherence Tomography (OCT) has been used as a promising diagnostic tool. The aim of the present study was to evaluate the effects of AgNPs against *Candida albicans* strains and their cytotoxicity potential in mammalian cells. Then, Optical Coherence Tomography (OCT) was used as a diagnostic tool in areas of interest in restorative dentistry: 1) evaluation of restorative materials submitted to microshear bond strength experiments; 2) and, a systematic review investigating OCT as an imaging method to diagnoses restorative failure. For this, fungal susceptibility tests to AgNPs, checkerboard assay, germ tube assay, and cytotoxicity tests were performed. Then, OCT images were obtained from dentin specimens (sound and demineralized) exposed to different femtosecond laser parameters (11 and 18 J/cm^2), restored and subjected to microshear test. Finally, a systematic review and quantitative meta-analysis were performed to investigate the use of OCT as a diagnostic tool for detecting restorative failure in composite resin restorations. The results of the experiments indicated activity of AgNPs on resistant *C. albicans* strains with lower cytotoxicity in mammalian cells than in fungal cells. OCT was a useful tool in identifying the bond strength pattern of restorative materials and in the early detection of restorative failures.

Keywords: metal nanoparticles; silver; Candida albicans; tomography, optical coherence; lasers; dental restoration failure.

LISTA DE ILUSTRAÇÕES

TESE

Figura 1 –	Esquema gráfico da síntese de nanopartículas de prata.	23
Figura 2 –	*Candida albicans* semeada e cultivada em placa de ágar *Sabouraud* Dextrose.	24
Figura 3 –	Soluções de estoque do fluconazol: diluição em série em RPMI-1640 tamponado com MOPS.	25
Figura 4 –	Cepa de *Candida albicans* cultivada em microplaca de 96 poços após exposição a diferentes concentrações de solução de PMAA-AgNPs. Esta placa foi submetida a revelação com resazurina para ilustrar o crescimento microbiano em poços com alteração da cor original (roxa) para a cor rosa.	26
Figura 5 –	*Candida albicans* semeada e cultivada em placa de ágar *Sabouraud* Dextrose para determinação de concentração fungicida mínima.	26
Figura 6 –	Espécime amostral incluso em resina acrílica e com duas regiões distintas irradiadas pelo laser *Ti:Sapphire* femtosegundo.	30
Figura 7 –	Divisão das amostras de dentina para formação dos grupos experimentais.	30
Figura 8 –	Imagem representativa de laser *Ti:Sapphire* irradiando espécime de dentina.	31
Figura 9 –	Amostra posicionada para aquisição de imagem no Tomógrafo por Coerência Óptica (*Spectral Domain* – OCT).	33
Figura 10 –	Amostra com cilindros de resina para realização de testes de microcisalhamento.	35

ARTIGO – OPTICAL COHERENCE TOMOGRAPHY AS DIAGNOSTIC TEST FOR FAILURE ANALYSIS OF COMPOSITE RESIN RESTORATIONS: SYSTEMATIC REVIEW AND META-ANALYSIS

Figura 1 –	PRISMA flowchart summarizing the search.	49
Figura 2 –	Quality assessment of studies included.	52
Figura 3 –	Forest plot of the summary correlation coefficient for the included studies (n = 6).	54
Figura 4 –	Funnel plot for the summary correlation coefficient analysis (n = 6).	55

LISTA DE TABELAS

TESE

Tabela 1 – Estratégias de busca. 37

ARTIGO – OPTICAL COHERENCE TOMOGRAPHY AS DIAGNOSTIC TEST FOR FAILURE ANALYSIS OF COMPOSITE RESIN RESTORATIONS: SYSTEMATIC REVIEW AND META-ANALYSIS

Tabela 1 – Characteristics of the studies included in the systematic review. 50

Tabela 2 – Quality assessment of studies included. 52

LISTA DE ABREVIATURAS E SIGLAS

AFM	Microscopia de força atômica / Do inglês, *atomic force microscope*
AgNPs	Nanopartículas de prata / Do inglês, *silver nanoparticles*
ATCC	Do inglês, *American Type Culture Collection*
BVS	Biblioteca Virtual em Saúde
C. albicans	*Candida albicans*
CC_{50}	Concentração citotóxica de 50% / Do inglês, *50% cytotoxic concentration*
CIM	Concentração Inibitória Mínima
CFM	Concentração Fungicida Mínima
CLSI	Do inglês, *Clinical & Laboratory Standards Institute*
CLSM	Do inglês, *confocal laser scanning microscopy*
DD	Dentina desmineralizada
DMEM	Meio de Eagle Modificado por Dulbecco
DOI	Do inglês, *Digital Object Identifier*
DS	Dentina saudável
E_p	Energia de pulso
FICI	Índice de Concentração Inibitória Fracionada
F_p	Fluência de pulso único
fs	Femtosegundo / Do inglês, *femtosecond*
GRADE	Do inglês, *Grading of Recommendations Assessment, Development and Evaluation*
IPEN	Instituto de Pesquisa em Energia Nuclear
LFBM	Laboratório de Fisiologia e Bioquímica de Microrganismos
MEV	Microscopia eletrônica de varredura
Micro-CT	Do inglês, *Micro-computed tomography*
MOPS	3-(N-morfolino) ácido propanossulfônico
MTT	Brometo de 3-(4,5-dimetiltiazol-2-il)-2,5-difenil tetrazólio
OCT	Tomografia por Coerência Óptica / Do inglês, *Optical Coherence Tomography*
PBS	Solução salina tamponada com fosfato

P_m	Potência média
PMAA	Ácido poli(metacrílico) / Do inglês, *poly(methacrylic acid)*
PRISMA-P	Do inglês, *Preferred Reporting Items for Systematic reviews and Meta-Analyses for Protocols*
QUADAS-2	Do inglês, *Quality Assessment of Diagnostic Accuracy Studies 2*
RPMI-1640	Do inglês, *Roswell Park Memorial Institute Medium*
SD-OCT	Do inglês, *Spectral-domain optical coherence tomography*
SEM	Do inglês, *Scan electron microscopy*
SFB	Soro fetal bovino
SPSS	Do inglês, *Statistical Package for Social Sciences*
SS-OCT	Do inglês, *Swept-source optical coherence tomography*
Ufc	Unidades formadoras de colônia
UV	Ultra-violeta

LISTA DE SÍMBOLOS

>	Maior que
<	Menor que
≥	Maior ou igual que
≤	Menor ou igual que
±	Mais ou menos
%	Por cento
°C	Graus Celsius
2D	Bidimensional
3D	Tridimensional
µg	Micrograma
µJ	Microjoule
µl	Microlitro
µm	Micrômetro
A	Área
$AgNO_3$	Nitrato de prata
$CaCl_2$	Cloreto de cálcio
cm	Centímetro
CO_2	Dióxido de carbono
dB	Decibéis
h	Hora
HCl	Ácido clorídrico
J	Joule
KH_2PO_4	Fosfato de potássio
kHz	Kilohertz
kV	Kilovolt
l	Litro
M	Molar
min	Minuto
mJ	Milijoule
ml	Mililitro

mm	Milímetro
mmol	Milimolar
mol	Molar
mW	Miliwatt
N	Newton
NaCl	Cloreto de sódio
nm	Nanômetro
pH	Potencial hidrogeniônico
R	Taxa de repetição de laser
rpm	Rotações por minuto
s	Segundos
W	Watt

SUMÁRIO

1	**INTRODUÇÃO**	**19**
2	**METODOLOGIA**	**22**
2.1	**Estudo 1. Atividade de nanopartículas de prata em cepas de *Candida albicans* resistentes ao fluconazol: efeitos sinérgicos e citotóxicos**	**22**
2.1.1	*Síntese e caracterização de PMAA-AgNPs*	*22*
2.1.2	*Cepas de Candida albicans e padronização do inóculo*	*23*
2.1.3	*Agentes antifúngicos*	*24*
2.1.4	*Atividade antifúngica*	*25*
2.1.5	*Ensaio checkerboard*	*27*
2.1.6	*Ensaio de formação de tubo germinativo*	*27*
2.1.7	*Ensaio de citotoxicidade*	*27*
2.1.8	*Análise estatística*	*28*
2.2	**Estudo 2. Efeitos da irradiação por laser femtosegundo na resistência de união de microcisalhamento em dentina saudável e dentina desmineralizada**	**28**
2.2.1	*Preparação da amostra*	*28*
2.2.2	*Grupos experimentais*	*29*
2.2.3	*Condicionamento a laser*	*31*
2.2.4	*Tomografia por coerência óptica*	*32*
2.2.5	*Microscopia eletrônica de varredura*	*33*
2.2.6	*Microscopia de força atômica*	*33*
2.2.7	*Teste de resistência de união ao microcisalhamento*	*34*
2.2.8	*Estudo do tipo de falha*	*34*
2.2.9	*Análise estatística*	*35*
2.3	**Estudo 3. Tomografia por coerência óptica como ferramenta de diagnóstico para análise de falha em restauração de resina composta: revisão sistemática e metanálise**	**35**
2.3.1	*Critérios de elegibilidade*	*36*

2.3.2 Bases de dados 36
2.3.3 Estratégia de busca 37
2.3.4 Seleção dos estudos 40
2.3.5 Extração de dados 40
2.3.6 Avaliação de risco de viés 41
2.3.7 Síntese de dados 41
2.3.8 Qualidade da evidência 41
3 RESULTADOS E DISCUSSÃO 42
4 ARTIGO – OPTICAL COHERENCE TOMOGRAPHY AS DIAGNOSTIC TEST FOR FAILURE ANALYSIS OF COMPOSITE RESIN RESTORATIONS: SYSTEMATIC REVIEW AND META-ANALYSIS 43
5 CONSIDERAÇÕES FINAIS 65
REFERÊNCIAS 66
APÊNDICE A – ACTIVITY OF POLY(METHACRYLIC ACID)-SILVER NANOPARTICLES ON FLUCONAZOLE RESISTANT *CANDIDA ALBICANS* STRAINS: SYNERGISTIC AND CYTOTOXIC EFFECTS 69
APÊNDICE B – EFFECTS OF FEMTOSECOND LASER IRRADIATION ON THE MICROSHEAR BOND STRENGTH OF SOUND AND DEMINERALIZED DENTIN 81

1 INTRODUÇÃO

A nanotecnologia, tecnologia de materiais nanométricos (1 – 100 nm), tem se mostrado de grande utilidade na obtenção de melhorias no diagnóstico, tratamento e prevenção de doenças bucais. Diante da revolução que a nanotecnologia tem proporcionado na formulação de novos biomateriais e técnicas odontológicas, fica claro seu vasto potencial ainda a ser explorado (DAS *et al*., 2022; DESAI; SOMASUNDARAM, 2020).

O desenvolvimento e aprimoramento de nanopartículas metálicas têm dado destaque as propriedades únicas que as tornam tão desejáveis na ciência dos materiais, na biologia e na área da saúde. Além de seus efeitos antimicrobianos, apresentam vantagens como: toxicidade relativamente baixa, hidrofilicidade e alta estabilidade (MUSSIN *et al*., 2019). As nanopartículas de prata (AgNPs) estão entre os nanomateriais mais estudados para aplicações biomédicas devido às suas potentes propriedades antimicrobianas, boa estabilidade química e biocompatibilidade (SINGH *et al*., 2019).

A utilização de AgNPs de maneira isolada ou em combinação com drogas antifúngicas disponíveis comercialmente tem sido investigada a fim de driblar a crescente resistência microbiana, bem como as complicações associadas ao uso prolongado de antifúngicos (MUSSIN *et al*., 2019). A atividade dessas nanopartículas contra *Candida albicans* já foi demonstrada (HAMIDA; ALI; GODA; REDHWAN, 2021; HAMPE *et al*., 2017; LEE *et al*., 2019; LONGHI; *et al*., 2016). Esta espécie fúngica faz parte da microbiota normal da maior parte das pessoas saudáveis, mas também é a principal espécie responsável pela candidíase: uma infecção oportunista que pode variar desde uma condição superficial a uma infecção sistêmica invasiva e com potencial risco de vida (R; RAFIQ, 2020). Além do surgimento de resistência fúngica, o espectro limitado dos fármacos disponíveis constitui uma grande barreira para o tratamento eficaz de infecções tanto locais como sistêmicas (NGUYEN; TRUONG; BRUNING, 2020).

Diante dessa situação, a busca por novas AgNPs com propriedades físico-químicas mais seguras para uso humano ainda é uma demanda urgente, pois seu potencial de citotoxicidade ainda não está bem estabelecido e tem sido motivo de questionamentos (PUNJABI *et al*., 2018). Assim, tem-se almejado não apenas um método inovador, econômico e ecologicamente correto para produzir estas

nanopartículas, mas também se tem buscado avaliar sua atividade antimicrobiana e sua biossegurança a fim de validar seu potencial terapêutico (RÓŻALSKA *et al*., 2018).

Além da nanotecnologia, as inovações ligadas à fotônica tem proporcionado novos horizontes para a pesquisa odontológica através de aplicações que incorporam os estudos da biofotônica (fotônica aplicada às áreas biológicas). Estudos voltados para a interação da luz com os tecidos dentários, bem como com materiais de aplicação na saúde bucal têm surgido como uma promessa de meios de diagnóstico mais precisos e de tecnologias menos invasivas. Nesse contexto, a Tomografia por Coerência Óptica (OCT), método de imagem já consolidado na cardiologia e na oftalmologia, tem sido vastamente explorada em diversas especialidades odontológicas.

OCT é uma técnica de imagem bem estabelecida para diagnóstico *in vivo* e *ex vivo* (HUANG *et al*., 1991) e em uma infinidade de tecidos e biomateriais (DING; LI; WANG, 2021). O princípio de operação da OCT é semelhante ao do ultrassom, utilizando ondas de luz em vez de ondas sonoras. A luz tem sido empregada para investigar propriedades estruturais de tecidos biológicos e materiais diversos, oferecendo vantagens não encontradas em outras técnicas de imagem. A técnica de OCT atinge resoluções espaciais longitudinais e laterais em escala micrométrica e detecta frações extremamente pequenas dos sinais refletidos ou retroespalhados (SWANSON; FUJIMOTO, 2017; WOJTKOWSKI, 2010) identificando detalhes e particularidades estruturais, indo além do alcance dos microscópios ópticos tradicionais, que não captam o interior do material.

Na dentística restauradora, a OCT tem sido explorada de maneira diversa para elucidar lacunas de pesquisas laboratoriais e clínicas, pois possui a vantagem de ser um método não-invasivo, fornecendo imagens transversais sem danificar amostras. Além disso, sob uma perspectiva do atendimento clínico, aponta para a possibilidade de eliminar a dose de radiação usual em diagnóstico por imagem (MATSUURA *et al*., 2018). Portanto, a técnica de OCT é um método de imagem prático, não destrutivo e não ionizante que tem direcionado novos panoramas em imagem, dando acesso a reconstruções volumétricas tridimensionais em escala de tempo praticamente real (WOJTKOWSKI, 2010), impactando aspectos na pesquisa, na prática clínica e em questões comerciais (SWANSON; FUJIMOTO, 2017).

Sendo assim, foi avaliada a atividade de nanopartículas de prata esféricas frente a cepas de *C. albicans*, bem como seu potencial de citotoxicidade em células de mamíferos. Em seguida, o tomógrafo por coerência óptica foi utilizado para investigação em áreas da dentística restauradora: avaliamos a morfologia e características de superfície de corpos de prova submetidos a experimentos de microcisalhamento, a fim de explicar as diferenças observadas na resistência de união; e, por fim realizamos uma revisão sistemática da literatura e meta-análise quantitativa para investigar o uso da OCT como ferramenta diagnóstica para a detecção de falha restauradora em restaurações de resina composta.

Como aspectos de originalidade essa tese traz nanopartículas de prata produzidas através de metodologia simples, de baixo custo e baixa geração de resíduos; e nunca antes testadas em células fúngicas. Estas nanopartículas testadas em cepas de *C. albicans* resistentes mostraram um resultado promissor principalmente quando comparado a sua citotoxicidade. No que se refere ao OCT destaca-se através de revisão sistemática sua importância como ferramenta diagnóstica diante de um dos grandes desafios clínicos da dentística restauradora.

2 METODOLOGIA

2.1 Estudo 1. Atividade de nanopartículas de prata (PMAA-AgNPs) em cepas de *Candida albicans* resistentes ao fluconazol: efeitos sinérgicos e citotóxicos

Os experimentos deste estudo foram realizados nos seguintes laboratórios: Laboratório de Fotônica e Biofotônica do Departamento de Física da Universidade Federal de Pernambuco, Laboratório de Fisiologia e Bioquímica de Microrganismos do Departamento de Antibióticos da Universidade Federal de Pernambuco e no Laboratório de Biologia de Patógenos do Departamento de Microbiologia do Instituto Aggeu Magalhães.

2.1.1 Síntese e caracterização de PMAA-AgNPs

Nanopartículas de prata (PMAA-AgNPs) foram sintetizados de acordo com metodologia previamente descrita por Carvalho *et al*. (2018). Em solução aquosa de nitrato de prata ($AgNO_3$, 50 ml, 5 mmol/l) foi adicionado ácido poli(metacrílico) (PMAA, 50 ml, 0,5 mmol/l), sendo em seguida submetida a agitação magnética a 25 °C durante 5 min. Esta solução foi exposta à luz UV (8 W, comprimento de onda central de 370 nm) durante 6 h para redução da prata (Figura 1). A solução foi armazenada em frasco âmbar (SPADARO *et al*., 2009). Tamanho e morfologia das PMAA-AgNPs obtidas foram analisados. A espectroscopia de transmissão visível (Espectrômetro Cary 50 UV-Vis, Varian/Agilent, Palo Alto, EUA) foi utilizada para verificar a conversão de cátions de prata em nanopartículas de prata. A nanoestrutura das amostras foi caracterizada por microscopia eletrônica de transmissão (JEOL, JEM-2100, Japão) operando em 200 kV e módulo espectrômetro fluorescente de raios X de energia dispersiva do Instituto de Pesquisa em Energia Nuclear (IPEN) – SP, Brasil. As medições de potencial zeta foram realizadas usando Zetasizer Nano (Malvern, Inglaterra) do Laboratório de Polímeros Não Convencionais, Departamento de Física – Universidade Federal de Pernambuco.

Figura 1 – Esquema gráfico da síntese de nanopartículas de prata.

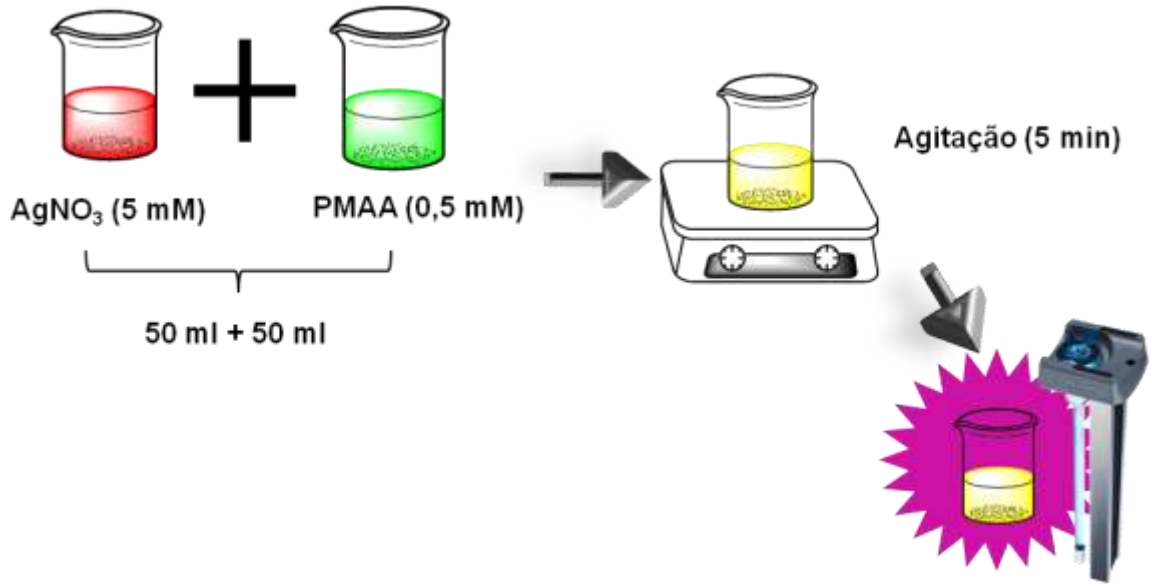

Fonte: a autora (2022)

2.1.2 Cepas de Candida albicans e padronização do inóculo

As cepas de *C. albicans* (n = 9) foram obtidas através de culturas de estoque mantidas no Laboratório de Fisiologia e Bioquímica de Microrganismos (LFBM) do Departamento de Antibióticos da Universidade Federal de Pernambuco. Essas cepas foram isoladas de urina (LFBM Ca01, LFBM Ca02, LFBM Ca03 e LFBM Ca04), cavidade oral (LFBM Ca05 e LFBM Ca06) e sangue (LFBM Ca07, LFBM Ca14 e LFBM Ca1002). *C. albicans* ATCC® 10231 foi utilizada como cepa padrão.

As culturas de *C. albicans* foram reativadas em caldo de *Sabouraud* Dextrose (DIFCO, EUA), semeadas em ágar *Sabouraud* Dextrose (DIFCO, EUA) e incubadas a 35 °C por 24 h (Figura 2). Para padronização do inóculo, foram selecionadas colônias únicas e a suspensão de levedura foi preparada em solução salina (0,85%). A turbidez destas suspensões foi ajustada para 90% de transmitância a 530 nm que é equivalente a 10^6 unidades formadoras de colônias por ml (ufc/ml). Em seguida, foram realizadas duas diluições para obtenção do inóculo final (10^3 ufc/ml). Primeiro, a cultura de *C. albicans* foi diluída em solução salina (1:100) seguida por uma segunda diluição (1:10) em *Roswell Park Memorial Institute Medium* (RPMI-1640, Gibco, EUA) tamponado com 3-(N-morfolino) ácido propanossulfônico (MOPS, *Sigma-Aldrich*, EUA), seguindo as diretrizes do *Clinical & Laboratory Standards Institute* (CLSI,

2017a). O crescimento de *C. albicans* na cultura foi confirmado por meio de contagem direta de células.

Figura 2 – *Candida albicans* semeada e cultivada em placa de ágar *Sabouraud* Dextrose.

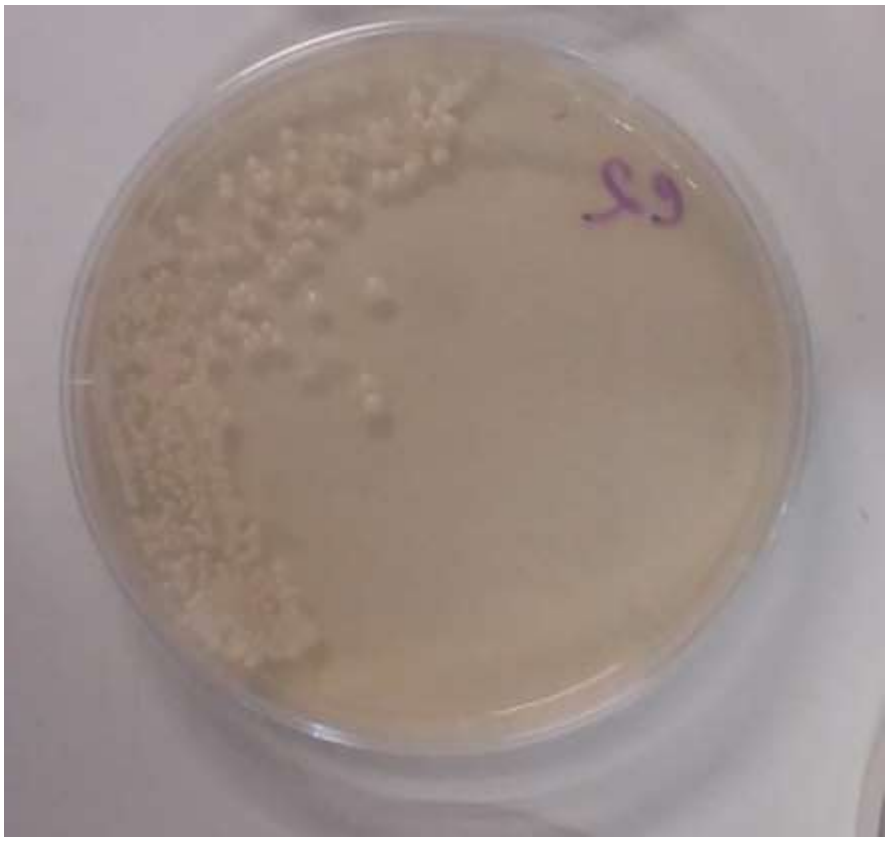

Fonte: a autora (2022)

2.1.3 Agentes antifúngicos

Anfotericina B, nistatina e fluconazol (*Sigma-Aldrich*, EUA) foram escolhidos como medicamentos de referência, considerando as diretrizes do *Guideline of Infectious Diseases Society of America* (PAPPAS *et al*., 2016). O perfil de resistência foi definido particularmente para cada droga, considerando a Concentração Inibitória Mínima (CIM) como os valores necessários para inibir o crescimento de 90% dos microrganismos: anfotericina B CIM > 1,0 µg/ml e fluconazol CIM ≥ 8,0 µg/ml. Para nistatina, CIM entre 8,0 e 32,0 µg/ml foi definida como suscetibilidade dose-dependente (CLSI, 2017a; CLSI, 2017b). Anfotericina B, nistatina e fluconazol foram solubilizados em dimetilsulfóxido/tween 80/água (1,0/0,5/8,5) enquanto nanopartículas de prata foram solubilizadas em água. *C. albicans* cultivada em meio

contendo dimetilsulfóxido/tween 80/água foi utilizada como controle negativo para excluir a possibilidade de efeitos tóxicos deste diluente sobre o patógeno.

2.1.4 Atividade antifúngica

A avaliação da suscetibilidade das cepas de *C. albicans* aos antifúngicos foi realizada pelo método de microdiluição, de acordo com a diretriz CLSI (2017a) com pequenas modificações. Soluções de estoque de PMAA-AgNPs, anfotericina B, nistatina e fluconazol foram diluídas em série em RPMI-1640 tamponado com MOPS para obter concentrações que variaram de 64,0 a 0,5 µg/ml, exceto para fluconazol, cuja concentração variou de 1.024 a 8,0 µg/ml (Figura 3). Alíquotas (100 µl) das soluções das drogas foram distribuídas em microplacas de 96 poços e, em seguida, uma suspensão padronizada de cepas de *C. albicans* (100 µl) foi adicionada. As microplacas foram incubadas a 35 °C durante 24 h (Figura 4). A CIM foi relatada como a menor concentração de compostos que inibiram o crescimento de *C. albicans* (CLSI, 2017a).

Figura 3 – Soluções de estoque do fluconazol: diluição em série em RPMI-1640 tamponado com MOPS.

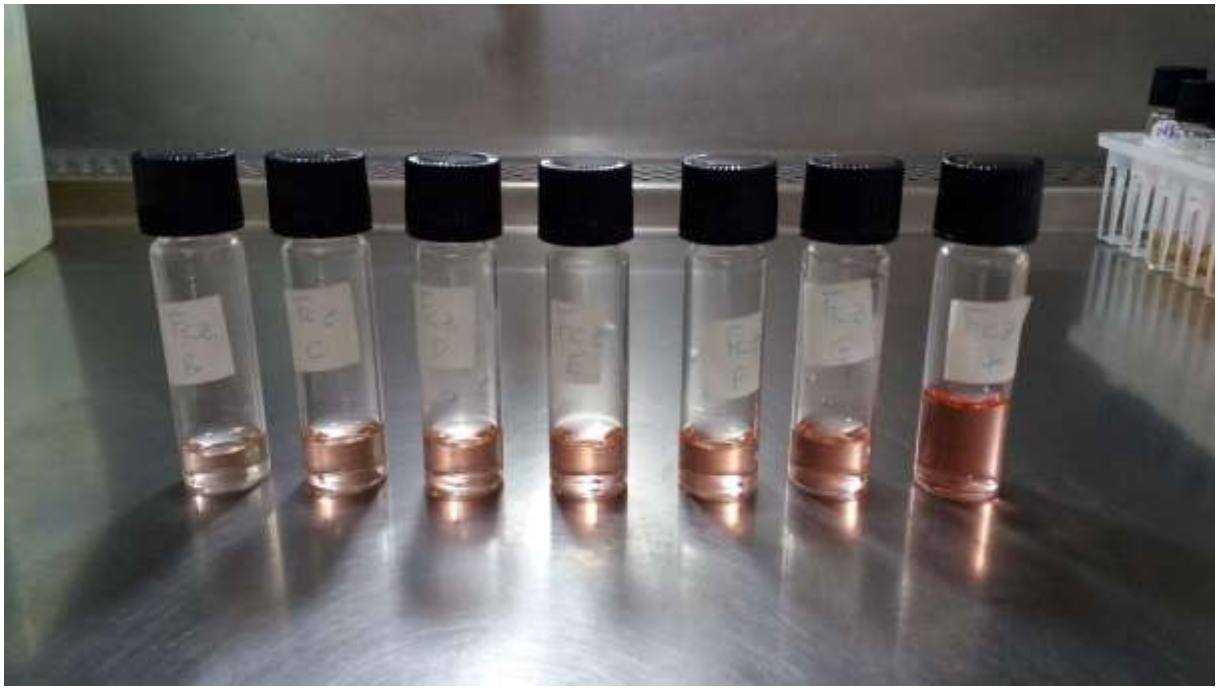

Fonte: a autora (2022)

Figura 4 – Cepa de *Candida albicans* cultivada em microplaca de 96 poços após exposição a diferentes concentrações de solução de PMAA-AgNPs. Esta placa foi submetida a revelação com resazurina: os poços evidenciados pela cor roxa indicam inibição do crescimento microbiano.

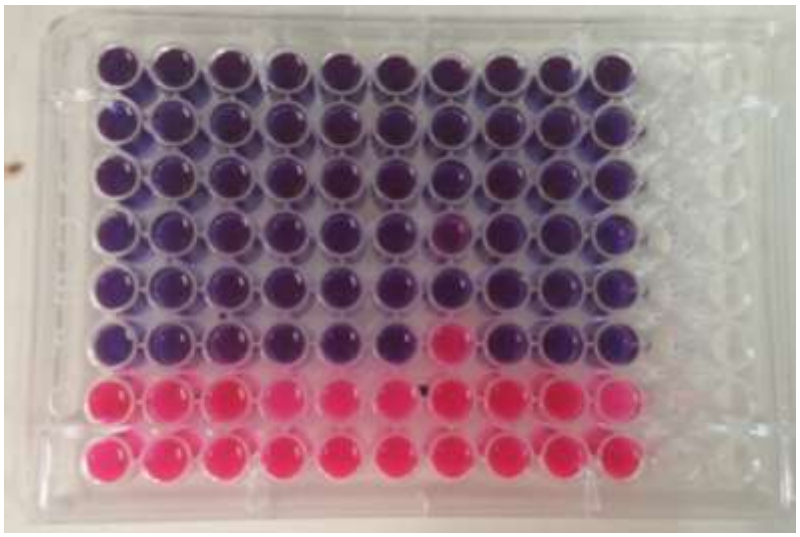

Fonte: a autora (2022)

Para determinar a Concentração Fungicida Mínima (CFM), definida como a concentração mais baixa capaz de matar mais de 99,9% do inóculo inicial, alíquotas (5 µl) de cada poço onde não foi detectado crescimento fúngico, foram semeadas em ágar *Sabouraud* Dextrose (Figura 5). Placas foram incubadas nas mesmas condições e o número de colônias foi determinado.

Figura 5 – *Candida albicans* semeada e cultivada em placa de ágar *Sabouraud* Dextrose para determinação de concentração fungicida mínima.

Fonte: a autora (2022)

2.1.5 Ensaio checkerboard

O ensaio *checkerboard* foi realizado de acordo com metodologia descrita por Odds (2003). Diluições apropriadas de PMAA-AgNPs (4,0 a 0,031 µg/ml) e fluconazol (1.024 a 0,5 µg/ml) foram preparadas em RPMI-1640. A partir dessas diluições, 50 µl foram adicionados em microplacas de 96 poços para obter uma concentração final correspondente a 1/8 e 1/12 do valor de CIM para PMAA-AgNPs e fluconazol, respectivamente. Em seguida, 100 µl de suspensão de células foram adicionados a cada poço (10^3 ufc/ml) e as microplacas foram incubadas a 35 °C por 24 h.

O Índice de Concentração Inibitória Fracionada (FICI) foi determinado como: (CIM PMAA-AgNPs em combinação com fluconazol/CIM do PMAA-AgNPs) + (CIM do fluconazol em combinação com PMAA-AgNPs/CIM do fluconazol).

O efeito da combinação foi definido como sinérgico se o FICI fosse ≤ 0,5, aditivo quando o FICI fosse > 0,5 a ≤ 1,0 e antagônico quando > 1,0 (ODDS, 2003).

2.1.6 Ensaio de formação do tubo germinativo

Para os testes de formação do tubo germinativo, uma cepa foi escolhida aleatoriamente (LFBM Ca06). Esta cepa foi cultivada em caldo de *Sabouraud* Dextrose a 35 °C durante 24 h. As culturas foram diluídas no mesmo caldo para obter suspensões padrão da levedura (10^3 ufc/ml). Essas suspensões foram expostas ao fluconazol, PMAA-AgNPs e suas combinações em concentrações sub-inibitórias. Alíquotas de 1 mL de cada cultura de *C. albicans* foram adicionadas a 1 mL de soro fetal bovino (SFB, Gibco, EUA). Os tubos de ensaio foram incubados a 37 °C por 3 h sob agitação suave. Amostras cultivadas em meio livre de drogas suplementado com SFB foram consideradas como controle positivo para formação do tubo germinativo. Uma gota de cada cultura de *C. albicans* foi colocada em uma lâmina e observada sob microscópio óptico com aumento de 400X (Olympus BX51, Tóquio, Japão) (MATARE; NZIRAMASANGA; GWANZURA; ROBERTSON, 2017). Foi considerado como tendo germinado se a formação do tubo germinativo fosse pelo menos duas vezes o comprimento da célula.

2.1.7 Ensaio de citotoxicidade

Os efeitos citotóxicos do PMAA-AgNPs em macrófagos J774.A1 (ATCC® TIB-67TM), células *Vero* (ATCC® CCL-81TM) e fibroblastos (ATCC® PCS-201-018) foram avaliados pelo ensaio colorimétrico MTT (MOSMANN, 1983). Cada tipo celular (10^5

células/ml) foi semeado em placas de 96 poços contendo RPMI-1640 para macrófagos e células *Vero,* ou Meio de Eagle Modificado por Dulbecco (DMEM) para fibroblastos, suplementado com 10% de SFB inativado. As culturas foram incubadas a 37 °C por 3 h em atmosfera de 5% de CO_2. As células não aderentes foram removidas por lavagem com solução salina tamponada com fosfato (PBS), pH 7,0. As células restantes foram incubadas por mais 48 h em RPMI-1640 na ausência ou na presença de PMAA-AgNPs (100 µl), em concentrações variando de 2,0 a 64,0 µg/ml. As células tratadas e não tratadas foram lavadas e incubadas a 37 °C por 3 h em meio de cultura fresco contendo 0,5 mg/ml de brometo de 3-(4,5-dimetiltiazol-2-il)-2,5-difenil tetrazólio (MTT) (*Sigma–Aldrich*, EUA). Após a incubação, o MTT foi removido e as células foram tratadas com (100 µl) isopropanol ácido (HCl 0,04 mol/l em isopropanol) para solubilização dos cristais de formazan derivados da redução do MTT. Alíquotas das amostras (100 µl) foram transferidas para microplacas de 96 poços e analisadas no Espectrofotômetro de Microplacas Benchmark Plus™ (*Bio-Rad*®, EUA) a 540 nm.

2.1.8 Análise estatística

Todos os ensaios foram realizados em triplicata em experimentos independentes e os resultados foram expressos como uma média dos ensaios. Os resultados do ensaio de citotoxicidade foram plotados como a porcentagem de células viáveis para células não tratadas. O valor da concentração citotóxica de 50% (CC_{50}) foi calculado por análise de regressão não linear. Os dados foram comparados por análise de variância unidirecional (ANOVA) seguida do pós-teste de Tukey usando *GraphPad Prism* 9.1.1 (*GraphPad Software*, EUA). Valor de $p < 0,05$ foi considerado estatisticamente significante.

2.2 Estudo 2. Efeitos da irradiação por laser femtosegundo na resistência de união de microcisalhamento em dentina saudável e dentina desmineralizada

2.2.1 Preparação da amostra

Este estudo foi aprovado pelo Comitê de Ética da Universidade Federal de Pernambuco, sob o protocolo nº 1.735.580. Vinte molares humanos recém-extraídos foram obtidos através do Banco de Dentes da Universidade Federal de Pernambuco. Os dentes selecionados foram previamente examinados para confirmar a ausência de danos em sua superfície, como sulcos profundos ou rachaduras, foram submetidos a

higienização com auxílio de água destilada e escovas de Robinson. Posteriormente, os dentes foram armazenados em solução de cloramina 0,5% durante 15 dias.

As porções radiculares foram seccionadas a uma distância de 2 mm da junção cemento-esmalte. O esmalte da superfície oclusal foi removido com auxílio de uma ponta diamantada de baixa rotação (Isomet, Buehler Ltd., IL, EUA) a fim de expor a superfície dentinária. Cada dente foi incluído em resina acrílica (Jet, Clássico, São Paulo, Brasil) para facilitar a manipulação das amostras. As superfícies dentinárias foram submetidas a polimento metalográfico (Biopdi, São Paulo, Brasil) com lixas em duas granulações (400 e 600), sob refrigeração, durante 60 s, para remoção de qualquer remanescente de esmalte, planificação da superfície a ser estudada e produção de camada de *smear layer* padronizada.

Dez espécimes selecionadas aleatoriamente, foram submetidas à procedimento de ciclagem de pH de 5 dias via imersão em ácido cítrico 0,05 M (pH 2,3, durante 10 min, 6 vezes por dia). No intervalo entre as imersões, os espécimes foram expostos a uma solução supersaturada (pH 7,0), consistindo em 1,5 mmol/l de $CaCl_2$, 1,0 mmol/l de KH_2PO_4 e 50 mmol/l de NaCl (ZERO *et al*., 1990), em temperatura ambiente (25 °C), sob agitação (30 rpm) durante 60 min. A etapa final de ciclagem consistiu em armazenar os espécimes na mesma solução supersaturada até o momento da irradiação por laser, que foi realizada dentro de um intervalo de 24h. As soluções foram renovadas diariamente, e seu pH verificado no início e no final de cada dia de experimento.

2.2.2 Grupos experimentais

Os vinte espécimes de dentina foram distribuídos aleatoriamente em grupos experimentais de acordo com a condição do substrato (desmineralizado ou não) e de acordo com os parâmetros adotados na utilização do laser. Dez espécimes compuseram o grupo controle dentina saudável (DS) e dez espécimes compuseram o grupo controle dentina desmineralizada (DD). Os grupos DS e DD foram distribuídos randomicamente em subgrupos entre espécimes irradiadas e não irradiadas (controle). Cada amostra irradiada, recebeu em duas regiões diferentes, intensidades de energia de pulso diferente. As regiões irradiadas possuíam afastamento suficiente para garantir que a condição de irradiação de uma região não interferisse na outra (Figura 6). A divisão dos grupos experimentais está resumida na Figura 7.

Figura 6 – Espécime amostral incluso em resina acrílica e com duas regiões distintas irradiadas pelo laser *Ti:Sapphire* femtosegundo.

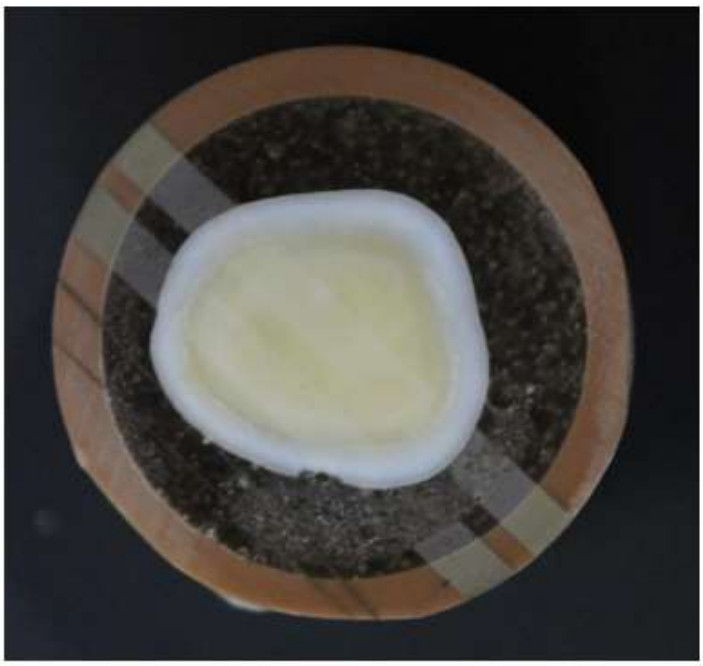

Fonte: a autora (2018)

Figura 7 - Divisão das amostras de dentina para formação dos grupos experimentais.

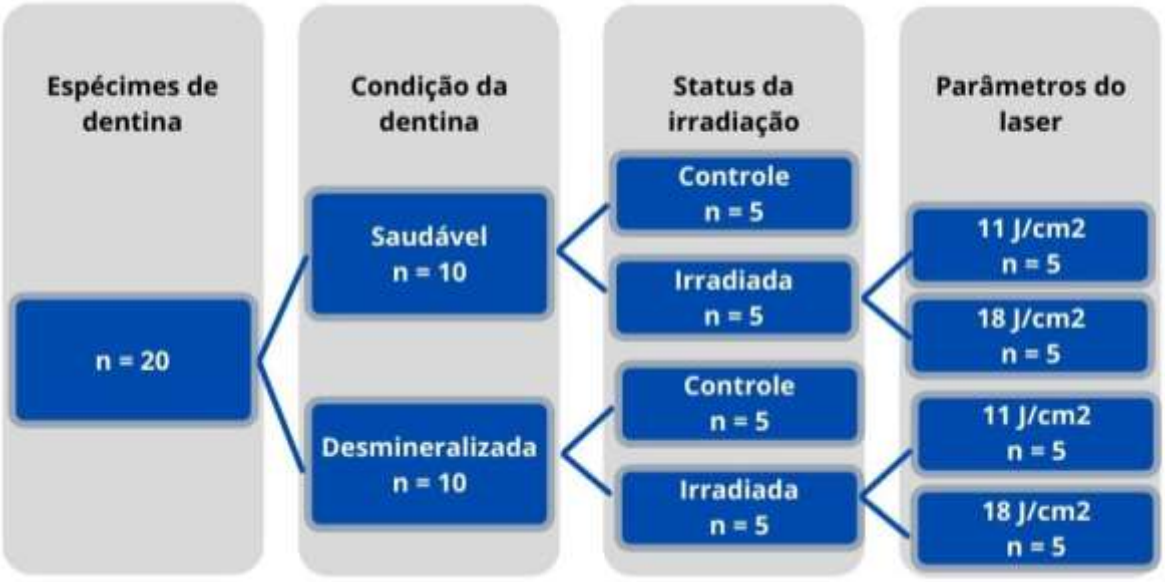

Fonte: a autora (2018)

2.2.3 Condicionamento a laser

O condicionamento a laser foi realizado utilizando um amplificador regenerativo pulsado de *Ti:Sapphire* (802 nm, 100 fs, 1 kHz, energia máxima de pulso de 1 mJ, Libra®, Coherent, EUA) (Figura 8). Dois valores de energia de pulso foram escolhidos (240 e 390 µJ) e aplicados em duas regiões distintas das amostras. A energia de pulso (E_p) foi calculada usando a potência média (P_m), através das fórmulas:

$$E_p = \frac{P_m}{R}$$

Onde, R é a taxa de repetição do laser (1 kHz). A potência média foi controlada por uma combinação de placa de Glan-Thompson/meia-onda, externa à cavidade do laser. O feixe de laser foi direcionado para a superfície da amostra usando uma lente objetiva (20×, abertura numérica de 0,3) para promover a ablação mediada por plasma.

Figura 8 – Imagem representativa de laser *Ti:Sapphire* irradiando espécime de dentina.

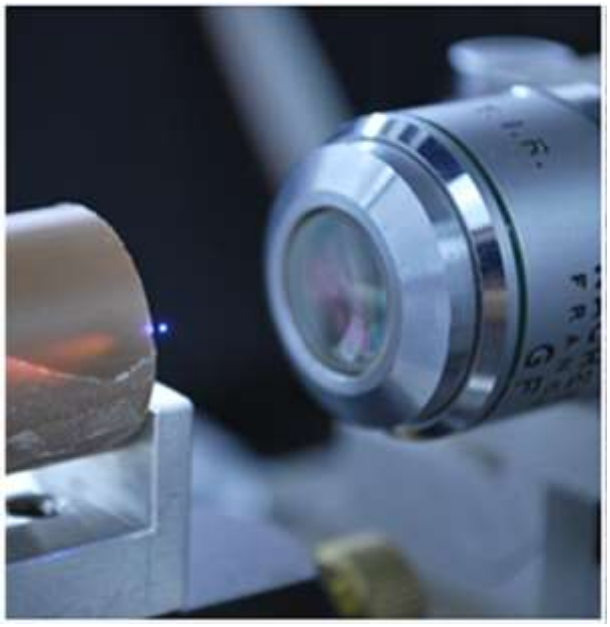

Fonte: a autora (2018)

As amostras foram fixadas em um suporte XYZ de precisão micrométrica, conectado a motores de passo controlados pela ferramenta LABVIEW®. Com o objetivo de aumentar a largura das linhas de varredura, diminuir danos térmicos e

mecânicos e, ainda, promover a remoção superficial da *smear layer*, a varredura a laser foi realizada com as amostras distantes 200 µm do foco na direção incidente (eixo Z), produzindo linhas de ablação com 90 µm de largura. Essa largura foi medida usando imagens de microscopia eletrônica de varredura das amostras irradiadas no estudo piloto a fim de estabelecer os melhores parâmetros do laser. A estrutura XYZ foi programada para se mover 2,5 cm na direção horizontal (eixo X), cobrindo toda a amostra. O comprimento horizontal foi suficiente para fazer duas medições independentes da resistência de união na mesma região irradiada pelo laser. Na direção vertical (eixo Y), foram produzidas 20 linhas de varredura, igualmente espaçadas em 90 µm, produzindo uma área irradiada com largura total de 1,8 mm. A velocidade de varredura foi de 30 mm/s. Considerando 90 µm como o diâmetro efetivo do feixe, esta velocidade de varredura promove a superposição de três pulsos por ponto de distância, aproximadamente. Usando a expressão:

$$F_p = \frac{E_p}{A}$$

onde, F_p é a fluência de pulso único e A corresponde a área do ponto, foi possível calcular as fluências totais em 1 kHz: ~11 J/cm^2 para 240 µJ e ~18 J/cm^2 para 390 µJ. Esses valores estão várias vezes acima dos valores de limiar de ablação citados na literatura para sistemas de laser equivalentes (PETROV; PECHEVA; WALMSLEY; DIMOV, 2018; PORTILLO MUÑOZ *et al*., 2012).

Sendo assim, o grupo composto por dentina saudável foi irradiada com densidade de energia de 11 J/cm^2 (DS-11) e de 18 J/cm^2 (DS-18). E o grupo composto por dentina desmineralizada, também foi irradiado pelos mesmos parâmetros do laser (DD-11 e DD-18).

2.2.4 Tomografia por coerência óptica

Cada espécime irradiado foi avaliado por OCT operando em *Spectral Domain* (SD-OCT, *Callisto Spectral Domain OCT System*, Thorlabs Inc., NJ, EUA), através de imagens 2D e 3D (Figura 9). A fonte de luz OCT é um diodo super luminescente com comprimento de onda central de 930 nm, largura de banda espectral de 100 nm e potência máxima de saída de 5 mW. As imagens geradas por este sistema apresentam resolução axial de 7/5,3 µm (ar/água), resolução lateral de 8 µm e profundidade máxima de imagem de 1,3 mm. A taxa de varredura axial do sistema é

de 1,2 kHz, capturando dois quadros por segundo com 105 dB de sensibilidade. Este sistema fornece perfis de profundidade que, somados às imagens transversais, possibilitam reconstruções tridimensionais. As amostras foram posicionadas em uma placa micrométrica XYZ movimentada manualmente. Todas as superfícies foram analisadas por linhas de varredura partindo da área de referência em direção à área irradiada, passando pela interface. O sistema SD-OCT gerou imagens 2D transversais com 1024 × 512 pixels (4 × 0,5 mm) e imagens 3D com 1024 × 512 pixels (3 × 3 mm). A discrepância entre a altura da área de referência e a superfície irradiada foi medida usando o programa *ImageJ* (JAVA, domínio público) para calcular a perda tecidual.

Figura 9 – Amostra posicionada para aquisição de imagem no Tomógrafo por Coerência Óptica (*Spectral Domain* – OCT).

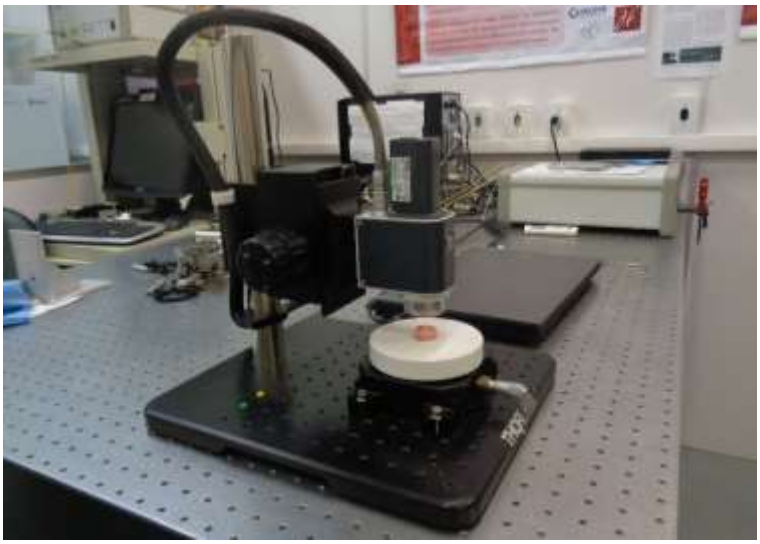

Fonte: a autora (2018)

2.2.5 Microscopia eletrônica de varredura

Microscopia eletrônica de varredura (Mira 3, Tescan, Brno, República Tcheca, 10 kV, magnificação de 5000x) de áreas irradiadas foram adquiridas de amostras adicionais (n = 2).

2.2.6 Microscopia de força atômica

Duas amostras adicionais foram preparadas para análise por meio de microscopia de força atômica (AFM, Alpha 300 RA, WITec, Ulm, Alemanha). A superfície foi sondada em “modo de contato”. A imagem foi realizada com um cantilever revestido de alumínio com constante de força de 0,2 N/m e ponto de

operação de 0,5 V. A taxa de varredura foi muito lenta com objetivo de alcançar detalhes da estrutura dentinária. As dimensões das imagens coletadas foram 30 μm × 30 μm, 256 × 256 pixels.

2.2.7 Teste de resistência de união ao microcisalhamento

O sistema adesivo testado (Clearfil SE Bond, Kuraray Noritake Dental Inc., Kurashiki, Okayama, Japão) foi aplicado nas superfícies dentinárias de acordo com as instruções do fabricante. Tubos transparentes de polietileno (diâmetro interno de 0,9 mm e altura de 1 mm) foram dispostos sobre fitas perfuradas de dupla face. A resina composta (Tetric N-Ceram A3, Ivoclar Vivadent, Schaan, Liechtenstein) foi cuidadosamente acondicionada dentro dos tubos e posteriormente fotopolimerizada por 20 s usando um diodo emissor de luz com 1200 mW/cm^2 (Radii-cal, SDI, Bayswater, Victoria, Austrália). As amostras foram armazenadas em água destilada por 24 horas a 37 °C. Tubo e fita dupla face foram removidos cautelosamente com auxílio de lâmina de bisturi (Figura 10). Estereomicroscópio (ampliação 10x) foi ferramenta utilizada para investigação de possíveis defeitos. Os corpos de prova foram testados em máquina universal de ensaios (EMIC, DL 10000, São José dos Pinhais-PR, Brasil). Um fio ortodôntico fino (0,2 mm) foi enrolado ao redor do cilindro alinhado configurado para garantir a orientação correta das forças aplicadas. A velocidade da cruzeta foi fixada em 0,5 mm/min até a falha. O software TESC 3.04 (EMIC, São José dos Pinhais-PR, Brasil) registrou os valores de resistência de união. Esses procedimentos foram aplicados a todos os grupos experimentais, e a resistência de união nos grupos controle (DS e DD) representam o protocolo clínico normal (sem condicionamento a laser).

2.2.8 Estudo do tipo de falha

A análise do tipo de falha foi realizada com auxílio de microscópio óptico com ampliação de 5x, 10x, 20x e 50x (Olympus BX51, Tóquio, Japão). A tomografia por coerência óptica foi realizada para obter imagens 2D e 3D. As falhas foram enquadradas nas seguintes nomenclaturas, de acordo com percentual de material livre de substrato como “falha do tipo adesiva” (falha identificada na interface resina-esmalte), “falha do tipo coesiva” (falha dentro do esmalte ou resina composta) e “falha do tipo mista” (falha variando entre interface resina-esmalte e falha do tipo coesiva).

Figura 10 - Amostra com cilindros de resina para realização de testes de microcisalhamento.

Fonte: a autora (2018)

2.2.9 Análise estatística

Os dados coletados foram analisados no programa SPSS 13.0 (*Statistical Package for Social Sciences*, Chicago, IL, EUA) para *Windows*. Estatísticas descritivas foram obtidas e o teste de Kruskal Wallis (p = 0,01) foi utilizado para comparar os resultados entre os grupos. Em caso de diferenças significativas, foi utilizado o teste de Mann Whitney para comparação pareada entre os grupos (p = 0,05).

2.3 Estudo 3. Tomografia por Coerência Óptica como ferramenta de diagnóstico para análise de falha em restauração de resina composta: revisão sistemática

O protocolo para a construção desta revisão sistemática foi escrito seguindo a diretriz do *Preferred Reporting Items for Systematic reviews and Meta-Analyses for Protocols* 2015 (PRISMA-P 2015) (MOHER; *et al*., 2015; SHAMSEER *et al*., 2015) e foi registrado na plataforma *Open Science Framework*, estando disponível em https://osf.io/z9qgn/. A pergunta de pesquisa desta revisão sistemática foi construída com base na estratégia “PIRD” (*Population; Index test; Reference test; Diagnosis*) e consiste em: “A Tomografia por Coerência Óptica é uma ferramenta eficaz para diagnóstico de falha restauradora em restaurações diretas de resina composta?”.

2.3.1 Critérios de elegibilidade

Quanto ao desenho do estudo – foram incluídos estudos do tipo ensaios laboratoriais (estudos *in vitro*) que utilizaram OCT para diagnóstico de falha restauradora em restaurações de resina composta.

Quanto aos participantes – restaurações em resina composta realizadas em dentes humanos ou dentes bovinos. Critérios de exclusão: restaurações indiretas, restauração em resina composta realizadas em dentes decíduos.

Quanto ao teste de índice – Tomografia por Coerência Óptica utilizada para auxiliar na detecção ou diagnóstico de falha de restauração em resina composta. Critérios de exclusão: estudos que avaliaram falha restauradora exclusivamente com OCT, sem comparação direta com outra técnica de avaliação.

Quanto aos testes padrões utilizados como referência – foram considerados como exames de referência: radiografias convencionais e digitais, microtomografia computadorizada, microscopia eletrônica de varredura, microscopia confocal de varredura a laser, microscopia óptica (corte histológico), infiltração de corante, estereomicroscópio.

Condição-alvo – Falha restauradora: integridade marginal, falhas adesivas, microinfiltração, rachaduras ou bolhas na interface resina-tecido dentário em restaurações de resina composta.

2.3.2 Bases de dados

As buscas sistemáticas foram executadas em um único dia (02 de julho de 2022) nas seguintes bases de dados sem restrições de idioma ou data de publicação: *Medline* via *Pubmed*, *Embase*, *Cochrane*, *Web of Science*, Scielo via *Web of Science*, *Scopus*, Lilacs via BVS. Pesquisa adicional foi realizada em: *Opengrey* e *Google Scholar*. Para garantir a saturação da literatura, foram feitas buscas manuais nas listas de referência dos estudos incluídos a fim de resgatar publicações adicionais não identificadas nas buscas eletrônicas realizadas.

2.3.3 Estratégia de busca

A estratégia de busca construída para o *Medline* via *Pubmed* está apresentada na Tabela 4. Após a finalização da estratégia utilizada no *Medline*, houve adaptação da estratégia para as demais bases de dados.

Tabela 1 – Estratégias de busca.

	Estratégia de busca
	Medline* via *Pubmed
#1	"Tomography, Optical Coherence"[Mesh]
#2	"Coherence Tomography, Optical" OR "OCT Tomography" OR "Tomography, OCT" OR "Optical Coherence Tomography"
#3 (#1 OR #2)	("Tomography, Optical Coherence"[Mesh]) OR ("Coherence Tomography, Optical" OR "OCT Tomography" OR "Tomography, OCT" OR "Optical Coherence Tomography")
#4	"Composite Resins"[Mesh]
#5	"Composite Resin" OR "Resin, Composite" OR "Resins, Composite"
#6 (#4 OR #5)	("Composite Resins"[Mesh]) OR ("Composite Resin" OR "Resin, Composite" OR "Resins, Composite")
#7	"Dental Marginal Adaptation"[Mesh]
#8	"Marginal integrity"
#9	"Interfacial integrity"
#10	"Cracks"
#11	"Dental Restoration Failure"
#12 (#6 OR #7 OR #8 OR #9 OR #10 OR #11)	((((((("Composite Resins"[Mesh]) OR ("Composite Resin" OR "Resin, Composite" OR "Resins, Composite")) OR ("Dental Marginal Adaptation"[Mesh])) OR ("Marginal integrity")) OR ("Interfacial integrity")) OR ("Cracks")) OR ("Dental Restoration Failure")
#13 (#3 AND #12)	(("Tomography, Optical Coherence"[Mesh]) OR ("Coherence Tomography, Optical" OR "OCT Tomography" OR "Tomography, OCT" OR "Optical Coherence Tomography")) AND (((((("Composite Resins"[Mesh]) OR ("Composite Resin" OR "Resin, Composite" OR "Resins, Composite")) OR ("Dental Marginal Adaptation"[Mesh])) OR ("Marginal integrity")) OR ("Interfacial integrity")) OR ("Cracks")) OR ("Dental Restoration Failure"))
	Embase
População	'resin'/exp OR 'resin' OR 'dental marginal adaptation'/exp OR 'dental marginal adaptation' OR 'dental restoration'/exp OR 'dental restoration'
Teste índice	'optical coherence tomography'

	('resin'/exp OR 'resin' OR 'dental marginal adaptation'/exp OR 'dental marginal adaptation' OR 'dental restoration'/exp OR 'dental restoration') AND 'optical coherence tomography'
	Cochrane
População	"Composite Resins" OR "Composite Resin" OR "Resin, Composite" OR "Resins, Composite" OR "Dental Marginal Adaptation" OR "Marginal integrity" OR "Interfacial integrity" OR Cracks OR "Dental Restoration Failure"
Teste índice	"Tomography, Optical Coherence" OR "Coherence Tomography, Optical" OR "OCT Tomography" OR "Tomography, OCT" OR "Optical Coherence Tomography"
	"Tomography, Optical Coherence" OR "Coherence Tomography, Optical" OR "OCT Tomography" OR "Tomography, OCT" OR "Optical Coherence Tomography" in All Text AND "Composite Resins" OR "Composite Resin" OR "Resin, Composite" OR "Resins, Composite" OR "Dental Marginal Adaptation" OR "Marginal integrity" OR "Interfacial integrity" OR Cracks OR "Dental Restoration Failure" in All Text - (Word variations have been searched)
	Web of Science
População	ALL=("Composite Resins" OR "Composite Resin" OR "Resin, Composite" OR "Resins, Composite" OR "Dental Marginal Adaptation" OR "Marginal integrity" OR "Interfacial integrity" OR Cracks OR "Dental Restoration Failure")
Teste índice	ALL=("Tomography, Optical Coherence" OR "Coherence Tomography, Optical" OR "OCT Tomography" OR "Tomography, OCT" OR "Optical Coherence Tomography")
	(ALL=("Composite Resins" OR "Composite Resin" OR "Resin, Composite" OR "Resins, Composite" OR "Dental Marginal Adaptation" OR "Marginal integrity" OR "Interfacial integrity" OR Cracks OR "Dental Restoration Failure")) AND ALL=("Tomography, Optical Coherence" OR "Coherence Tomography, Optical" OR "OCT Tomography" OR "Tomography, OCT" OR "Optical Coherence Tomography")
	Scielo via *Web of Science*
População	TS=("Composite Resins" OR "Composite Resin" OR "Resin, Composite" OR "Resins, Composite" OR "Dental Marginal Adaptation" OR "Marginal integrity" OR "Interfacial integrity" OR Cracks OR "Dental Restoration Failure")

Teste índice	TS=(“Tomography, Optical Coherence" OR "Coherence Tomography, Optical" OR "OCT Tomography" OR "Tomography, OCT" OR "Optical Coherence Tomography”)
	(TS=("Composite Resins" OR "Composite Resin" OR "Resin, Composite" OR "Resins, Composite" OR "Dental Marginal Adaptation" OR "Marginal integrity" OR "Interfacial integrity" OR Cracks OR "Dental Restoration Failure")) AND TS=(“Tomography, Optical Coherence" OR "Coherence Tomography, Optical" OR "OCT Tomography" OR "Tomography, OCT" OR "Optical Coherence Tomography”)
	Scopus
TITLE-ABS-KEY	("Composite Resins" OR "Composite Resin" OR "Resin, Composite" OR "Resins, Composite" OR "Dental Marginal Adaptation" OR "Marginal integrity" OR "Interfacial integrity" OR cracks OR "Dental Restoration” Failure") AND ("Tomography, Optical Coherence" OR "Coherence Tomography, Optical" OR "OCT Tomography" OR "Tomography, OCT" OR "Optical Coherence Tomography")
	BVS/LILACS (Inglês)
População	"Composite Resins" OR "Composite Resin" OR "Resin, Composite" OR "Resins, Composite" OR "Dental Marginal Adaptation" OR "Marginal integrity" OR "Interfacial integrity" OR Cracks OR "Dental Restoration Failure"
Teste índice	"Tomography, Optical Coherence" OR "Coherence Tomography, Optical" OR "OCT Tomography" OR "Tomography, OCT" OR "Optical Coherence Tomography"
	("Composite Resins" OR "Composite Resin" OR "Resin, Composite" OR "Resins, Composite" OR "Dental Marginal Adaptation" OR "Marginal integrity" OR "Interfacial integrity" OR Cracks OR "Dental Restoration Failure") AND ("Tomography, Optical Coherence" OR "Coherence Tomography, Optical" OR "OCT Tomography" OR "Tomography, OCT" OR "Optical Coherence Tomography")
	BVS/LILACS (Português)
População	“Resinas Compostas” OR Compósitos OR “Resina Composta” OR “Adaptação Marginal Dentária” OR “Falha de Restauração Dentária”
Teste índice	“Tomografia de Coerência Óptica”
	(“Resinas Compostas” OR Compósitos OR “Resina Composta” OR “Adaptação Marginal Dentária” OR “Falha de Restauração Dentária”) AND (“Tomografia de Coerência Óptica”)

	BVS/LILACS (Espanhol)
População	“Resinas Compuestas” OR Composite OR “Resina Compuesta” OR “Adaptación Marginal Dental” OR “Fracaso de la Restauración Dental”
Teste índice	“Tomografía de Coherencia Óptica”
	(“Resinas Compuestas” OR Composite OR “Resina Compuesta” OR “Adaptación Marginal Dental” OR “Fracaso de la Restauración Dental”) AND (“Tomografía de Coherencia Óptica”)
	Google Scholar
	("Resin" OR "Dental Marginal Adaptation" OR "Dental Restoration Failure") AND "Optical Coherence Tomography"
	Open Grey
	("Composite Resin" OR "Dental Marginal Adaptation") AND "Optical Coherence Tomography"

Fonte: a autora (2022)

2.3.4 Seleção dos estudos

<u>*Gerenciamento de referências*</u> – Os estudos identificados pelas estratégias de busca foram importados para o *EndNote* (*Clarivate Analytics*, Filadélfia, EUA) para gerenciamento de referências. Artigos duplicados foram removidos.

<u>*Processo de seleção dos estudos*</u> – O processo de seleção foi realizado com auxílio do *Software Rayyan©*. Dois revisores (C.M.B.C e S.R.M.V) selecionaram e avaliaram independentemente os resultados de todas as buscas para inclusão, em duas etapas: 1) leitura dos títulos e resumos; 2) leitura dos artigos na íntegra. Em cada uma dessas etapas de seleção, houve uma reunião de consenso e, caso houvesse divergências, um terceiro revisor (G.Q.M) seria consultado. Os motivos de exclusão dos estudos avaliados na íntegra foram registrados.

2.3.5 Extração de dados

A extração dos dados foi feita por dois revisores, de forma independente, em formulário específico para este estudo. As discordâncias entre os dois revisores foram resolvidas por consenso. Em caso de não se estabelecer consenso, um terceiro revisor faria a avaliação para uma decisão final.

Os seguintes dados foram registrados para cada artigo: informações gerais (autor, título, periódico, ano, país, DOI), informações do desenho do estudo (tipo de estudo, detalhes do projeto, teste padrão de referência), características da amostra (tipo de dente, número de restaurações avaliadas, classificação do preparo cavitário, tipo de adesivo e resina composta), características do equipamento de OCT (tipo de OCT, resolução axial, resolução transversal, comprimento de onda, profundidade de penetração, tipo de imagem adquirida, velocidade de aquisição da imagem, software de aquisição de imagem, pós-processamento de imagem), resultados do estudo (tipo de avaliação realizada com dados de OCT, critérios de mensuração, variáveis de comparação diagnóstica).

Os resultados foram extraídos em todas as formas de dados (contínuo, dicotômico ou ordinal) conforme relatado nos estudos incluídos. Foram coletados dados de correlação, porcentagem, média e desvio padrão. Para as variáveis dicotômicas foi considerado número de dentes/restaurações submetidos aos testes índice e de referência, número de verdadeiros positivos, verdadeiros negativos, falsos positivos e falsos negativos. Para as variáveis ordinais, foram considerados os valores dos escores.

2.3.6 Avaliação de risco de viés

O risco de viés dos estudos foi avaliado usando a ferramenta *Cochrane Collaboration* – QUADAS-2 (*Quality Assessment of Diagnostic Accuracy Studies 2*) baseando-se nos quatro domínios: seleção de participantes, teste índice, padrão de referência e fluxo e tempo (WHITING *et al*., 2011).

2.3.7 Síntese de dados

Se os estudos apresentassem homogeneidade em termos de desenho e comparação de dados quantitativos, a síntese seria realizada.

2.3.8 Qualidade da evidência

A qualidade da evidência para todos os resultados foi julgada usando a metodologia do grupo de trabalho *Grading of Recommendations Assessment, Development and Evaluation* e usando a ferramenta online GRADEPro (www.guidelinedevelopment.org). A qualidade da evidência foi avaliada em todos os domínios de risco de viés, consistência, objetividade e precisão (ZHANG *et al*., 2019).

3 RESULTADOS E DISCUSSÃO

Os resultados e discussão destes estudos serão apresentados a seguir por meio de 3 artigos científicos. O estudo 1 está descrito no artigo "*Activity of poly(methacrylic acid)-silver nanoparticles on fluconazole resistant Candida albicans strains: synergistic and cytotoxic effects*", publicado no periódico *Journal of Applied Microbiology* (Fator de impacto: 3.772, Qualis: A2), DOI: 10.1111/jam.15542 (Apêndice A). Nesta pesquisa, fui responsável pelo desenho de estudo, execução de todos os experimentos microbiológicos, análise de resultados e construção do artigo.

O artigo intitulado "*Effects of femtosecond laser irradiation on the microshear bond strength of sound and demineralized dentin*", referente ao estudo 2, foi publicado no periódico *Journal of Laser Applications* (Fator de impacto: 1.636, Qualis: B2), DOI: 10.2351/1.5053222 – Apêndide B. Neste trabalho, fui responsável pela obtenção e avaliação de todas as imagens do tecido dentinário através da Tomografia por Coerência Óptica e do microscópio óptico para avaliação da morfologia do tecido e das características da superfície.

O terceiro estudo resultou no artigo "*Optical Coherence Tomography as diagnostic test for failure analysis of composite resin restorations: systematic review and meta-analysis*". Este estudo será submetido no periódico *Journal of Dentistry* (Fator de impacto: 4.379, Qualis: A1).

4 ARTIGO – OPTICAL COHERENCE TOMOGRAPHY AS DIAGNOSTIC TEST FOR FAILURE ANALYSIS OF RESIN COMPOSITE RESTORATIONS: SYSTEMATIC REVIEW AND META-ANALYSIS

Cecília Maria Cruz Falcão*[a], Sirley Raiane Mamede Veloso[b], Gabriela Queiroz Monteiro[b], Renata de Albuquerque Cavalcanti Almeida[b], Anderson Stevens Leonidas Gomes[a,c].

a Graduate Program in Dentistry, Federal University of Pernambuco, Recife, Brazil.
b University of Pernambuco, Recife, Brazil.
c Department of Physics, Federal University of Pernambuco

*Corresponding author: Cecília Maria Cruz Falcão. ceciliaodonto@gmail.com Professor Moraes Rego Avenue, Department of Prosthesis and Oral Surgery, Federal University of Pernambuco, Recife, PE, Brazil. CEP 50670-901

ABSTRACT

Background This study aimed to perform a systematic review and meta-analysis to investigate the use of OCT as a diagnostic tool to detect restorative failures in resin composite restorations in different populations (human teeth and bovine teeth) when compared to standard reference tests. **Methods** *In vitro* studies that used OCT to diagnose a restorative failure in direct resin composite restorations in human teeth or bovine teeth when compared to standard reference tests were included. Studies that evaluated restorative failure exclusively with OCT, without direct comparison with another evaluation technique were excluded. Information sources: Medline/Pubmed, Embase, Cochrane, Web of Science, Scielo, Scopus, Lilacs/BVS were searched. Quality Assessment of Diagnostic Accuracy Studies 2 (QUADAS-2) was applied for risk of bias. A random-effects model was used and meta-analysis was conducted. **Results** The search identified 1048 results. The initial screening of titles and abstracts resulted in 91 studies. Twelve studies were included and one additional relevant study was found by checking citations of the selected papers. Thirteen studies were included in the systematic review and six studies were included in the meta-analysis. The estimated average correlation coefficient was 0.9717 (95% CI 0.9624 to 0.9811). There was no significant amount of heterogeneity. **Conclusion** The clinical applicability of

the findings of this review is not yet well established because datasets of *in vitro* studies are not representative of a general dental setting. OCT showed a high correlation of suggestive images of gaps compared to other imaging methods. OCT seems to be a potential tool to diagnose the early restorative failure. **Registration** Open Science Framework platform (https://osf.io/z9qgn/).

INTRODUCTION

Failures at the tooth-restoration interface are a factor that compromises the longevity of direct resin composite restorations[1;2]. The presence of postoperative sensitivity, marginal discoloration, and secondary caries leads to restoration replacement[1], remaining a critical issue in adhesive dentistry. The interfacial degradation results from chemical, mechanical, and morphological changes in the restorative materials and the surrounding dental tissues[3]. Additionally, the presence of internal voids (air bubbles) affects the resin composites' mechanical properties, lowering their fatigue resistance[4].

However, the diagnosis of restorative failure can be pretty challenging. The decision to replace existing restorations and treatment planning are sometimes highly subjective. Confirming that a tooth is healthy using a detection method is essential to avoid the unnecessary interventional treatment[5]. To general dental practitioners, dental radiography is frequently used to assess the margin quality of resin composite restorations. Perfect marginal integrity is difficult to assess using the conventional diagnostic method. Radiographs do not present sufficient sensitivity to detect early lesions, particularly caries adjacent to restoration, because of the overlap of adjacent structures[6].

Given the limitations of dental radiography, other imaging methods have been sought in clinical and *in vitro* research to fill this lack, such as micro-computed tomography (micro-CT)[4,7], confocal laser scanning microscopy (CLSM)[3,6,8], scan electron microscopy (SEM)[9]. In this context, optical coherence tomography (OCT) has emerged as a potential tool to evaluate the sealing performances nondestructively. OCT is a high-resolution, cross-sectional imaging technique that permits non-invasive imaging of the underlying defects in a biological system[10]. Unlike any radiographic imaging technique, it is a non-ionizing tool, which makes it safe for the pediatric and pregnant patients[11].

OCT was previously used to detect gap defects at the tooth–restoration interfaces[12,13] and voids or air bubbles of different sizes within the composite restoration[4]. OCT has shown a remarkable ability to detect and quantifying micro gaps under the restorations non-invasively. Better understanding and a direct comparison with other methods of the mode of action of OCT are required to develop into a commercially viable device that can easily be deployed and interpreted by the clinician[5].

This study aimed to perform a systematic review of the literature and quantitative meta-analysis to investigate the use of OCT as a diagnostic tool for detecting a restorative failure in resin composite restorations in different populations (human teeth and bovine teeth) when compared to standard reference tests.

METHODS

The protocol was written following the guideline of Preferred Reporting Items for Systematic reviews and Meta-Analyses for Protocols 2015 (PRISMA-P 2015)[14,15] and was registered in the Open Science Framework platform (https://osf.io/z9qgn/).

Eligibility criteria

Study design – Studies such as laboratory tests (*in vitro* studies) that use OCT to diagnose a restorative failure in resin composite restorations were included.

Participants – Direct resin composite restorations in human permanent teeth or bovine teeth.

Index test – OCT is used for the detection or diagnosis of dental restoration failure. Exclusion criteria: studies that evaluated restorative failure exclusively with OCT, without direct comparison with another evaluation technique.

Reference standards – Reference standard tests were considered: conventional and digital radiographs, micro-computed tomography, scanning electron microscopy, confocal laser scanning microscopy, optical microscopy (histological section), dye infiltration, stereomicroscope.

Target conditions – Restorative failure: failure in marginal integrity, adhesive failures, microleakage, cracks or bubbles at the resin-dental tissue interface in resin composite restorations.

Information sources

Systematic searches were carried out in a single day (July 02, 2022), in the following databases without language or publication status restrictions: Medline/Pubmed, Embase, Cochrane, Web of Science, Scielo/Web of Science, Scopus, Lilacs/BVS. An additional search was performed on: Opengrey and Google Scholar. Manual searches were made in reference lists of included studies to identify additional publications not identified in electronic searches ensuring literature saturation[16,17].

Search strategy

A Medline/Pubmed search strategy is presented in Appendix A. After the Medline/Pubmed strategy was finalized, it was adapted to the syntax and subject headings of the other databases.

Study records

Data management – Studies identified by search strategies were imported to EndNote (Clarivate Analytics, Philadelphia, USA) for reference management. Duplicate articles were removed.

Selection process – The selection process was carried out using the Rayyan© Software. Two review authors independently screened and assessed the results of all searches for inclusion in two stages: 1) reading of titles and abstracts; 2) reading entire articles. Consensus meetings were done in both stages, and if there were any disagreements, a third reviewer was consulted. The reasons for the exclusion of studies evaluated in full text were recorded.

Data items

Two reviewers performed data extraction, independently and in duplicate. Disagreements between the two reviewers were resolved by consensus. If there were no consensus, a third reviewer would assess a final decision[17].

For each study, the following data were recorded: setting (author, title, journal, year, country), study information (type of study, design details, reference standard), sample characteristics (type of tooth, number of evaluated restorations, classification of cavity preparation, type of adhesive and resin composite material), OCT characteristics (OCT type, axial resolution, transverse resolution, wavelength, penetration depth, type of image acquired, image acquisition speed, image acquisition software, post-processing of imaging), study results (type of evaluation performed with OCT data, measurement criteria, diagnostic comparison variables).

Results were extracted in all forms of data (continuous, dichotomous or ordinal) as reported in the included studies. Correlation, percentage, mean and standard deviation data were collected. For dichotomous variables, the number of teeth/restorations submitted to index and reference tests were considered, the number of true positives, true negatives, false positives and false negatives. For ordinal variables, score values were considered.

Risk of bias individual studies

The risk of bias in individual studies was assessed using the Cochrane Collaboration tool – QUADAS-2 (Quality Assessment of Diagnostic Accuracy Studies 2). The applicability of primary diagnostic studies was evaluated in four domains: participant selection, index test, reference standard and flow and time[17].

Data synthesis

Studies were sufficiently homogeneous in terms of design and quantitative data synthesis using a random-effects model was performed. The meta-analysis was conducted using Jamovi 2.2.5 Software. A funnel plot based on standard errors was used as a visual tool to investigate publication bias.

Confidence in the cumulative estimate

The quality of evidence for all outcomes was judged using the Grading of Recommendations Assessment, Development and Evaluation working group methodology and the GRADEPro online tool (www.guidelinedevelopment.org). The quality of evidence was assessed across the domains of risk of bias, consistency, directness and precision. These have been considered narratively when statistical methods were not available[18].

RESULTS

Study selection

The search identified 1,048 results and 512 remained after duplicated removal, as shown in flow diagram[19] (Figure 1). The initial screening of titles and abstracts resulted in 91 studies being considered for inclusion. We retrieved full papers for these studies, and after further review of the full text, we included 12 studies. Reports were excluded for the following reasons: not comparison studies (a lack of reference standard) (n = 38); OCT was used only as representative and/or qualitative images (n = 33); conference report abstracts (n = 4); *in vivo* study (n = 1) and data in another article (n = 3). One additional relevant study was found by checking references and citations of the selected papers. Therefore, 13 studies were included in the systematic review. Only six studies were included in meta- analysis.

Study characteristics

The included studies were published between 2011 and 2021 (Table 1). Six studies used bovine incisors teeth[3,4,7,8,12,20], while the other seven used human permanent teeth (anterior[9], premolar[11,21], and molars[6,22-24]). Regardless of the area evaluated, all studies opted for a cavity preparation with a maximum depth of 2 mm.

Five studies evaluated enamel margins on the cavity surface (enamel/resin composite interface) and cavity floor (dentin/resin composite interface), with four in bovine teeth[4,8,12,20] and one in human teeth[23]. Two studies observed only the enamel/resin composite interface (human teeth)[6,9] while five studies observed only dentin/resin composite interface[3,7,11,22,24]. In addition to evaluating enamel/resin composite and dentin/resin composite interface, one study also investigated the cement/resin composite interface (human teeth)[21]. The total sample size was 393 (ranging from 1[4] to 80[21]).

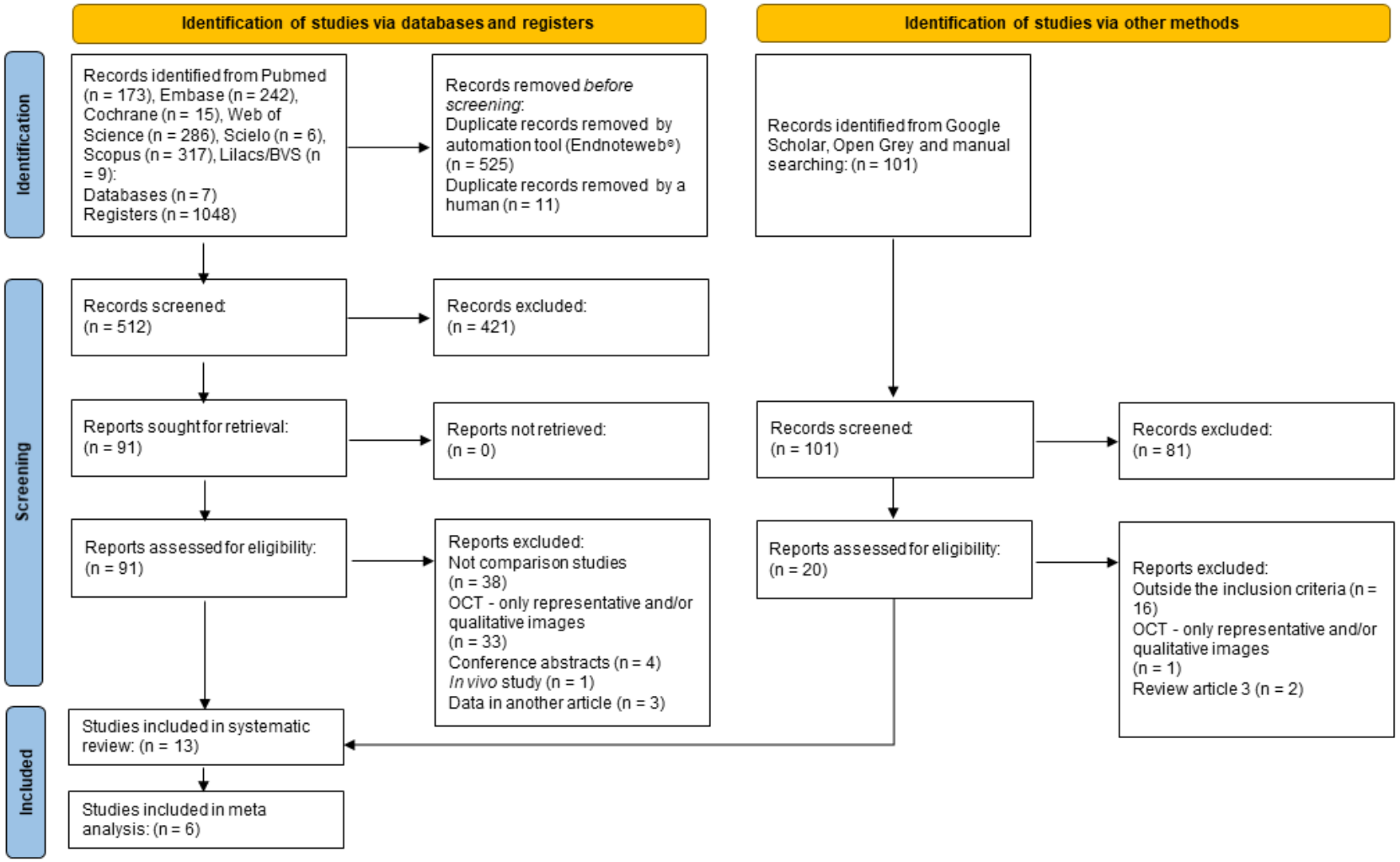

Figure 1. PRISMA flowchart summarizing the search.

Table 1. Characteristics of the studies included in the systematic review.

Study	Teeth	(n)	Interface evaluated	OCT	Reference Standard	Diagnostic variable
Alshahni, 2019[8]	Bovine	36	Enamel/composite and dentin/composite	SS-OCT (1,260 to 1,360 nm)	CLSM	Gap lenght
Bakhsh, 2011[11]	Human	21	Dentin/composite	SS-OCT (1,260 to 1,360 nm)	CLSM	Gap lenght
Bista, 2013[12]	Bovine	9	Enamel/composite and dentin/composite	SS-OCT (1,260 to 1,360 nm)	CLSM	% Sealed interface
Han, 2016[7]	Bovine	24	Dentin/composite	SS-OCT (1,260 to 1,360 nm)	Micro-CT	% Defective spots
Horie, 2016[6]	Human	60	Enamel/composite	SS-OCT (1,330 ± 100 nm)	CLSM	% Gap lenght
Makishi, 2011[20]	Bovine	24	Enamel/composite and dentin/composite	SS-OCT (1,319 ± 100 nm)	CLSM	Detection of gap
Matsuura, 2018[22]	Human	40	Dentin/composite	SS-OCT (1,240 to 1,380 nm)	Digital radiograph	Detection of carie
Nazari, 2013[4]	Bovine	1	Enamel/composite and dentin/composite	SS-OCT (1,310 ± 100 nm)	Micro-CT	Gap volume (mm^3)
Sadr, 2011[24]	Human	10	Dentin/composite	SS-OCT (1,260 to 1,360 nm)	CLSM	% Gap lenght
Schneider, 2019[9]	Human	8	Enamel/composite interface	SD-OCT (1,310 ±107 nm)	SEM	Detection of gap
Senawongse, 2011[21]	Human	80	Enamel/composite and dentin/composite	SS-OCT (1,315 to 1,340 nm)	Dye Leakage	Gap (mm)
Zhou, 2016[23]	Human	40	Enamel/composite and dentin/composite	SS-OCT (1,260 to 1,360 nm)	CLSM	Gap length
Zhou, 2021[3]	Bovine	40	Dentin/composite	SS-OCT (1,260 to 1,360 nm)	CLSM	Gap scale

Most studies used the swept-source OCT (SS-OCT), except for one study that used the spectral domain (SD-OCT) system[9]. All OCT systems operated at 1240 – 1380 nm, centered at approximately 1310nm.

Most studies used CLSM as the reference standard (n = 8). Micro-CT (n = 2), SEM (n = 1), digital radiography (n = 1) and conventional dye leakage (n = 1) were also used. Despite the method of comparison, the measurements of the gaps were either linear (mm), area (mm^2), or volume (mm^3).

Results of individual studies

All studies pointed to OCT as a tool to identify restorative failure by detecting gaps, voids, or bubbles. There was no difference between the internal adaptations measured by SS-OCT and those measured by CLSM, micro-CT, and SEM. However, the statistical analysis revealed a significant difference between the gap measured by SS-OCT and dye leakage ($p < 0.01$). The observation with SS-OCT demonstrated greater gap formation than the observation with dye leakage[21]. SS-OCT demonstrated significantly higher sensitivity, specificity and agreement when compared with digital dental radiography.

Except for Nazari (2013), who evaluated air bubbles inside composite[4], all studies related white clusters and bright zones on OCT images. These images were attributed to the increased intensity of backscattered light in the B-scan images, corresponding to the enamel/resin composite and dentin/resin composite interfacial gaps. There is a significant correlation between the length of the cluster with brighter pixels along the cavity floor from the SS-OCT and the actual length of the gap at the corresponding location measured under CLSM, SEM or Micro-CT[11]. Even when using contrast agent (silver nitrate) regions with gap showed increased brightness on the SS-OCT images[20]. No increase in signal intensity at most of the cavity interface, demonstrated a good seal at the bonded tooth–restoration interface[12].

Dentin beneath the restorations appeared dark and was discriminated from the restoration even at a 2 mm thickness. Dentin with caries appeared as a bright zone beneath the restorations and was clearly distinguished from intact dentin. However, SS-OCT values for detecting caries beneath resin composite restorations were lower for the 2-mm thick resin composite than for the 1-mm thick. This decrease in sensitivity for the 2-mm thick restoration can be explained by attenuation of the signal through the restoration[22].

Methodological quality of included studies

The included studies were ranked based on standardized criteria for diagnostic research using the QUADAS-2[25] tool for quality assessment of diagnostic accuracy studies. (Table 2 and Figure 2).

Table 2. Quality assessment of the included studies.

Study	RISK OF BIAS				APPLICABILITY CONCERNS		
	PATIENT SELECTION	INDEX TEST	REFERENCE STANDARD	FLOW AND TIMING	PATIENT SELECTION	INDEX TEST	REFERENCE STANDARD
Alshahni, 2019	?	☺	?	☺	?	☺	☺
Bakhsh, 2011	?	?	?	?	?	☺	☺
Bista, 2013	?	?	?	?	?	☺	☺
Han, 2016	?	?	?	☺	?	☺	☺
Horie, 2016	☺	?	?	?	☺	☺	☺
Makishi, 2011	?	?	?	?	?	☺	☺
Matsuura, 2018	?	☺	☺	?	?	☺	☺
Nazari, 2013	?	?	?	?	?	☺	☺
Sadr, 2011	?	?	?	?	?	☺	☺
Schneider, 2019	?	☺	☺	?	☹	☺	☺
Senawongse, 2011	?	?	?	?	?	☺	☺
Zhou, 2016	?	?	?	?	?	☺	☺
Zhou, 2021	?	?	?	?	☺	☺	☺

☺: low risk; ☹: high risk; ?: unclear risk.

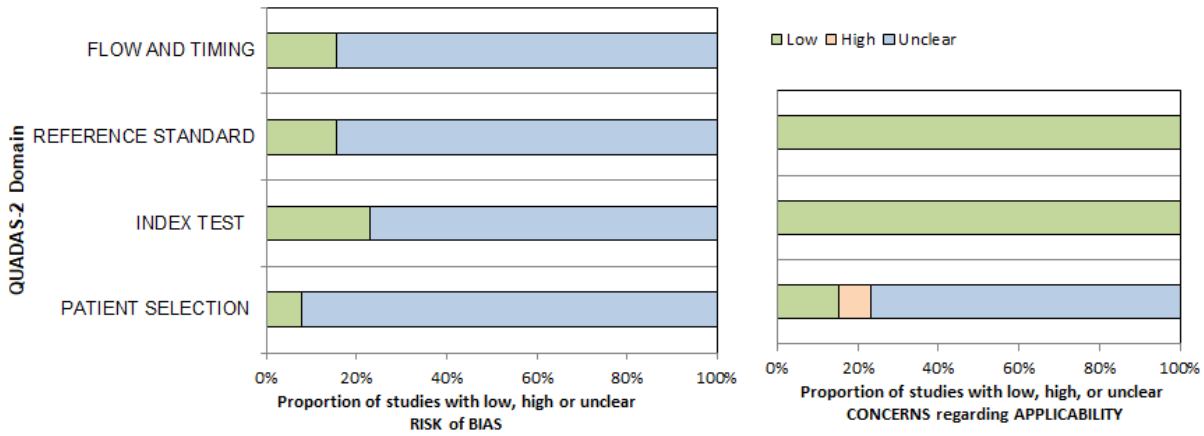

Figure 2. Quality assessment of the included studies.

No study was designated as high or low risk of bias. The unclear risk of bias in each of the four domains (patient selection, index test, reference standard, and flow

and timing) was 92%, 77%, 85%, and 85%, respectively. In contrast, the percentage designated as low risk were 8%, 23%, 15%, and 15%, respectively. The available studies' uncertain methodological quality was due the absence of clear information about (1) the randomization process of samples and exclusion criteria, (2) blinded index test and reference standard interpretation, and (3) interval or storage methods between index and reference standard.

Regarding applicability, the index test and reference standard were well conducted in all studies, showing a low risk in this domain. Unlike patient selection, 77% of the studies were classified as "unclear". One study was designated as high risk about patient selection because teeth had been included suspected of restorative failure that would be more straightforward to detect, introducing bias and influencing sensitivity and specificity[5].

Quantitative synthesis – Meta-analysis

From the 13 studies selected for qualitative analysis, only six studies, that used the same test index (CLSM) and presented results such as Pearson's correlation and linear regression, were included in the meta-analysis. The other seven studies were excluded for the following reasons: five studies employed other tests index (SEM[9], Micro-CT[4,7], dye leakage[21] and digital radiograph[22]); one study showed sensitivity/specificity results, which alone do not allow quantitative synthesis[20]; and one another study, provided only Spearman's correlation[3].

The observed Pearson's correlation coefficients ranged from 0.913 to 0.978, with the majority estimates being positive (100%). The estimated average correlation coefficient based on the random-effects model was 0.9717 (95% CI 0.9624 to 0.9811; Figure 3). Therefore, the average outcome differed significantly from zero ($z = 203.3654$, $p < 0.0001$).

According to the Q-test, there was no significant amount of heterogeneity in the true outcomes ($Q(5) = 6.5202$, $p = 0.2588$, $tau^2 = 0.0000$, $I^2 = 4.1049\%$). A 95% prediction interval for the true outcomes is given by 0.9611 to 0.9824. Hence, even though there may be some heterogeneity, the true outcomes of the studies are generally in the same direction as the estimated average outcome. An examination of the studentized residuals revealed that there was no indication of outliers in the context of this model. According to the Cook's distances, none of the studies could be considered to be overly influential.

Egger's regression test indicated funnel plot asymmetry (p = 0.0480), which was consistent with an asymmetrical funnel plot (Figure 4) with missing studies in the lower right.

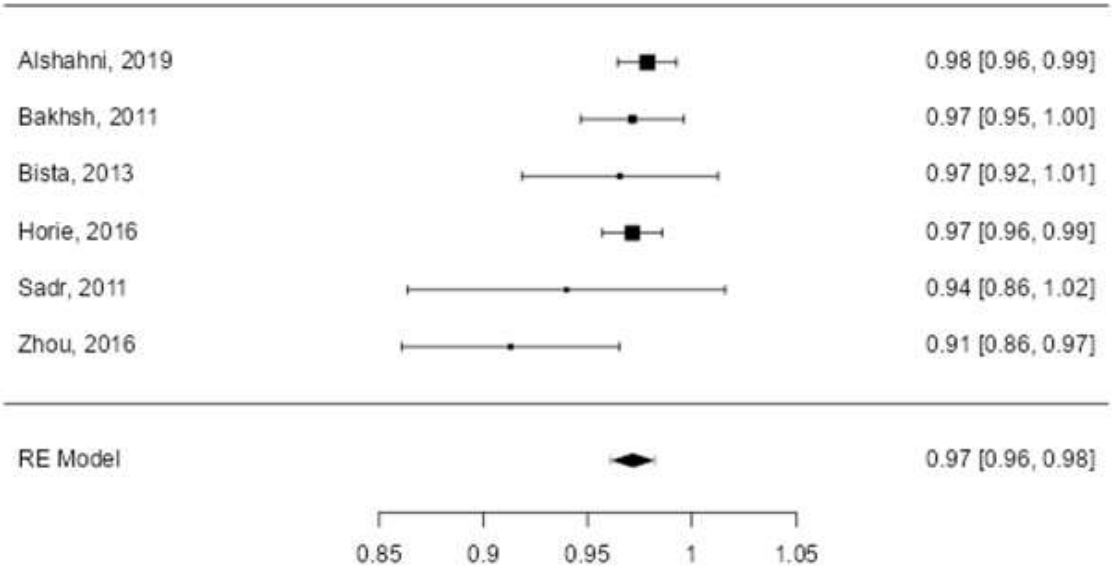

Random-Effects Model (k = 6)

	Estimate	se	Z	p	CI Lower Bound	CI Upper Bound
Intercept	0.972	0.00478	203	< .001	0.962	0.981
	.	.	.	.	.	.

Note. Tau² Estimator: Restricted Maximum-Likelihood

Heterogeneity Statistics

Tau	Tau²	I²	H²	R²	df	Q	p
0.003	0 (SE= 1e-04)	4.1%	1.043	.	5.000	6.520	0.259

Figure 3. Forest plot of the summary correlation coefficient for the included studies (n = 6).

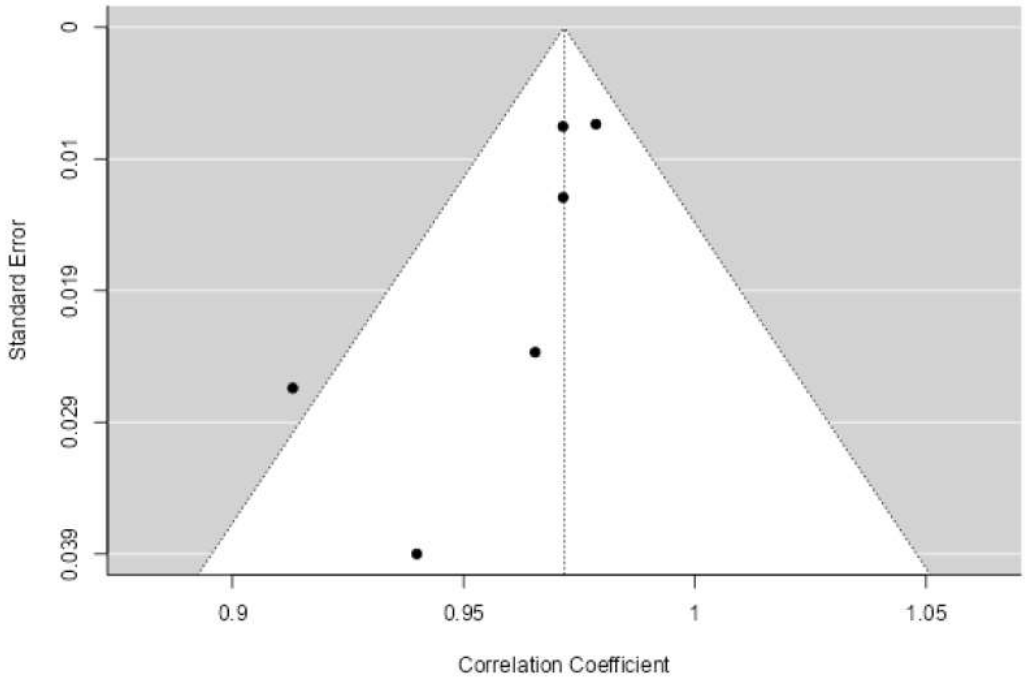

Figure 4. Funnel plot for the summary correlation coefficient analysis (n = 6).

We rated the certainty of the evidence as moderate. We downgraded 1 level in the total due to the indirectness arising from the *in vitro* studies and the imprecision of the estimates.

DISCUSSION

We conducted a systematic review with meta-analysis to investigate the use of OCT as a tool for diagnosing restorative failure. Sufficient studies provided correlation data, enabling a meta-analysis. We showed a high correlation between the images suggestive of gaps obtained with OCT compared to other imaging methods was observed.

Dental radiograph, micro-CT, SEM, and CLSM were the imaging methods found in the selected studies for meta-analysis. Each equipment has its characteristics as a tool for evaluation. Radiographs do not have sufficient sensitivity to detect early restorative failures. Micro-CT has no limitation for evaluating the restoration in terms of cavity depth, unlike OCT has depth limitations. Even though SS-OCT shows very clear images within the penetrating depth of the laser[7]. On the other hand, one of the main advantages of OCT imaging is the capacity to eliminate the radiation dose from visual diagnostic approaches in dentistry[22]. SEM and CLSM can diagnose restorative

failures accurately, although they are available only to *in vitro* assays because they are destructive methods.

SS-OCT and SD-OCT were used in the selected studies to observe interfacial gap, marginal integrity, and air bubbles around the resin composite restorations. The OCT imaging mechanism for distinguishing between different materials is based on their composition, light scattering properties, and refractive indexes[4,11]. Light will be reflected and refracted according optical variation between restorative material, air, and tooth structure. In OCT imaging the signal intensity of investigated structure is affected by adjacent superior structures. A Fresnel phenomenon reflects a fraction of light at an interface between two media with different refractive indexes, which depends on the incidence angle and the contrast of refractive indexes[11]. Dental resin composites are mostly transparent substrates that allow transmission of visible and near-infrared light; therefore, OCT is generally suitable for assessing marginal integrity[6]. Moreover, gaps showed much brighter than lesions on OCT because more water or dentinal fluid existed in interfacial gaps than in demineralized tissues[23].

Gap images were generally clear with high-intensity bright clusters or white spots[7]. A high correlation was found between the lengths of the bright cluster and the length of the gap. A different finding was noticed when OCT detected voids or air bubbles, as voids filled with air, reflect back most of the light from their boundaries. Such strong backscattering from within the resin composite occasionally prevents effective signal acquisition from the deeper region of the structure. The light attenuation due to multiple reflections at the defect boundaries results in a dark area with low signal intensity underneath the defect[12]. However, it was not expected that the OCT with an axial resolution of 11 µm would accurately measure gaps only a few micrometers in height[11]. The light is scattered and attenuated with depth[7]. The interfacial defect in a cavity is a 3D phenomenon and would be best described by 3D analysis[11].

Few studies (n = 2) reported data regarding sensibility and specificity[20,22]. These data are essential for systematic reviews of diagnostic studies and the search for evidence of test index accuracy. Meanwhile, most studies that employed CLSM as index test (n = 6) provided Pearson's correlation and linear regression data sufficient for quantitative synthesis.

There was no significant amount of heterogeneity despite variability across the study protocols and methodologies assumed. The included studies were diverse in their sample population (bovine and human teeth) and area evaluated.

The frequent score of "unclear" is because studies did not offer enough details about the randomization process of samples and exclusion criteria. QUADAS-2 emphasizes the importance of adequate sample randomization and explicitness in exclusion criteria. Sample straightforward to diagnose should not participate, as it may overestimate the accuracy of the test. The blinding of index test and reference standard interpretation was not clearly reported, leaving the risk of bias uncertain. In general, the studies did not report the interval or storage methods between the index and reference standard. Theoretically, in these *in vitro* assays, the diagnostic time between the two tests does not affect the restorative failure. However, inappropriate storage methods adds a risk of sample alteration.

The available studies' uncertain methodological quality was due to the absence of clear information about (1) the randomization process of samples and exclusion criteria; (2) blinded index test and reference standard interpretation; and (3) interval or storage methods between the index and reference standard. We could not categorize any study as low or high risk of bias or concerns for applicability across all domains.

Publication bias was evident in the correlation analysis, as shown by an asymmetrical funnel plot. However, considering the extensive literature search described in the methodology, this result should be analyzed with caution. Tests that currently use standard errors to assess publication bias for diagnostic accuracy studies may lead to uncertainty and misleading results[26].

The strengths of this review is the rigorous application of evidence synthesis methodology through transparent and reproducible methods.

The clinical applicability of the findings of this review is not yet well established because datasets of *in vitro* studies are not representative of a general dental setting. Furthermore, there is a question of whether the utilization of OCT devices provides sufficient benefit to justify the cost. Studies may be conducted to investigate the use of OCT in a general dental practice setting[5].

CONCLUSION

OCT seems to be a potential tool to diagnoses the early restorative failure, identifying failure in marginal integrity, gaps, voids, and air bubbles. However, it is limited regarding evaluating deep restorations. There was a strong correlation between the images obtained with OCT and other reference imaging methods. Considering the limitations of this review, OCT can become a valuable tool in restorative dentistry.

REFERENCES

1. Heintze SD. 2007. Systematic reviews: I. The correlation between laboratory tests on marginal quality and bond strength. Ii. The correlation between marginal quality and clinical outcome. J Adhes Dent. 9 Suppl 1:77-106.

2. Stewart CA, Finer Y. 2019. Biostable, antidegradative and antimicrobial restorative systems based on host-biomaterials and microbial interactions. Dent Mater. 35(1):36-52.

3. Zhou Y, Matin K, Shimada Y, Wang G, Sadr A, Tagami J. 2021. Detection and analysis of early degradation at resin-dentin interface by optical coherence tomography (oct) and confocal laser scanning microscope (clsm). J Dent. 106:103583.

4. Nazari A, Sadr A, Saghiri MA, Campillo-Funollet M, Hamba H, Shimada Y, Tagami J, Sumi Y. 2013. Non-destructive characterization of voids in six flowable composites using swept-source optical coherence tomography. Dent Mater. 29(3):278-286.

5. Macey R, Walsh T, Riley P, Hogan R, Glenny AM, Worthington HV, Clarkson JE, Ricketts D. 2021. Transillumination and optical coherence tomography for the detection and diagnosis of enamel caries. Cochrane Database Syst Rev. 1:CD013855.

6. Horie K, Shimada Y, Matin K, Ikeda M, Sadr A, Sumi Y, Tagami J. 2016. Monitoring of cariogenic demineralization at the enamel-composite interface using swept-source optical coherence tomography. Dent Mater. 32(9):1103-1112.

7. Han SH, Sadr A, Tagami J, Park SH. 2016. Non-destructive evaluation of an internal adaptation of resin composite restoration with swept-source optical coherence tomography and micro-ct. Dent Mater. 32(1):e1-7.

8. Alshahni RZ, Shimada Y, Zhou Y, Yoshiyama M, Sadr A, Sumi Y, Tagami J. 2019. Cavity adaptation of composite restorations prepared at crown and root: Optical assessment using ss-oct. Dent Mater J. 38(5):779-789.

9. Schneider H, Steigerwald-Otremba AS, Häfer M, Krause F, Scholz M, Haak R. 2019. Is optical coherence tomography a potential tool to evaluate marginal adaptation of class iii/iv composite restorations. Oper Dent. 44(3):242-253.

10. Huang D, Swanson EA, Lin CP, Schuman JS, Stinson WG, Chang W, Hee MR, Flotte T, Gregory K, Puliafito CA. 1991. Optical coherence tomography. Science. 254(5035):1178-1181.

11. Bakhsh TA, Sadr A, Shimada Y, Tagami J, Sumi Y. 2011. Non-invasive quantification of resin-dentin interfacial gaps using optical coherence tomography: Validation against confocal microscopy. Dent Mater. 27(9):915-925.
12. Bista B, Sadr A, Nazari A, Shimada Y, Sumi Y, Tagami J. 2013. Nondestructive assessment of current one-step self-etch dental adhesives using optical coherence tomography. J Biomed Opt. 18(7):76020.
13. Monteiro GQ, Montes MA, Gomes AS, Mota CC, Campello SL, Freitas AZ. 2011. Marginal analysis of resin composite restorative systems using optical coherence tomography. Dent Mater. 27(12):e213-223.
14. Moher D, Shamseer L, Clarke M, Ghersi D, Liberati A, Petticrew M, Shekelle P, Stewart LA, Group P-P. 2015. Preferred reporting items for systematic review and meta-analysis protocols (prisma-p) 2015 statement. Syst Rev. 4:1.
15. Shamseer L, Moher D, Clarke M, Ghersi D, Liberati A, Petticrew M, Shekelle P, Stewart LA, Group P-P. 2015. Preferred reporting items for systematic review and meta-analysis protocols (prisma-p) 2015: Elaboration and explanation. BMJ. 350:g7647.
16. De Vet H, Eisinga A, Riphagen I, Aertgeerts B, Pewsner D. 2008. Cochrane handbook for systematic reviews of diagnostic test accuracy version 0.4. Elsevier.
17. McGrath TA, Alabousi M, Skidmore B, Korevaar DA, Bossuyt PMM, Moher D, Thombs B, McInnes MDF. 2017. Recommendations for reporting of systematic reviews and meta-analyses of diagnostic test accuracy: A systematic review. Syst Rev. 6(1):194.
18. Zhang Y, Coello PA, Guyatt GH, Yepes-Nuñez JJ, Akl EA, Hazlewood G, Pardo-Hernandez H, Etxeandia-Ikobaltzeta I, Qaseem A, Williams Jr JW. 2019. Grade guidelines: 20. Assessing the certainty of evidence in the importance of outcomes or values and preferences—inconsistency, imprecision, and other domains. Journal of Clinical Epidemiology. 111:83-93.
19. Page MJ, McKenzie JE, Bossuyt PM, Boutron I, Hoffmann TC, Mulrow CD, Shamseer L, Tetzlaff JM, Akl EA, Brennan SE et al. 2021. The prisma 2020 statement: An updated guideline for reporting systematic reviews. BMJ. 372:n71.
20. Makishi P, Shimada Y, Sadr A, Tagami J, Sumi Y. 2011. Non-destructive 3d imaging of composite restorations using optical coherence tomography: Marginal adaptation of self-etch adhesives. J Dent. 39(4):316-325.

21. Senawongse P, Pongprueksa P, Harnirattisai C, Sumi Y, Otsuki M, Shimada Y, Tagami J. 2011. Non-destructive assessment of cavity wall adaptation of class v composite restoration using swept-source optical coherence tomography. Dent Mater J. 30(4):517-522.

22. Matsuura C, Shimada Y, Sadr A, Sumi Y, Tagami J. 2018. Three-dimensional diagnosis of dentin caries beneath composite restorations using swept-source optical coherence tomography. Dent Mater J. 37(4):642-649.

23. Zhou Y, Shimada Y, Matin K, Sadr A, Sumi Y, Tagami J. 2016. Assessment of bacterial demineralization around composite restorations using swept-source optical coherence tomography (ss-oct). Dent Mater. 32(9):1177-1188.

24. Swept source optical coherence tomography for quantitative and qualitative assessment of dental composite restorations. Lasers in Dentistry XVII; 2011: SPIE.

25. Whiting PF, Rutjes AW, Westwood ME, Mallett S, Deeks JJ, Reitsma JB, Leeflang MM, Sterne JA, Bossuyt PM, Group Q-. 2011. Quadas-2: A revised tool for the quality assessment of diagnostic accuracy studies. Ann Intern Med. 155(8):529-536.

26. Deeks JJ, Macaskill P, Irwig L. 2005. The performance of tests of publication bias and other sample size effects in systematic reviews of diagnostic test accuracy was assessed. J Clin Epidemiol. 58(9):882-893.

APPENDIX A – Search strategy

	Query
	Pubmed via Medline
#1	"Tomography, Optical Coherence"[Mesh]
#2	"Coherence Tomography, Optical" OR "OCT Tomography" OR "Tomography, OCT" OR "Optical Coherence Tomography"
#3 (#1 OR #2)	("Tomography, Optical Coherence"[Mesh]) OR ("Coherence Tomography, Optical" OR "OCT Tomography" OR "Tomography, OCT" OR "Optical Coherence Tomography")
#4	"Composite Resins"[Mesh]
#5	"Composite Resin" OR "Resin, Composite" OR "Resins, Composite"
#6 (#4 OR #5)	("Composite Resins"[Mesh]) OR ("Composite Resin" OR "Resin, Composite" OR "Resins, Composite")
#7	"Dental Marginal Adaptation"[Mesh]
#8	"Marginal integrity"
#9	"Interfacial integrity"
#10	"Cracks"
#11	"Dental Restoration Failure"
#12 (#6 OR #7 OR #8 OR #9 OR #10 OR #11)	((((((("Composite Resins"[Mesh]) OR ("Composite Resin" OR "Resin, Composite" OR "Resins, Composite")) OR ("Dental Marginal Adaptation"[Mesh])) OR ("Marginal integrity")) OR ("Interfacial integrity")) OR ("Cracks")) OR ("Dental Restoration Failure")
#13 (#3 AND #12)	(("Tomography, Optical Coherence"[Mesh]) OR ("Coherence Tomography, Optical" OR "OCT Tomography" OR "Tomography, OCT" OR "Optical Coherence Tomography")) AND (((((("Composite Resins"[Mesh]) OR ("Composite Resin" OR "Resin, Composite" OR "Resins, Composite")) OR ("Dental Marginal Adaptation"[Mesh])) OR ("Marginal integrity")) OR ("Interfacial integrity")) OR ("Cracks")) OR ("Dental Restoration Failure"))
	Embase
Population	'resin'/exp OR 'resin' OR 'dental marginal adaptation'/exp OR 'dental marginal adaptation' OR 'dental restoration'/exp OR 'dental restoration'
Index	'optical coherence tomography'
	('resin'/exp OR 'resin' OR 'dental marginal adaptation'/exp OR 'dental marginal adaptation' OR 'dental restoration'/exp OR 'dental restoration') AND 'optical coherence tomography'
	Cochrane
Population	"Composite Resins" OR "Composite Resin" OR "Resin, Composite" OR "Resins, Composite" OR "Dental Marginal Adaptation" OR "Marginal

	integrity" OR "Interfacial integrity" OR Cracks OR "Dental Restoration Failure"
Index	"Tomography, Optical Coherence" OR "Coherence Tomography, Optical" OR "OCT Tomography" OR "Tomography, OCT" OR "Optical Coherence Tomography"
	"Tomography, Optical Coherence" OR "Coherence Tomography, Optical" OR "OCT Tomography" OR "Tomography, OCT" OR "Optical Coherence Tomography" in All Text AND "Composite Resins" OR "Composite Resin" OR "Resin, Composite" OR "Resins, Composite" OR "Dental Marginal Adaptation" OR "Marginal integrity" OR "Interfacial integrity" OR Cracks OR "Dental Restoration Failure" in All Text - (Word variations have been searched)
	Web of Science
Population	ALL=("Composite Resins" OR "Composite Resin" OR "Resin, Composite" OR "Resins, Composite" OR "Dental Marginal Adaptation" OR "Marginal integrity" OR "Interfacial integrity" OR Cracks OR "Dental Restoration Failure")
Index	ALL=("Tomography, Optical Coherence" OR "Coherence Tomography, Optical" OR "OCT Tomography" OR "Tomography, OCT" OR "Optical Coherence Tomography")
	(ALL=("Composite Resins" OR "Composite Resin" OR "Resin, Composite" OR "Resins, Composite" OR "Dental Marginal Adaptation" OR "Marginal integrity" OR "Interfacial integrity" OR Cracks OR "Dental Restoration Failure")) AND ALL=("Tomography, Optical Coherence" OR "Coherence Tomography, Optical" OR "OCT Tomography" OR "Tomography, OCT" OR "Optical Coherence Tomography")
	Scielo via Web of Science
Population	TS=("Composite Resins" OR "Composite Resin" OR "Resin, Composite" OR "Resins, Composite" OR "Dental Marginal Adaptation" OR "Marginal integrity" OR "Interfacial integrity" OR Cracks OR "Dental Restoration Failure")
Index	TS=(“Tomography, Optical Coherence" OR "Coherence Tomography, Optical" OR "OCT Tomography" OR "Tomography, OCT" OR "Optical Coherence Tomography”)
	(TS=("Composite Resins" OR "Composite Resin" OR "Resin, Composite" OR "Resins, Composite" OR "Dental Marginal Adaptation" OR "Marginal integrity" OR "Interfacial integrity" OR Cracks OR "Dental Restoration Failure")) AND TS=(“Tomography, Optical Coherence" OR "Coherence

	Tomography, Optical" OR "OCT Tomography" OR "Tomography, OCT" OR "Optical Coherence Tomography")
	Scopus
TITLE-ABS-KEY	("Composite Resins" OR "Composite Resin" OR "Resin, Composite" OR "Resins, Composite" OR "Dental Marginal Adaptation" OR "Marginal integrity" OR "Interfacial integrity" OR cracks OR "Dental Restoration Failure") AND TITLE-ABS-KEY ("Tomography, Optical Coherence" OR "Coherence Tomography, Optical" OR "OCT Tomography" OR "Tomography, OCT" OR "Optical Coherence Tomography")
	BVS/LILACS (English)
Population	"Composite Resins" OR "Composite Resin" OR "Resin, Composite" OR "Resins, Composite" OR "Dental Marginal Adaptation" OR "Marginal integrity" OR "Interfacial integrity" OR Cracks OR "Dental Restoration Failure"
Index	"Tomography, Optical Coherence" OR "Coherence Tomography, Optical" OR "OCT Tomography" OR "Tomography, OCT" OR "Optical Coherence Tomography"
	("Composite Resins" OR "Composite Resin" OR "Resin, Composite" OR "Resins, Composite" OR "Dental Marginal Adaptation" OR "Marginal integrity" OR "Interfacial integrity" OR Cracks OR "Dental Restoration Failure") AND ("Tomography, Optical Coherence" OR "Coherence Tomography, Optical" OR "OCT Tomography" OR "Tomography, OCT" OR "Optical Coherence Tomography")
	BVS/LILACS (Portuguese)
Population	“Resinas Compostas” OR Compósitos OR “Resina Composta” OR “Adaptação Marginal Dentária” OR “Falha de Restauração Dentária”
Index	“Tomografia de Coerência Óptica”
	(“Resinas Compostas” OR Compósitos OR “Resina Composta” OR “Adaptação Marginal Dentária” OR “Falha de Restauração Dentária”) AND (“Tomografia de Coerência Óptica”)
	BVS/LILACS (Spanish)
Population	“Resinas Compuestas” OR Composite OR “Resina Compuesta” OR “Adaptación Marginal Dental” OR “Fracaso de la Restauración Dental”
Index	“Tomografía de Coherencia Óptica”
	(“Resinas Compuestas” OR Composite OR “Resina Compuesta” OR “Adaptación Marginal Dental” OR “Fracaso de la Restauración Dental”) AND (“Tomografía de Coherencia Óptica”)

	Google Scholar
	("Resin" OR "Dental Marginal Adaptation" OR "Dental Restoration Failure") AND "Optical Coherence Tomography"
	Open Grey
	("Composite Resin" OR "Dental Marginal Adaptation") AND "Optical Coherence Tomography")

5 CONSIDERAÇÕES FINAIS

Foi possível concluir que:

- Houve sinergismo entre PMAA-AgNPs com fluconazol contra cepas resistentes de *C. albicans* indicando que PMAA-AgNPs podem superar a resistência ao fluconazol. Apesar das PMAA-AgNPs apresentarem citotoxicidade dose-dependente nas células de mamíferos testadas, o efeito inibitório dessas nanopartículas isoladas ou em combinação foi maior em *C. albicans* do que nas células hospedeiras. Essa combinação pode ser usada com cuidado como agente antifúngico em formulações tópicas para combater a candidíase resistente. Ainda são necessários mais estudos *in vivo* para avaliar as propriedades toxicológicas e farmacêuticas das PMAA-AgNPs, visando garantir sua segurança e eficácia na prática clínica.

- OCT possibilitou quantificar a perda de tecido dentinário após irradiação com laser de femtosegundo *Ti:Sapphire*. Constatou-se que o laser fez ablação com sucesso da camada de *smear layer* da dentina, abrindo os túbulos dentinários, aumentando a rugosidade da superfície, melhorando a adesão, e trazendo maior resistência ao microcisalhamento. OCT também possibilitou a avaliação do tipo de falha após os ensaios de microcisalhamento.

- OCT parece ser uma ferramenta em potencial para diagnosticar *in vitro* falhas restauradoras precoces, identificando falhas na integridade marginal, *gaps*, vazios e bolhas de ar, embora haja limitações na avaliação de restaurações profundas. Houve forte correlação entre as imagens obtidas com OCT e outros métodos de imagem de referência. Considerando as limitações, a OCT pode se tornar uma ferramenta valiosa na odontologia restauradora.

REFERÊNCIAS

CARVALHO, M.; SANTANA, G.; ANDRADE, A.; CABRAL, A. et al. Exploiting silver nanoparticles with PMAA against *Aedes aegypti* larvae development: potential larvicidal activity. In: **Colloidal Nanoparticles for Biomedical Applications XIII.** SPIE, v. 10507, p.80-86, 2018.

CLINICAL AND LABORATORY STANDARDS INSTITUTE. Performance standards for antifungal susceptibility testing of yeasts. **CLSI supplement M60. Wayne, PA: CLSI**, 2017.

CLINICAL AND LABORATORY STANDARDS INSTITUTE. Reference Method for Broth Dilution Antifungal Susceptibility Testing of Yeasts. **CLSI standard M27. Wayne, PA: CLSI,** 2017b.

DAS, A.; RAPOSO, G. C. C.; LOPES, D. S.; DA SILVA, E. J. et al. Exploiting Nanomaterials for Optical Coherence Tomography and Photoacoustic Imaging in Nanodentistry. **Nanomaterials (Basel)**, v. 12, n. 3, 2022.

DESAI, K.; SOMASUNDARAM, J. Nanodentistry-An Overview. **European Journal of Molecular & Clinical Medicine**, v. 7, n. 1, p. 2879-2887, 2020.

DING, Z.; LI, P.; WANG, R. R. Introduction to the Special Issue on Optical Coherence Tomography (OCT). **World Scientific**, v. 14, p. 2102001, 2021.

HAMIDA, R. S.; ALI, M. A.; GODA, D. A.; REDHWAN, A. Anticandidal Potential of Two Cyanobacteria-Synthesized Silver Nanoparticles: Effects on Growth, Cell Morphology, and Key Virulence Attributes of. **Pharmaceutics**, v. 13, n. 10, 2021.

HAMPE, I. A. I.; FRIEDMAN, J.; EDGERTON, M.; MORSCHHÄUSER, J. An acquired mechanism of antifungal drug resistance simultaneously enables *Candida albicans* to escape from intrinsic host defenses. **PLoS Pathog**, v. 13, n. 9, p. e1006655, 2017.

HUANG, D.; SWANSON, E. A.; LIN, C. P.; SCHUMAN, J. S. et al. Optical coherence tomography. **Science**, v. 254, n. 5035, p. 1178-1181, 1991.

KEMALOGLU, H.; KARACOLAK, G.; TURKUN, L. S. Can Reduced-Step Polishers Be as Effective as Multiple-Step Polishers in Enhancing Surface Smoothness? **J Esthet Restor Dent**, v. 29, n. 1, p. 31-40, 2017.

LEE, B.; LEE, M. J.; YUN, S. J.; KIM, K. et al. Silver nanoparticles induce reactive oxygen species-mediated cell cycle delay and synergistic cytotoxicity with 3-bromopyruvate in. **Int J Nanomedicine**, v. 14, p. 4801-4816, 2019.

LONGHI, C.; SANTOS, J. P.; MOREY, A. T.; MARCATO, P. D. et al. Combination of fluconazole with silver nanoparticles produced by *Fusarium oxysporum* improves antifungal effect against planktonic cells and biofilm of drug-resistant *Candida albicans*. **Med Mycol**, v. 54, n. 4, p. 428-432, 2016.

MATARE, T.; NZIRAMASANGA, P.; GWANZURA, L.; ROBERTSON, V. Experimental Germ Tube Induction in. **Biomed Res Int**, v. 2017, p. 1976273, 2017.

MATSUURA, C.; SHIMADA, Y.; SADR, A.; SUMI, Y. et al. Three-dimensional diagnosis of dentin caries beneath composite restorations using swept-source optical coherence tomography. **Dent Mater J**, v. 37, n. 4, p. 642-649, 2018.

MOHER, D.; SHAMSEER, L.; CLARKE, M.; GHERSI, D. et al. Preferred reporting items for systematic review and meta-analysis protocols (PRISMA-P) 2015 statement. **Syst Rev**, 4, p. 1, 2015.

MOSMANN, T. Rapid colorimetric assay for cellular growth and survival: application to proliferation and cytotoxicity assays. **J Immunol Methods**, v. 65, n. 1-2, p. 55-63, 1983.

MUSSIN, J. E.; ROLDÁN, M. V.; ROJAS, F.; SOSA, M. L. Á. et al. Antifungal activity of silver nanoparticles in combination with ketoconazole against *Malassezia furfur*. **AMB Express**, v. 9, n. 1, p. 131, 2019.

NGUYEN, S.; TRUONG, J. Q.; BRUNING, J. B. Targeting Unconventional Pathways in Pursuit of Novel Antifungals. **Front Mol Biosci**, v. 7, p. 621366, 2020.

ODDS, F. C. Synergy, antagonism, and what the chequerboard puts between them. **J Antimicrob Chemother**, v. 52, n. 1, p. 1, 2003.

PAPPAS, P. G.; KAUFFMAN, C. A.; ANDES, D. R.; CLANCY, C. J. et al. Clinical Practice Guideline for the Management of Candidiasis: 2016 Update by the Infectious Diseases Society of America. **Clin Infect Dis**, v. 62, n. 4, p. e1-50, 2016.

PETROV, T.; PECHEVA, E.; WALMSLEY, A. D.; DIMOV, S. Femtosecond laser ablation of dentin and enamel for fast and more precise dental cavity preparation. **Mater Sci Eng C Mater Biol Appl**, v. 90, p. 433-438, 2018.

PORTILLO MUÑOZ, M.; LORENZO LUENGO, M. C.; SÁNCHEZ LLORENTE, J. M.; PEIX SÁNCHEZ, M. et al. Morphological alterations in dentine after mechanical treatment and ultrashort pulse laser irradiation. **Lasers Med Sci**, v. 27, n. 1, p. 53-58, Jan 2012.

PUNJABI, K.; MEHTA, S.; CHAVAN, R.; CHITALIA, V. et al. Efficiency of Biosynthesized Silver and Zinc Nanoparticles Against Multi-Drug Resistant Pathogens. **Front Microbiol**, v. 9, p. 2207, 2018.

R, A. N.; RAFIQ, N. B. Candidiasis. **StatPearls Publishing**, v. 2020, 2020.

RÓŻALSKA, B.; SADOWSKA, B.; BUDZYŃSKA, A.; BERNAT, P. et al. Biogenic nanosilver synthesized in *Metarhizium robertsii* waste mycelium extract - As a modulator of *Candida albicans* morphogenesis, membrane lipidome and biofilm. **PLoS One**, v. 13, n. 3, p. e0194254, 2018.

SHAMSEER, L.; MOHER, D.; CLARKE, M.; GHERSI, D. et al. Preferred reporting items for systematic review and meta-analysis protocols (PRISMA-P) 2015: elaboration and explanation. **BMJ**, v. 350, p. g7647, 2015.

SINGH, B. R.; GUPTA, V. K.; DEEBA, F.; BAJPAI, R. et al. Non-Toxic and Ultra-Small Biosilver Nanoclusters Trigger Apoptotic Cell Death in Fluconazole-Resistant. **Biomolecules**, v. 9, n. 2, 2019.

SPADARO, D.; BARLETTA, E.; BARRECA, F.; CURRÒ, G. et al. PMA capped silver nanoparticles produced by UV-enhanced chemical process. **Applied Surface Science**, v. 255, n. 20, p. 8403-8408, 2009.

SWANSON, E. A.; FUJIMOTO, J. G. The ecosystem that powered the translation of OCT from fundamental research to clinical and commercial impact [Invited]. **Biomed Opt Express**, v. 8, n. 3, p. 1638-1664, 2017.

WHITING, P. F.; RUTJES, A. W.; WESTWOOD, M. E.; MALLETT, S. et al. QUADAS-2: a revised tool for the quality assessment of diagnostic accuracy studies. **Ann Intern Med**, v. 155, n. 8, p. 529-536, 2011.

WOJTKOWSKI, M. High-speed optical coherence tomography: basics and applications. **Appl Opt**, v. 49, n. 16, p. D30-61, 2010.

ZERO, D. T.; RAHBEK, I.; FU, J.; PROSKIN, H. M. et al. Comparison of the iodide permeability test, the surface microhardness test, and mineral dissolution of bovine enamel following acid challenge. **Caries Res**, v. 24, n. 3, p. 181-188, 1990.

ZHANG, Y.; COELLO, P. A.; GUYATT, G. H.; YEPES-NUÑEZ, J. J. et al. GRADE guidelines: 20. Assessing the certainty of evidence in the importance of outcomes or values and preferences—inconsistency, imprecision, and other domains. **Journal of Clinical Epidemiology**, v. 111, p. 83-93, 2019

APÊNDICE A – ACTIVITY OF POLY(METHACRYLIC ACID)-SILVER NANOPARTICLES ON FLUCONAZOLE RESISTANT *CANDIDA ALBICANS* STRAINS: SYNERGISTIC AND CYTOTOXIC EFFECTS

Received: 13 January 2022 | Revised: 11 March 2022 | Accepted: 21 March 2022

Journal of Applied Microbiology

DOI: 10.1111/jam.15542

ORIGINAL ARTICLE

Activity of poly(methacrylic acid)- silver nanoparticles on fluconazole- resistant *Candida albicans* strains: Synergistic and cytotoxic effects

Cecília Maria Cruz Falcão[1] | Audrey Andrade[2,3] | Vanderlan Nogueira Holanda[4] | Regina Celia Bressan Queiroz de Figueiredo[4] | Eulália Azevedo Ximenes[5] | Anderson Stevens Leonidas Gomes[1,2]

[1]Postgraduate Program in Dentistry, Federal University of Pernambuco, Recife, Brazil

[2]Department of Physics, Federal University of Pernambuco, Recife, Brazil

[3]Laboratory of Microscope and Microanalysis, Strategic Technologies Center of Northeast, Recife, Brazil

[4]Department of Microbiology, Aggeu Magalhaes Research Centre, Recife, Brazil

[5]Department of Antibiotics, Federal University of Pernambuco, Recife, Brazil

Correspondence
Cecília Maria Cruz Falcão, Postgraduate Program in Dentistry, Federal University of Pernambuco, 50670- 901, Recife, Prince Edward Island, Brazil.
Email: ceciliaodonto@gmail.com

Funding information
Conselho Nacional de Desenvolvimento Científico e Tecnológico, Grant/Award Number: PQ- 1A 307259/2015- 3; Coordenação de Aperfeiçoamento de Pessoal de Nível Superior, Grant/Award Number: 001CAPES- UFPE; Instituto Nacional de Fotônica, Grant/Award Number: INCT 465763/2014- 6

Abstract

Aims: To synthesize and evaluate the antifungal activity of poly(methacrylic acid)-silver nanoparticles (PMAA-A gNPs) against nine *Candida albicans* isolated from clinical specimens.

Methods and Results: The effects of PMAA- AgNPs- fluconazole combination was analysed by checkerboard methodology. The synergistic potential of PMAA-A gNPs-fluconazole was determined by the fractional inhibitory concentration index (FICI). The inhibition of germ tube formation and the determination of PMAA- AgNPs cytotoxicity were also performed. All *C. albicans* strains were susceptible to PMAA- AgNPs and resistant to fluconazole. PMAA- AgNPs at subinhibitory concentrations restored the susceptibility of resistant *C. albicans* to fluconazole, whose FICI ranged from 0.3 to 0.5. The synergistic interaction of the combination was observed in eight of nine strains. The PMAA- AgNPs- fluconazole combination was also able to inhibit the germ tube formation. PMAA-A gNPs showed a dose-dependent decrease in vi- ability for cells tested, with 50% cytotoxic concentration (CC_{50}) values of 6.5, 4.9 and 6.8 μg ml^{-1} for macrophages, fibroblasts and Vero cells, respectively.

Conclusions: This study demonstrated that, in general, PMAA-A gNPs acts synergistically in combination with fluconazole, inhibiting fluconazole- resistant *C. albicans* strains. PMAA- AgNPs- fluconazole combination was also able to inhibit germ tube formation, an important virulence factor. Inhibitory effect of PMAA- AgNPs alone or in combination was higher in *C. albicans* than in mammalian cells.

Significance and Impact of Study: This study shows the potential of PMAA- AgNPs combined with fluconazole to inhibit fluconazole- resistant *C. albicans* strains.

KEYWORDS
Candida albicans, fluconazole, germ tube, silver nanoparticles, synergism

INTRODUCTION

Candidiasis is an opportunistic pathology ranging from superficial to systemic and life- threatening infection, being *Candida albicans* the most prevalent species (Arya & Rafiq, 2020). Usually, infections caused by *Candida* are treated by different classes of antifungals including: azoles, polyenes and echinocandins (Pappas et al., 2016). Besides the emergence of resistance, the limited spectrum of available antifungals constitutes a major barrier to the effective treatment of systemic and local fungal infections (Nguyen et al., 2020).

The development of resistance to the currently used antifungals has been an important health concern. In this regard, the search of novel antifungal alternatives to traditional antibiotics, aiming to overcome this limitation, represents an urgent need in the field. (Pimentel et al., 2022; Nadhe et al., 2019).

Metal nanoparticles have been demonstrated to have not only antimicrobial effects, but also advantages such as: lower toxicity, hydrophilicity, biocompatibility and high stability. These nanoparticles alone or in combination with currently antifungal agents can be used to circumvent the fungal resistance, as well as the complications associated with prolonged use of antifungals (Mussin et al., 2019). Silver nanoparticles (AgNPs) are among the most studied nanomaterials for biomedical applications due to their potent antimicrobial properties, good chemical stability and biocompatibility (Singh et al., 2019). The activity of these nanoparticles against *C. albicans* has been already demonstrated (Hamida et al., 2021; Hampe et al., 2017; Lee et al., 2019; Longhi et al., 2016). However, the search of novel AgNPs with more suitable physicochemical properties and lower cytotoxicity with antifungal activity is still an urgent need.

Although nanoparticles are considered as a promising tool in the areas of science and technology, their cytotoxicity potential has been a matter of concern (Punjabi et al., 2018). Development of AgNPs with antifungal activity, environmentally harmless and cheap procedures in AgNP production has been sought. Thus, it is necessary to develop not only an innovative, cost- effectively and eco- friendly method to produce AgNPs, but also to evaluate its antimicrobial activity and biosafety to prove their therapeutic potential (Różalska et al., 2018).

In a previous study, a solution of silver nitrate and biocompatible poly(methacrylic acid) (PMAA) polymer were used as starting point to prepare spherical AgNPs (PMAA- AgNPs), with diameter smaller than 40 nm (Carvalho et al., 2018). To the best of our knowledge, studies on the effect of PMAA-AgNPs combined with antifungal agents against *C. albicans* have not yet been published. In this regard, this study aims to evaluate the in vitro effects of the combination of PMAA- AgNPs with fluconazole against *C. albicans* strains isolated from different clinical samples, the ability of these nanoparticles to inhibit the germ tube formation as well the determination of its cytotoxicity potential on mammalian cells.

MATERIALS AND METHODS

Synthesis and characterization of PMAA-AgNPs

Poly(methacrylic acid)- silver nanoparticles (PMAA-AgNPs) were synthesized according to the methodology described by Carvalho et al. (2018). Aqueous solution of silver nitrate ($AgNO_3$, 50 ml, 5 mmol L^{-1} was mixed with PMAA (sodium salt, 50 ml, 0.5 mmol L^{-1}) and magnetically stirred at 25°C for 5 min. This solution was exposed to UV light (8 W, central wavelength 370 nm) for 6 h for silver reduction and stored in amber vials (Spadaro et al., 2009). Then, size and morphology of synthesized PMAA- AgNPs was analysed. UV– Visible transmission spectroscopy (Cary 50 UV– Vis spectrometer; Varian/ Agilent) was used to verify the conversion of silver cations to AgNPs. Nanostructure of samples were characterized by transmission electron microscopy (JEOL; JEM- 2100) operating at 200 kV and energy dispersive X- ray fluorescent spectrometer module of the Nuclear and Energy Research Institute (SP, Brazil). The zeta potential measurements were performed using Zetasizer Nano from the laboratory of Non- Conventional Polymers, Department of Physics– Federal University of Pernambuco.

Candida albicans strains and inoculum standardization

Candida albicans strains (n = 9) were obtained from stock cultures maintained in the Laboratory of Physiology and Biochemistry of Microorganisms (LFBM), Department of Antibiotics— Federal University of Pernambuco. These strains were isolated from urine (LFBM Ca01, LFBM Ca02, LFBM Ca03 and LFBM Ca04), oral cavity (LFBM Ca05 and LFBM Ca06) and blood (LFBM Ca07, LFBM Ca14 and LFBM Ca1002). *C. albicans* ATCC® 10231 was used as standard strain.

Candida albicans cultures were reactivated in Sabouraud Dextrose Broth (DIFCO), seeded onto Sabouraud Dextrose Agar (DIFCO) and incubated at 35°C for 24 h. For standardization of the inoculum, single colonies were selected and yeast suspension was prepared in saline solution (0.85%). Turbidity of these suspensions was adjusted to 90% transmittance at 530 nm which is equivalent to 10^6 colony forming units per ml (cfu ml^{-1}). Then, two dilutions were performed to obtain a final inoculum (10^3 cfu ml^{-1}). First, *C. albicans* culture were diluted in saline solution (1:100) following by a second dilution (1:10) in Roswell Park Memorial Institute Medium (RPMI-1640; Gibco) buffered with 3- (*N*-morpholino)propanesulfonic acid (MOPS; Sigma-Aldrich) (CLSI, 2017b). *Candida albicans* growth in the culture was confirmed by direct cell counting.

Antifungal agents

Amphotericin B, nystatin and fluconazole (Sigma-Aldrich) were chosen as reference drugs, based on Guideline of Infectious Diseases Society of America (Pappas et al., 2016). Resistance was defined for each case, considering minimal inhibitory concentration (MIC) values required to inhibit the growth of 90% of organisms: amphotericin B MIC >1.0 μg ml^{-1}, fluconazole MIC ≥8.0 μg ml^{-1}. For nystatin, MIC between 8.0 and 32.0 μg ml^{-1} was defined as dose-dependent susceptibility (CLSI, 2017a, 2017b). Amphotericin B, nystatin and fluconazole were solubilized in dimethyl sulfoxide/tween 80/water (1.0/0.5/8.5) while AgNPs were solubilized in water. *Candida albicans* cultivated in medium containing dimethyl sulfoxide/tween 80/water was used as negative control to exclude the possibility of toxic effects of this diluent on the pathogen.

Antifungal activity

Susceptibility of *C. albicans* to antibiotics was carried out using broth microdilution method, in accordance with CLSI M27-A 4 guideline with slight modifications. Stock solution of PMAA- AgNPs, amphotericin B, nystatin and fluconazole were serially diluted in RPMI- 1640 buffered with MOPS to obtain concentrations that ranged from 64.0 to 0.5 μg ml^{-1}, except to fluconazole, whose concentration ranged from 1024 to 8.0 μg ml^{-1}. Aliquots (100 μl) of drugs solutions were distributed in sterile 96-w ell microplates and then a standardized suspension of *C. albicans* strains (100 μl) was added to wells. These plates were incubated at 35°C for 24 h. Minimal inhibitory concentration was reported as the lowest concentration of compounds that inhibited *C. albicans* growth (CLSI, 2017b).

To determine the minimal fungicidal concentration (MFC), defined as the lowest concentration that killed more than 99.9% of the initial inoculum, aliquots (5 μl) of each well, where no growth was detected, were seeded onto Sabouraud Dextrose Agar. These plates were incubated under the same conditions and the number of colonies was determined.

Checkerboard assay

Checkerboard assay was performed according to the methodology described by Odds (2003). Appropriate dilutions of PMAA- AgNPs (4.0–0 .031 μg ml^{-1}) and fluconazole (1024– 0.5 μg ml^{-1}) were prepared into RPMI- 1640. From these dilutions, 50 μl were added into 96-w ell microplates to obtain a final concentration corresponding to 1/8 and 1/12 of MIC value for PMAA- AgNPs and fluconazole, respectively. Then, 100 μl of cell suspension was added to each well (10^3 cfu ml^{-1}) and microplates were incubated at 35°C for 24 h.

Fractional inhibitory concentration index (FICI) was determined as: (MIC of the PMAA- AgNPs in combination with fluconazole/MIC of the PMAA-AgNPs) + (MIC of fluconazole in combination with PMAA- AgNPs/MIC of fluconazole).

The effect of the combination was defined as synergistic if FICI was ≤0.5, additive when the FICI was >0.5 to ≤1.0 and antagonistic when >1.0 (Odds, 2003).

Germ tube formation assay

LFBM Ca06 strain was randomly chosen for the germ tube formation tests. This strain was cultivated on Sabouraud Dextrose Broth at 35°C for 24 h. Cultures were diluted in the same broth to obtain yeast standard suspensions (10^3 cfu ml^{-1}). These suspensions were exposed to fluconazole, PMAA- AgNPs and their combination in subinhibitory concentrations. Aliquots of 1 ml of each *C. albicans* culture were added to 1 ml of fetal bovine serum (FBS; Gibco). The test tubes were incubated at 37°C for 3 h under gently shaking. Samples cultivated in free-d rug medium supplemented with FBS were considered as positive control of germ tube formation. A drop of each *C. albicans* culture was placed on a slide and observed under light microscope at 400× magnification (Olympus BX51) (Matare et al., 2017). Yeasts were considered to have germinated if the germ tube formation was at least twice the length of the cell.

Cytotoxicity assay

Cytotoxic effects of the PMAA-A gNPs on J774.A1 macrophages (ATCC TIB-6 7TM), Vero cells (ATCC CCL- 81TM) and fibroblasts (ATCC PCS- 201- 018) were evaluated by 3- (4,5- dimethylthiazol- 2- yl)- 2,5- di phenyl tetrazolium bromide (MTT) colorimetric assay (Mosmann, 1983). For each cell types, 10^5 cells ml^{-1} was seeded in 96-w ell plates containing RPMI-1640 for macrophages and Vero cells, or Dulbecco's Modified Eagle Medium for fibroblasts, supplemented with 10% inactivated FBS. Cultures were incubated at 37°C for 3 h in 5% CO_2 atmosphere. Nonadherent cells were removed by washing with phosphate buffered saline, pH 7.0. Remaining cells were allowed to grow for additional 48 h in RPMI-1 640 in the absence or the presence of PMAA- AgNPs (100 µl), at concentrations ranging from 2.0 to 64.0 µg ml^{-1}. Treated and untreated cells were washed and incubated at 37°C for 3 h in fresh culture media containing 0.5 mg ml^{-1} of MTT (Sigma– Aldrich). After incubation, MTT was removed and the cells were treated with an (100 µl) acid isopropanol (0.04 N HCl in isopropanol) for formazan crystal solubilization derived from MTT reduction. Samples aliquots (100 µl) were transferred to 96- well microplates and analysed at Benchmark Plus™ Microplate Spectrophotometer (Bio- Rad®) at 540 nm.

Statistical analysis

All assays were performed in triplicate on two independent experiments and the results were expressed as an average of the assays. Cytotoxicity assay results were plotted as the percentage of viable cells normalized to untreated cells. The cytotoxic concentration 50% value (CC_{50}) was calculated by nonlinear regression analysis. Data were compared by one-w ay analysis of variance followed by the Tukey posttest using GraphPad Prism 9.1.1 (GraphPad Software). *p*- value <0.05 was considered statistically significant.

RESULTS

Synthesis and characterization of PMAA-AgNPs

Poly(methacrylic acid)- silver nanoparticles showed maximum intensity of the extinction spectrum in 420 nm (Figure 1), which is correlated to the plasmon absorption peak of spherical AgNPs (Maier, 2007). Monodispersed AgNPs, spherical and without significant agglomeration, were observed in transmission electron microscopy image (Figure 2a). Particle size distribution ranges from 10 to 40 nm with a mean size of 15 nm (Figure 2b). The presence of PMAA prevented the particles clustering while they remain in suspension. Poly(methacrylic acid)- silver nanoparticles presented a zeta potential of −41.83 mV.

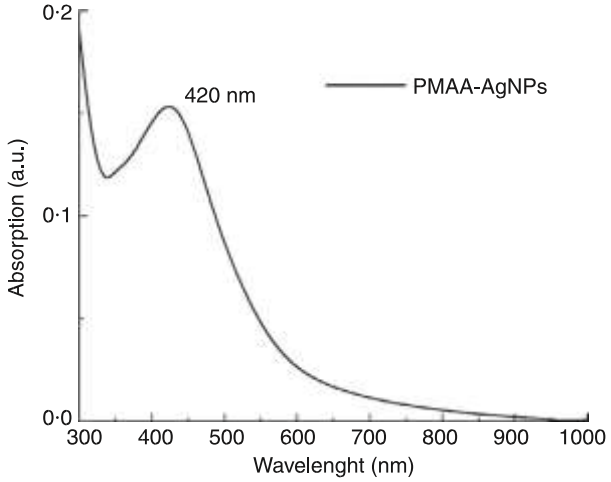

FIGURE 1 UV– visible absorption spectra of PMAA- AgNPs. PMMA- AgNPs, poly(methacrylic acid)- silver nanoparticles

Antifungal activity

Minimal inhibitory concentration and MFC values of PMAA- AgNPs and antifungals against *C. albicans* are presented in Table 1. Poly(methacrylic acid)-silver nanoparticles showed activity against all *C. albicans* strains tested, including *C. albicans* ATCC 10231 (MIC 4.0– 8.0 μg ml^{-1}). Compared to nystatin and fluconazole, amphotericin B showed the strongest activity whose MIC values ranging from 1.0 to 2.0 μg ml^{-1}. However, three strains (LFBM Ca01, LFBM Ca05 and LFBM Ca14) showed resistance to this antifungal (MIC 2.0 μg ml^{-1}).

All *C. albicans* strains were susceptible to nystatin treatment in a dose- dependent manner. On the other hand, all strains tested showed to be resistant to fluconazole, exhibiting MIC values equal or greater than 1024 μg ml^{-1}. In this regard, fluconazole was selected for the study of the interaction with PMAA-AgNPs.

Checkerboard assay

Minimal inhibitory concentration and FICI values obtained by the combination of PMAA- AgNPs with fluconazole against *C. albicans* strains are presented in Table 2.

Subinhibitory concentrations of PMAA- AgNPs (≤ 0.5 × MIC) enhanced the anti- *Candida* activity of fluconazole. Among all *C. albicans* strains tested, five (LFBM Ca02, LFBM Ca04, LFBM Ca05, LFBM Ca14, LFBM Ca1002) had their sensitivity to fluconazole restored (initial MIC 1024 μg ml^{-1}; final MIC 4.0– 2.0 μg ml^{-1}). Synergistic interaction (FICI ≤ 0.5) was detected in eight strains leading to a reduction of MIC values (PMAA- AgNPs ≥ 50%; fluconazole ≥ 96.8%). Isobole curve corroborates the synergistic association between PMAA- AgNPs and fluconazole (Figure 3). The greater synergistic interactions of PMAA- AgNPs + fluconazole was observed for LFBM Ca05 and LFBM Ca07 strains (FICI = 0.3). For these yeasts, the MIC value for fluconazole alone (≥ 1024 μg ml^{-1}) was lowered to 1/32– 1/256 fold (combined MIC 32.0–4 .0 μg ml^{-1}), respectively, when it was used in combination with PMAA- AgNPs. Although additive effect was observed against LFBM Ca01 strain (FICI = 0.6), PMAA- AgNPs tested at MIC = 2.0 μg ml^{-1} was able to lower the MIC of fluconazole (individual MIC ≥1024 μg ml^{-1}; combined MIC = 128.0 μg ml^{-1}).

Germ tube formation assay

The treatment of *C. albicans* (LFBM Ca06 strain) subinhibitory concentrations of PMAA-A gNPs (2.0 or 1.0 μg ml^{-1}) or fluconazole (16.0 μg ml^{-1}) did not inhibit the germ tube formation (Figure 4a–c). However, when these cultures were exposed at PMAA-A gNPs- fluconazole combination at MIC of 2.0– 16.0 or 1.0– 16.0 μg ml^{-1} for 3 h, an inhibition of germ tube formation could be observed (Figure 4d). It is noteworthy that germ tube inhibition occurred at concentration 1/64 × MIC for fluconazole when in combination with ≤1/2 × MIC of PMAA-A gNPs.

Cytotoxicity assay

MTT assay showed a dose-d ependent decrease in the viability for all the cell types tested, with CC_{50} values equal to 6.5 μg ml^{-1} (±0.56), 4.9 μg ml^{-1} (±0.25) and 6.8 μg ml^{-1} (±0.36), for macrophages, fibroblasts and Vero Cells, respectively (Figure 5).

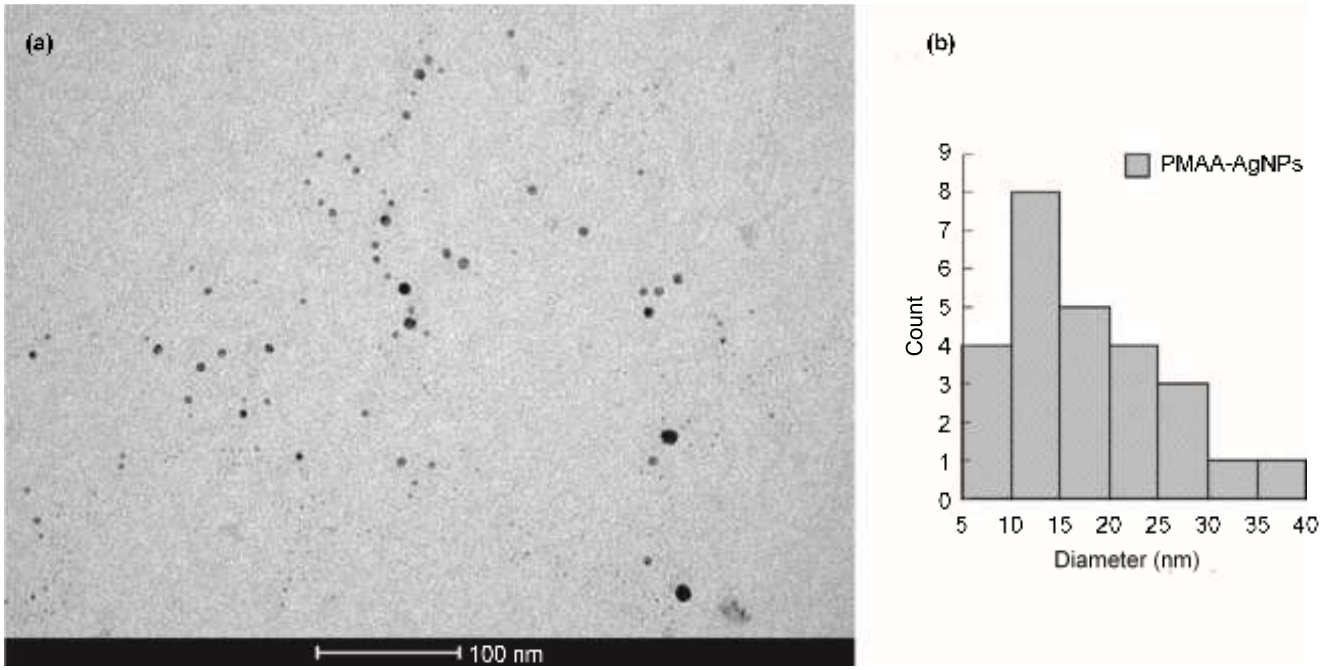

FIGURE 2 Transmission electron microscopy image of PMAA- AgNPs taken after synthesis (a); particle size distribution (b). PMMA- AgNPs, poly(methacrylic acid)- silver nanoparticles.

TABLE 1 Minimal inhibitory and minimal fungicidal concentration (MIC/MFC) of PMAA-A gNPs and antifungals against *Candida albicans* strains

	MIC/MFC (μg ml^{-1})			
***Candida albicans* strains**	**PMAA- AgNPs**	**Amphotericin B**	**Nystatin**	**Fluconazole**
LFBM Ca01	4.0/8.0	2.0/2.0	16.0/32.0	>1024
LFBM Ca02	4.0/8.0	1.0/2.0	16.0/32.0	>1024
LFBM Ca03	4.0/8.0	1.0/2.0	16.0/32.0	>1024
LFBM Ca04	4.0/8.0	1.0/2.0	16.0/32.0	>1024
LFBMCa05	4.0/8.0	2.0/2.0	16.0/32.0	>1024
LFBM Ca06	4.0/8.0	1.0/2.0	16.0/32.0	>1024
LFBM Ca07	8.0/16.0	1.0/2.0	16.0/32.0	>1024
LFBM Ca14	4.0/8.0	2.0/4.0	16.0/32.0	>1024
LFBM Ca1002	4.0/8.0	1.0/2.0	16.0/32.0	>1024

Abbreviations: LFBM Ca, Laboratory of Physiology and Biochemistry of Microorganisms *Candida albicans*; MFC, minimal fungicidal concentration; MIC, minimal inhibitory concentration; PMMA- AgNPs, poly(methacrylic acid)- silver nanoparticles.

TABLE 2 Combination testing of the PMAA- AgNPs with fluconazole against *Candida albicans* strains

Candida albicans strains	PMAA- AgNPs/FLC MIC (μg ml^{-1})	PMAA- AgNPs/FLC Individual FIC	FICI	% MIC reduced
LFBM Ca01	2.0/128.0	0.5/0.125	0.6	50.0/87.5
LFBM Ca02	2.0/4.0	0.5/0.004	0.5	50.0/99.6
LFBM Ca03	2.0/16.0	0.5/0.02	0.5	50.0/98.4
LFBM Ca04	2.0/2.0	0.5/0.002	0.5	50.0/99.8
LFBM Ca05	1.0/4.0	0.25/0.004	0.3	75.0/99.6
LFBM Ca06	2.0/16.0	0.5/0.02	0.5	50.0/98.4
LFBM Ca07	2.0/32.0	0.25/0.03	0.3	75.0/96.8
LFBM Ca14	2.0/2.0	0.5/0.002	0.5	50.0/99.8
LFBM Ca1002	2.0/2.0	0.5/0.002	0.5	50.0/99.8

Note: % MIC Reduced = (MIC alone – MIC combined) × 100/MIC alone.

Abbreviations: FICI, fractional inhibitory concentration index; FLC, fluconazole; LFBM Ca, Laboratory of Physiology and Biochemistry of Microorganisms *Candida albicans*; MIC, minimal inhibitory concentration; PMAA-A gNPs, poly(methacrylic acid)- silver nanoparticles.

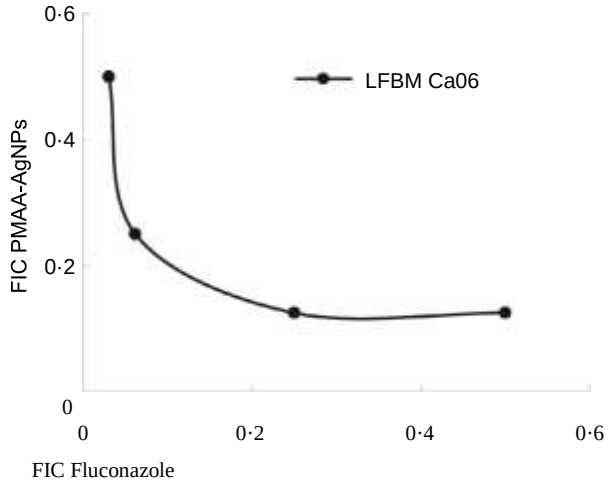

FIGURE 3 Isobole curve revealing the synergistic effect of PMAA- AgNPs with fluconazole against *Candida albicans* LFBM Ca06. PMMA- AgNPs, poly(methacrylic acid)- silver nanoparticles

DISCUSSION

Silver nanoparticles are promising antimicrobial compounds applied in nanomedicine. Different methods of synthesis, as well the composition of the stabilizer used, produce nanoparticles with singular properties, which depend on the structure, size and shape of nanoparticle (Akter et al., 2018; Nogueira et al., 2019). The surface characteristics of nanoparticles have an important role on their pharmacological cytotoxic activities (Das et al., 2017). For instance, both the size and the large surface contact area of these nanomaterials can influence its mechanism of action, allowing them to attach to the target cell membrane and easily penetrate, causing damage to cell structure (Hamida et al., 2021; Nogueira et al., 2019).

In this study, AgNPs were synthesized by a fast and easy to perform, nature-f riendly method. For this, water is used as a solvent whereas ultra- violet radiation is employed as a catalytic agent of AgNPs, resulting in small size PMAA- AgNPs with great potential for technological development of novel nanocomposites (Carvalho et al., 2018). This method was first described by Spadaro et al. (2009) aimed to make the synthesis of nanoparticles simpler, minimizing the generation of final reaction by- products.

Because PMAA have been described as biocompatible, hydrophilic and cost- effective polymer, this compound was selected in our study as both: a reducer of the silver ions present in aqueous solution (from the precursor $AgNO_3$), in presence of UV radiation, and a stabilizer, which prevents the formation of clusters in the colloidal solution (Luo et al., 2010). In addition, chemical structure of PMAA presents negatively charged carboxylic groups (– COO−), attached along the polymeric segments and acts as templates for incoming Ag^+ ions. PMAA offers the advantage of obtaining nanoparticles with more defined size and shape

minimizing the chances of clustering and nonhomogeneous distribution of AgNPs (Bajpai et al., 2013).

Consistently, zeta potential value of PMAA- AgNPs (−41.83 mV) corroborates a good dispersion and stability of these nanoparticles in solution (Shah et al., 2020), due to surface charge- based repulsion. Furthermore, negatively charged surface also facilitates the interaction between nanoparticle and target cell membranes (Nogueira et al., 2019).

An interesting finding of our study was the ability of PMAA- AgNPs to effectively act as an antifungal agent against fluconazole- resistant *C. albicans* strains at low concentrations (4.0– 8.0 μg ml^{-1}). It is already reported in the literature that AgNPs affect multiple cellular targets in *C albicans*, altering the morphology and fluidity of its surface membrane, causing rupture of cellular microenvironment and interfering with the ergosterol content and fatty acid composition, especially oleic acid (Radhakrishnan, Dwivedi, et al., 2018; Radhakrishnan, Reddy Mudiam, et al., 2018). These effects could ultimately lead to the shrunk and collapse of yeast (Hamida et al., 2021; Khatoon et al., 2019).

The widespread use of azoles has led to the emergence of acquired resistance in fungal pathogens. Yeasts such as *C. albicans* can be resistant to fluconazole by at least three mechanisms: (1) change in the target enzyme to reduce drug- binding, (2) increase in the amount of target enzyme or (3) prevention from intracellular drug accumulation. A usual resistance mechanism of *C. albicans* to antifungal is the active transport of drugs out of the cell by overexpression of efflux pumps, reducing the levels of azoles within the cell (Morschhäuser, 2016; Zavrel & White, 2015). Inhibiting and/or modulating the function of efflux pumps as well as the use of drug combinations has been an effective strategy to combat the multidrug resistance of pathogenic microorganisms (Hussain et al., 2019; Singh et al., 2018). Sun et al. (2016) showed that association of AgNPs with fluconazole could decrease expression levels of *CDR1* in *C. albicans*, the gene responsible for decoding of a major drug efflux pump. Thus, AgNPs may reverse resistance to fluconazole, further decreasing dose-dependent side effects and improving efficacy for the treatment.

Our results showed that PMAA- AgNPs combined with fluconazole in subinhibitory concentrations (≤0.5 × MIC) was able to reverse fluconazole resistance in five *C. albicans* clinical strains. These results agree with Hampe et al. (2017). Silver nanoparticles combined with antifungal drugs may reduce the amount of drug and consequently, the cost of treatment and drug-related toxicity, thus providing a safer, more effective and economical alternative compared to the monotherapy (Ahmad et al., 2016).

Similar results were obtained by Longhi et al. (2016) whom evaluated the activity of AgNPs against fluconazole- resistant *C. albicans* (MIC = 4.35 μg ml^{-1}). These authors showed a reduction of MIC values by 50% (2.17 μg ml^{-1}). However, no synergistic effect was found. On the other hand, the treatment with our PMAA- AgNPs caused a decrease of MIC by 75% and a synergistic effect in eight of nine strains when combined with fluconazole. Furthermore, compared to fluconazole alone, our results showed a significant susceptibility of *C. albicans* treated at lower concentration of AgNPs. Hussain et al. (2019) found that combined therapy of fluconazole with AgNPs against *C. albicans* induced drastic morphological depletion.

Germ tube formation is the first step in adhesion to host tissues playing important role in the mechanism of cell invasion by *C. albicans*. Therefore, morphological transition (yeast to hyphal) is pivotal for virulence and biofilm formation. Targeting virulence factors of *C. albicans* can be a useful strategy for the treatment of fungal infections (Halbandge et al., 2019; Khatoon et al., 2019). In the present study, PMAA- AgNPs were able to inhibit the germ tube formation, at subinhibitory concentrations when combined with fluconazole.

According to Różalska et al. (2018), the germ tube formation was also impaired in the presence of AgNPs, in both inhibitory and subinhibitory concentrations (0.5 × MIC = 3.125 μg ml^{-1}). Halbandge et al. (2019) suggested that AgNPs may affect signal transduction pathways in *C. albicans* by downregulating the expression of cell elongation gene (*ECE1*) and hyphal

inducer gene (*TEC1*), which are important for yeast-hyphal transition. In this regard, the ability of AgNPs acting on multiple molecular and cellular targets can be crucial to overcoming drug resistance and pathogenicity of fungal cells (Radhakrishnan, Reddy Mudiam, et al., 2018).

The most important parameter to determine the therapeutic application of a given compound is its putative toxicity (Punjabi et al., 2018). Although AgNPs provide many benefits, little is known about their overall toxicity due to the absence of precise comparative analysis among AgNPs with different shapes, sizes and capping agents. Silver nanoparticles' agglomeration and concentration range are important factors affecting the toxicity of these nanoparticles to cells (Akter et al., 2018). Therefore, we have also investigated the effects of PMAA- AgNPs against mammalian cells.

Although in our study a dose- dependent effect of PMAA- AgNPs cytotoxicity can be observed in all the cell type tested, the concentrations required to reduce the mammalian cell viability were considerably higher than those found to inhibit the *C. albicans* growth. Furthermore, none of the tested concentrations were able to reduce the mammalian cells viability by 100%. The treatment with PMAA- AgNPs were able to significantly reduce Vero cells viability only at concentration superior or equal to 8.0 μg ml^{-1}. This result is comparable to MFC of most *C. albicans* strains tested. Vero cell line is effective in evaluating the

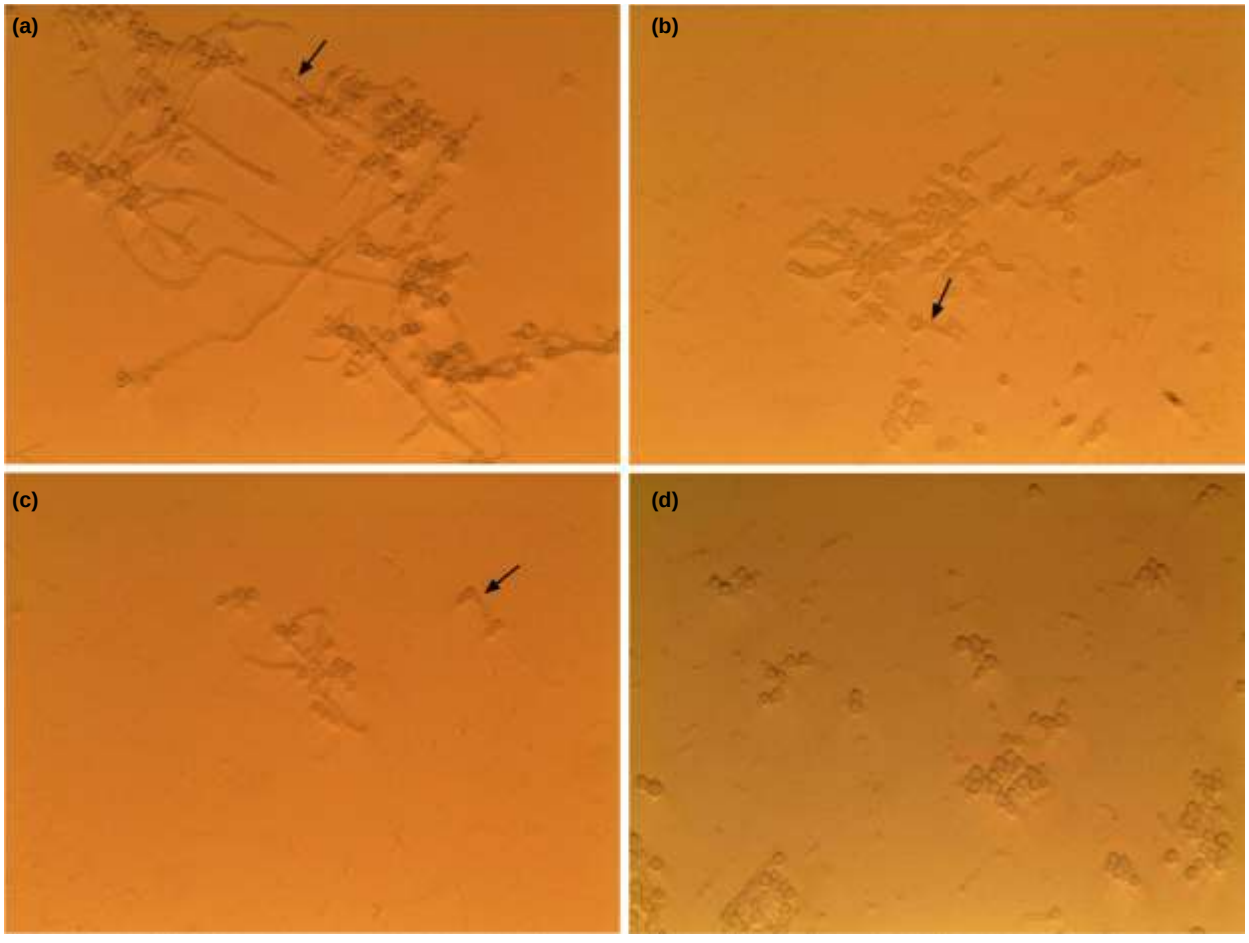

FIGURE 4 Germ tube formation by *Candida albicans* LFBM Ca06 in fetal bovine serum (a); exposed to fluconazole at 16.0 μg ml^{-1} (b); PMAA-AgNPs at 2.0 μg ml^{-1} (c) and germ tube inhibition by PMAA- AgNPsfluconazole (2.0 μg ml^{-1}/16.0 μg ml^{-1}) combination (d). Arrows indicate germ tube formation. PMMA- AgNPs, poly(methacrylic acid)- silver nanoparticles

nephrotoxic potential of drug candidate, with a good association between in vivo and in vitro results (Menezes et al., 2013). At subinhibitory concentration (2.0 μg ml^{-1}), no significant reduction in the mammalian cell viability was observed. However, the germ tube formation was efficiently inhibited at this same concentration of nanoparticles in combination with fluconazole (16.0 μg ml^{-1}).

Hussain et al. (2019) found that spherical AgNPs sizes range between 10 and 90 nm (average size = 80 nm) presented negligible cytotoxicity, suggesting that its use in human at lower concentration is safe, with minimal cell damage to the human cells. It is well known that the cytotoxicity of nanoparticles can be strongly affected by the presence of polymer coatings and surface charge (Akter et al., 2018).

The biocompatibility and bioavailability of nanoparticles are important factors that should be not neglected (Colino et al., 2021). Therefore, the development of novel nanoparticles should be optimized to improve its bioavailability in controlled release formulations. In this regard, PMAA could be a promising drug carrier for the development of smart-controlled release drugs in biomedical applications (Luo et al., 2010).

Synergism between PMAA- AgNPs with fluconazole against resistant *C. albicans* strains indicates that PMAA- AgNPs can overcome fluconazole resistance. Although PMAA- AgNPs presented dose- dependent cytotoxicity on the mammalian cells tested, the inhibitory effect of this nanoparticles alone or in combination was higher in *C. albicans* than in the host cells. This combination can be used carefully as antifungal agent in topical formulations to combat resistant candidiasis. Further in vivo studies are still needed to evaluate the toxicological and pharmaceutical proprieties of PMAA- AgNPs, alone or in combination with fluconazole, aiming to ensure its safety and efficacy in the clinical practice.

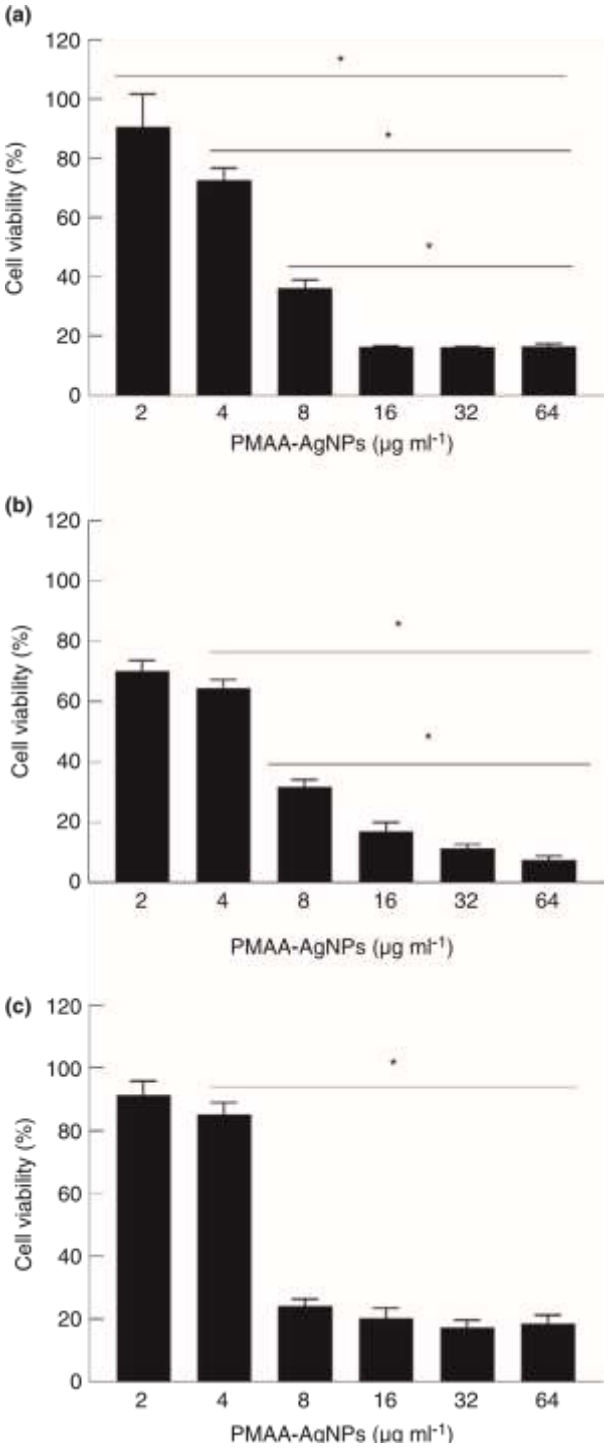

FIGURE 5 Effect of PMAA- AgNPs on viability of J774A.1 macrophages (a), fibroblasts (b) and Vero cells (c). Asterisks (*) denote a statistically significant difference compared to each other ($p \leq 0.05$). PMMA- AgNPs, poly(methacrylic acid)- silver nanoparticles

ACKNOWLEDGEMENTS

This work was supported by CNPq/FACEPE/CAPES through the National Institute of Photonics (Grant INCT 465763/2014- 6). ASLG thanks the financial support from CNPq through grant PQ- 1A 307259/2015-3 . Support from CAPES to the Graduate Program in Dentistry is also acknowledged (001CAPES- UFPE).

CONFLICT OF INTEREST

No conflict of interest declared.

ORCID

Cecília Maria Cruz Falcão https://orcid. org/0000-0002-8323-0949

REFERENCES

Ahmad, A., Wei, Y., Syed, F., Tahir, K., Taj, R., Khan, A.U. et al. (2016) Amphotericin B- conjugated biogenic silver nanoparticles as an innovative strategy for fungal infections. *Microbial Pathogenesis*, 99, 271– 281.

Akter, M., Sikder, M.T., Rahman, M.M., Ullah, A.K.M.A., Hossain, K.F.B., Banik, S. et al. (2018) A systematic review on silver nanoparticles- induced cytotoxicity: physicochemical properties and perspectives. *Journal of Advanced Research*, 9, 1–1 6.

Bajpai, S., Chand, N. & Mahendra, M. (2013) In situ formation of silver nanoparticles in poly (methacrylic acid) hydrogel for antibacterial applications. *Polymer Engineering & Science*, 53, 1751– 1759.

Carvalho, M.T., de Santana, G.S., de Andrade, A.N., Cabral, A., da Silva Rosa- Leão, N., de Melo- Santos, M.A.V. et al. (2018) Exploiting silver nanoparticles with PMAA against Aedes aegypti larvae development: potential larvicidal activity. *Colloidal Nanoparticles for Biomedical Applications XIII*, 10507. https:// doi.org/10.1117/12.2291573

CLSI. (2017a) *Performance standards for antifungal susceptibility testing of yeasts*, 1st edition. Wayne, PA: Clinical and Laboratory Standards Institute.

CLSI. (2017b) *Reference method for broth dilution antifungal susceptibility testing of yeasts*. Wayne, PA: Clinical and Laboratory Standards Institute.

Colino, C.I., Lanao, J.M. & Gutierrez- Millan, C. (2021) Recent advances in functionalized nanomaterials for the diagnosis and treatment of bacterial infections. *Materials Science & Engineering C, Materials for Biological Applications*, 121, 111843.

Das, B., Tripathy, S., Adhikary, J., Chattopadhyay, S., Mandal, D., Dash, S.K. et al. (2017) Surface modification minimizes the toxicity of silver nanoparticles: an *in vitro* and *in vivo* study. *Journal of Biological Inorganic Chemistry*, 22, 893– 918.

Halbandge, S.D., Jadhav, A.K., Jangid, P.M., Shelar, A.V., Patil, R.H. & Karuppayil, S.M. (2019) Molecular targets of biofabricated silver nanoparticles in *Candida albicans*. *Journal of Antibiotics (Tokyo)*, 72, 640–6 44.

Hamida, R.S., Ali, M.A., Goda, D.A. & Redhwan, A. (2021) Anticandidal potential of two *Cyanobacteria*- synthesized silver nanoparticles: effects on growth, cell morphology, and key virulence attributes of *Candida albicans*. *Pharmaceutics*, 13, 1688.

Hampe, I.A.I., Friedman, J., Edgerton, M. & Morschhäuser, J. (2017) An acquired mechanism of antifungal drug resistance simultaneously enables *Candida albicans* to escape from intrinsic host defenses. *PLoS Pathogens*, 13, e1006655.

Hussain, M.A., Ahmed, D., Anwar, A., Perveen, S., Ahmed, S., Anis, I. et al. (2019) Combination therapy of clinically approved antifungal drugs is enhanced by conjugation with silver nanoparticles. *International Microbiology*, 22, 239–2 46.

Khatoon, N., Sharma, Y., Sardar, M. & Manzoor, N. (2019) Mode of action and anti- *Candida* activity of *Artemisia annua* mediated-synthesized silver nanoparticles. *Journal of Mycology Medicine*, 29, 201– 209.

Lee, B., Lee, M.J., Yun, S.J., Kim, K., Choi, I.H. & Park, S. (2019) Silver nanoparticles induce reactive oxygen species-m ediated cell cycle delay and synergistic cytotoxicity with 3- bromopyruvate in *Candida albicans*, but not in *Saccharomyces cerevisiae*. *International Journal of Nanomedicine*, 14, 4801–4 816.

Longhi, C., Santos, J.P., Morey, A.T., Marcato, P.D., Durán, N., Pinge-Filho, P. et al. (2016) Combination of fluconazole with silver nanoparticles produced by *Fusarium oxysporum* improves antifungal effect against planktonic cells and biofilm of drug-resistant *Candida albicans*. *Medical Mycology*, 54, 428– 432.

Luo, Y.L., Xu, F., Feng, Q.S., Chen, Y.S. & Ma, C. (2010) Preparation and characterization of PMAA/MWCNTs nanohybrid hydrogels with improved mechanical properties. *Journal of Biomedical Materials Research. Part B, Applied Biomaterials*, 92, 243– 254.

Maier, S.A. (2007) *Plasmonics: fundamentals and applications*. New York: Springer Science & Business Media.

Matare, T., Nziramasanga, P., Gwanzura, L. & Robertson, V. (2017) Experimental germ tube induction in *Candida albicans*: an evaluation of the effect of sodium bicarbonate on morphogenesis and comparison with pooled human serum. *BioMed Research International*, 2017, 1976273.

Menezes, C., Valério, E. & Dias, E. (2013) The kidney Vero- E6 cell line: a suitable model to study the toxicity of microcystins. *New Insights into Toxicity and Drug testing*, 2, 29–4 8.

Morschhäuser, J. (2016) The development of fluconazole resistance in *Candida albicans* - an example of microevolution of a fungal pathogen. *Journal of Microbiology*, 54, 192– 201.

Mosmann, T. (1983) Rapid colorimetric assay for cellular growth and survival: application to proliferation and cytotoxicity assays. *Journal of Immunological Methods*, 65, 55– 63.

Mussin, J.E., Roldán, M.V., Rojas, F., de los Ángeles Sosa, M., Pellegri, N. & Giusiano, G. (2019) Antifungal activity of silver nanoparticles in combination with ketoconazole against *Malassezia furfur*. *AMB Express*, 9, 1– 9.

Nadhe, S.B., Singh, R., Wadhwani, S.A. & Chopade, B.A. (2019) *Acinetobacter sp*. mediated synthesis of AgNPs, its optimization, characterization and synergistic antifungal activity against *C. albicans*. *Journal of Applied Microbiology*, 127, 445– 458.

Nguyen, S., Truong, J.Q. & Bruning, J.B. (2020) Targeting unconventional pathways in pursuit of novel antifungals. *Frontiers in Molecular Biosciences*, 7, 621366.

Nogueira, S.S., de Araujo-N obre, A.R., Mafud, A.C., Guimarães, M.A., Alves, M.M.M., Plácido, A. et al. (2019) Silver nanoparticle

stabilized by hydrolyzed collagen and natural polymers: synthesis, characterization and antibacterial-a ntifungal evaluation. *International Journal of Biological Macromolecules*, 135, 808–814.

Odds, F.C. (2003) Synergy, antagonism, and what the chequerboard puts between them. *The Journal of Antimicrobial Chemotherapy*, 52, 1.

Pappas, P.G., Kauffman, C.A., Andes, D.R., Clancy, C.J., Marr, K.A., Ostrosky- Zeichner, L. et al. (2016) Clinical practice guideline for the management of candidiasis: 2016 update by the Infectious Diseases Society of America. *Clinical Infectious Diseases*, 62, e1–e50.

Pimentel, B.N.A.S., Marin- Dett, F.H., Assis, M., Barbugli, P.A., Longo, E. & Vergani, C.E. (2022) Antifungal activity and biocompatibility of α- $AgVO_3$, α- Ag_2WO_4, and β- Ag_2MoO_4 using a three-dimensional coculture model of the oral mucosa. *Frontiers in Bioengineering and Biotechnology*, 10, 826123.

Punjabi, K., Mehta, S., Chavan, R., Chitalia, V., Deogharkar, D. &Deshpande, S. (2018) Efficiency of biosynthesized silver and zinc nanoparticles against multi- drug resistant pathogens. *Frontiers in Microbiology*, 9, 2207.

Arya, N.R. & Rafiq, N.B. (2020) *Candidiasis*. Treasure Island (FL): StatPearls Publishing.

Radhakrishnan, V.S., Dwivedi, S.P., Siddiqui, M.H. & Prasad, T. (2018) In vitro studies on oxidative stress-i ndependent, Ag nanoparticles-induced cell toxicity of. *International Journal of Nanomedicine*, 13, 91– 96.

Radhakrishnan, V.S., Reddy Mudiam, M.K., Kumar, M., Dwivedi, S.P., Singh, S.P. & Prasad, T. (2018) Silver nanoparticles induced alterations in multiple cellular targets, which are critical for drug susceptibilities and pathogenicity in fungal pathogen. *International Journal of Nanomedicine*, 13, 2647– 2663.

Różalska, B., Sadowska, B., Budzyńska, A., Bernat, P. & Różalska, S. (2018) Biogenic nanosilver synthesized in *Metarhizium robertsii* waste mycelium extract - as a modulator of *Candida albicans* morphogenesis, membrane lipidome and biofilm. *PLoS One*, 13, e0194254.

Shah, Z., Hassan, S., Shaheen, K., Khan, S.A., Gul, T., Anwar, Y. et al. (2020) Synthesis of AgNPs coated with secondary metabolites of *Acacia nilotica*: an efficient antimicrobial and detoxification agent for environmental toxic organic pollutants. *Materials Science & Engineering. C, Materials for Biological Applications*, 111, 110829.

Singh, B.R., Gupta, V.K., Deeba, F., Bajpai, R., Pandey, V., Naqvi, A.H. et al. (2019) Non- toxic and ultra- small biosilver nanoclusters trigger apoptotic cell death in fluconazole-r esistant. *Biomolecules*, 9, 47.

Singh, S., Fatima, Z., Ahmad, K. & Hameed, S. (2018) Fungicidal action of geraniol against *Candida albicans* is potentiated by abrogated CaCdr1p drug efflux and fluconazole synergism. *PLoS One*, 13, e0203079.

Spadaro, D., Barletta, E., Barreca, F., Currò, G. & Neri, F. (2009) PMA capped silver nanoparticles produced by UV- enhanced chemical process. *Applied Surface Science*, 255, 8403– 8408.

Sun, L., Liao, K., Li, Y., Zhao, L., Liang, S., Guo, D. et al. (2016) Synergy between polyvinylpyrrolidone- coated silver nanoparticles and azole antifungal against drug-r esistant *Candida albicans*. *Journal of Nanoscience and Nanotechnology*, 16, 2325– 2335.

Zavrel, M. & White, T.C. (2015) Medically important fungi respond to azole drugs: an update. *Future Microbiology*, 10, 1355– 1373.

How to cite this article: Falcão, C.M., Andrade, A., Holanda, V.N., de Figueiredo, R.C., Ximenes, E.A. & Gomes, A.S. (2022) Activity of poly(methacrylic acid)- silver nanoparticles on fluconazole- resistant *Candida albicans* strains: Synergistic and cytotoxic effects. *Journal of Applied Microbiology*, 00, 1–10. Available from: https://doi.org/10.1111/jam.15542

APÊNDICE B – EFFECTS OF FEMTOSECOND LASER IRRADIATION ON THE MICROSHEAR BOND STRENGTH OF SOUND AND DEMINERALIZED DENTIN

J. Laser Appl. **31,** 012002 (2019); https://doi.org/10.2351/1.5053222. **31,** 012002 © 2019 Laser Institute of America.

Effects of femtosecond laser irradiation on the microshear bond strength of sound and demineralized dentin

Cite as: J. Laser Appl. 31, 012002 (2019); doi: 10.2351/1.5053222

Submitted: 22 August 2018 · Accepted: 19 December 2018 · View Online Export Citation CrossMark Published Online: 7 January 2019

P. F. Cassimiro-Silva,[1] Francisco de Assis M. G. Rego Filho,[2] Luciana Santos Afonso de Melo,[3] Tereza Januária Costa Dias,[1] Cecília Cruz Falcão,[1] Gabriela Queiroz de Melo Monteiro,[4] and Anderson Stevens L. Gomes[1,3,a)]

AFFILIATIONS [1] Graduate Program in Dentistry, Federal University of Pernambuco, Recife, PE 50670-901, Brazil [2] Institute of Physics, Federal University of Alagoas, Maceió, AL 57072-900, Brazil [3] Physics Department, Federal University of Pernambuco, Recife, PE 50670-901, Brazil [4] Faculty of Dentistry, University of Pernambuco, Camaragibe, PE 54753-020, Brazil [a)]

Author to whom correspondence should be addressed; electronic mail: anderson@df.ufpe.br Telephone: +55 81 2126-7636.

ABSTRACT

The aim of this in vitro study was to assess the microshear bond strength (μSBS) of an adhesive system in sound (SD) and demineralized dentin (DD) after femtosecond (fs) laser treatment. Twenty specimens of human dentin were randomly divided into two main groups: sound and demineralized dentin (n = 10). In each of them, three different tissue conditions were produced: SD control group, SD etched with two different fluences of an fs laser (11 and 18 J/cm^2, SD_{11} and SD_{18}, respectively), DD control group, and DD irradiated with the same laser parameters (DD_{11} and DD_{18}). An adhesive system was applied to the dentin surface, and a resin composite was light-cured to bond to the dentin surface. The μSBS was measured, and the fracture analysis was performed using an optical microscope. The data were analyzed using the Mann Whitney test ($p < 0.05$). Tissue morphology was assessed via 2D and 3D optical coherence tomography images, scanning electron microscopy, and atomic force microscopy. The optimum bond strength was recorded for the SD_{11} group (16.42 ± 4.63 MPa), and the minimum bond strength was recorded for the DD (8.89 ± 0.99 MPa) group. The Kruskal Wallis test revealed that sample groups were significantly different ($p < 0.01$). The Mann Whitney test demonstrated statistical differences between DD and all the other groups. The imaging techniques showed the opening of the dentinal tubules and that the bond strength could be related to laser-induced roughness. Femtosecond laser radiation was successfully able to remove smear layers, producing surface alterations that caused higher dentin-resin adhesion.

Key words: femtosecond laser, dentin bonding agents, tooth demineralization, optical coherence tomography, atomic force microscopy

I. INTRODUCTION

Dental demineralization is defined as the tissue loss from the tooth surface promoted by the action of acid or chelating substances, without bacterial involvement.[1] It is related to nutritional and individual factors, degenerating the dentin structure in more advanced stages. Consequently, the structural integrity of the tooth and its aesthetics are compromised, making restorative treatments necessary.[2]

Despite the great advances in adhesive dentistry, adhesion to tooth structure remains a challenge, especially to demineralized dentin (DD). Its continuous exposure to acids can result in complex histological changes, which is a problem for the quality of adhesion to the substrate.[3,4] Tooth demineralization leads to the dissolution of hydroxyapatite crystals, the increase of the tubules' diameter, and the exposure of highly mechanically resistant collagen fibrils network.[2,5,6] This scenario prevents the penetration of adhesive systems and the formation of hybrid layers.[7]

Therefore, new techniques have been proposed to improve the adhesion and the simplification of clinical procedures. Laser sources have been used as an alternative to promote ablation without chemical or morphological changes on the tooth surface, which could positively influence the adhesion.[8,9] However, ablation promoted by long-pulsed lasers produces microcracks, carbonization, and recrystallizations that compromise adhesion.[10,11] In this context, a laser source that promotes low-damage tissue ablation, combined with the use of more adequate irradiation parameters, is recommended.[12]

Femtosecond (fs) laser is a promising tool to ablate enamel[13–15] and dentin[16] tissues with high degree of accuracy and negligible thermal damage to the surrounding tissue,[17] which could be applied for cavity preparation.[18–20] Femtosecond (10^{-15} s) pulses generate peak powers high enough to produce plasma, which further ablates the dental tissue. The ultrafast interaction makes slower processes, such as heat conduction (which depends on the temperature gradient and thermal diffusivity), almost impossible to occur.[21,22] The ablation process ejects most of the dental matter into the air, preventing smear layer production, leaving the dentinal tubules open,[23] facilitating the adhesive penetration. Since then, extensive efforts have been made to find irradiation parameters able to produce considerable ablation rates, with minimum damage for the surrounding hard tissues.[24,25]

Femtosecond lasers have several applications in dentistry, such as multiphoton imaging,[26] its influence on the shear bond strength in orthodontics,[27,28] and Zirconia-based materials.[29–31] Surface modifications that reduce cell adhesion and biofilm formation,[32–34] bone micromachining,[35] and the improvement of the ablation rates promoted by fs sources have also been studied.[18,22] Additionally, some studies in the literature have reported the use of the femtosecond lasers to treat dentin prior to adhesive procedures.[9,19,36] However, the influence of femtosecond laser pretreatment on the adhesion to demineralized dentin have not yet been reported.

The aim of this in vitro study was to assess the microshear bond strength of an adhesive system to sound (SD) and demineralized dentin after smear layer removal by femtosecond laser with different irradiation parameters. Scanning electron microscopy (SEM), atomic force microscopy (AFM), and optical coherence tomography (OCT) were used to assess the tissue morphology and surface characteristics in order to explain the observed differences in the bond strength when comparing experimental groups.

II. MATERIALS AND METHODS

A. Specimen preparation

This study was approved by the Ethics Committee of the Federal University of Pernambuco, under the protocol #1.735.580. Twenty freshly extracted human

molars were selected for this study and were visually examined to confirm the absence of physical damage, such as deep grooves or cracks. The specimens were cleaned with distilled water and brushes, and further disinfected in 0.5% chloramine for 2 weeks.

The roots were sectioned at a 2 mm distance from the enamel-cementum junction, and the occlusal enamel was removed with a low-speed diamond saw (Isomet, Buehler Ltd., IL, USA) to expose the dentin surface. Each specimen was embedded in acrylic resin (Jet, Clássico, São Paulo, Brazil) to facilitate handling. The dentin surfaces were submitted to metallographic polishing (Biopdi, São Paulo, Brazil) with 400 and 600-grit water-cooled sandpaper for 60 s each to remove any residual enamel, to planify the target surface, and to produce standardized and clinically relevant smear layers.

B. Demineralization cycle

Ten specimens were submitted to pH cycling for 5 days via immersion in 0.05M citric acid (pH 2.3, 10 min, 6× per day). Between the acid attacks, the specimens were immersed in a supersaturated solution (pH 7.0), consisting of 1.5 mmol/l of $CaCl_2$, 1.0 mmol/l of KH_2PO_4, and 50 mmol/l of NaCl,[37] at room temperature (25 °C), and agitated for 60 min at 30 rpm on a shaker. The final step of the pH cycle consisted of storing the specimens in the same supersaturated solution until irradiation, performed at the following day. The solutions were renewed every day, and the pH of the solutions was checked at the beginning and at the end of each experimental day.

C. Experimental groups

Twenty dentin specimens were randomly assigned to experimental groups according to the substrate condition (demineralized or not) and laser parameters. Five specimens composed the SD control group, and five specimens composed the DD control group. The remaining ten specimens were randomly assigned to the etched groups. Each sample was irradiated in two different regions, each with different pulse energy. The irradiated regions were made sufficiently away to guarantee that the irradiation condition of one region did not interfere with the other. The first group was composed of sound dentin irradiated with a Ti:Sapphire fs laser with a fluence of 11 J/cm^2 (SD_{11}). The second group was similarly produced using a fluence of 18 J/cm^2 (SD_{18}). Finally, the five specimens of demineralized dentin, etched with the same laser parameters, formed two other groups (DD_{11} and DD_{18}). The details of the fluence calculation are described in Sec. II D. The sample division is summarized in Fig. 1. In each sample, two resin samples were bonded sufficiently far away from each other, resulting in ten independent measurements, used for statistical calculations.

D. Laser etching

Laser irradiation was performed using a pulsed Ti:Sapphire regenerative amplifier (802 nm, 100 fs, 1 kHz, maximum pulse energy of 1 mJ, Libra®, Coherent, USA). Two values of pulse energy were chosen (240 and 390 μJ) and applied onto two distinct regions of the samples. The pulse energy E_p was calculated using the measured average power (P_{av}) by the formulae E_p ¼ P_{av}=R, where R is the laser repetition rate (1 kHz). P_{av} was controlled by a Glan-Thompson/half-wave plate combination, external to the laser cavity. The laser beam was directed onto the sample surface by using an objective lens (20×, 0.3 numerical aperture) in order to promote plasma-mediated ablation. The samples were attached to a micrometric precision XYZ mount, connected to stepper motors controlled by a LABVIEW® routine. In order to increase the width of the scanning lines, decrease the thermal and mechanical damage, and to promote superficial removal of the smear layer, the laser scanning was performed with the samples moved 200 μm away from the focus in the incident direction (Z-axis), producing ablation lines with 90 μm width. This width was measured using scanning

electron microscopy images of the samples irradiated in the pilot study to establish the best laser parameters.

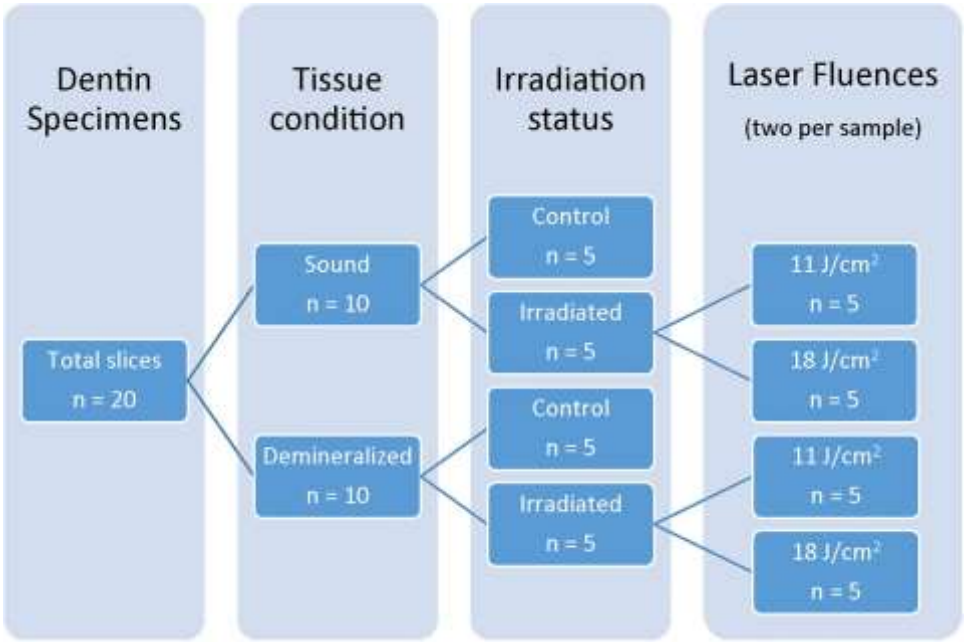

FIG. 1. Division of dentin specimens to form the experimental groups.

The XYZ mount was programmed to move 2.5 cm in the horizontal direction (X-axis), covering the whole sample. The horizontal length was large in order to make two independent measurements of the bond strength in the same laser-etched region. In the vertical direction (Y-axis), 20 scanning lines were produced, equally spaced by 90 µm, producing an etching area with total width of 1.8 mm. The scanning velocity was fixed at 30 mm/s. Considering 90 µm to be the effective beam diameter, this scanning speed promotes the superposition of three pulses per spot distance, at a crude approximation. Using the expression F_p ¼ E_p=A (F_p the single pulse fluence and A the area of the spot), the calculated total fluences at 1 kHz are ~11 J/cm^2 for 240 µJ and ~18 J/cm^2 for 390 µJ. These values are several times above ablation threshold values cited in the literature for equivalent laser systems.[20,21,38,39]

E. Microshear bond strength (µSBS) test

The tested adhesive system (Clearfil SE Bond, Kuraray Noritake Dental Inc., Kurashiki, Okayama, Japan) was applied to the dentin surfaces according to manufacturer's instructions. Transparent polyethylene tubes (Ø = 0.9 mm, h = 1 mm) were positioned over double-faced perforated tapes. The resin composite (Tetric N-Ceram A3, Ivoclar vivadent, Schaan, Liechtenstein) was carefully packed inside the tubes and was subsequently light-cured for 20 s using a light-emitting diode with 1200 mW/cm^2 (Radii-cal, SDI, Bayswater, Victoria, Australia).

The samples were kept in distilled water for 24 h at 37 °C. The tube and the double-faced tape were carefully removed with a blade, exposing the resin composite cylinders. The samples were examined under a stereomicroscope (×10 magnification) to observe possible defects. The specimens were tested in a universal testing machine (EMIC, DL 10000, São José dos Pinhais-PR, Brazil). A thin orthodontic wire (0.2 mm) was looped around the cylinder aligned with the

setup to ensure the correct orientation of the applied forces. The crosshead speed was set at 0.5 mm/min until failure. The computer software TESC 3.04 (EMIC, São José dos Pinhais-PR, Brazil) registered the bond strength values. These procedures were applied to all experimental groups, and the bond strengths in control groups (SD and DD) represent the normal clinical protocol (without laser etching).

F. Failure mode examination

Failure mode analysis was performed with an optical microscope at 5×, 10×, 20×, and 50× magnification (Olympus BX51, Tokyo, Japan). OCT was performed to obtain 2D and 3D images to confirm the results. The failure modes were classified into three categories, based on the percentage of substrate-free material as "adhesive" (failure at the resin/ enamel interface), "cohesive" (failure exclusively within enamel or resin composite), and "mixed" (failure at the resin–enamel interface that include cohesive failure of the neighboring substrates).

G. Optical coherence tomography

Before applying the resin composite and measuring the μSBS, each irradiated specimen was carefully analyzed through 2D and 3D images using a spectral domain SD-OCT (Callisto Spectral Domain OCT System, Thorlabs Inc., NJ, USA). The OCT light source is a super luminescent diode with central wavelength of 930 nm, spectral bandwidth of 100 nm, and maximum output power of 5 mW. Images generated by this system present axial resolution of 7/5.3 μm (air/water), lateral resolution of 8 μm, and maximum imaging depth at 1.3 mm. The axial scan rate of the system is 1.2 kHz, capturing two frames per second with 105 dB of sensitivity. This system provides depth profiles that, added to cross-sectional images, generate tridimensional reconstructions. Specimens were positioned on a manually controlled micrometric XYZ stage. All surfaces were analyzed by scanning lines starting from the reference area toward the irradiated area, passing by the interface. The SD-OCT system generated cross-sectional 2D images with 1024 × 512 pixels (4 × 0.5 mm) and 3D images with 1024 × 512 pixels (3 × 3 mm). The discrepancy between the height of the reference area and the irradiated surface was measured using the IMAGEJ program (JAVA, public domain) in order to calculate the tissue loss.

H. Scanning electron microscopy

Photomicrographs of representative areas of the irradiated surfaces were obtained via SEM. For this evaluation, two additional samples were prepared. Specimens were sputtercoated with gold and analyzed under SEM (Mira 3, Tescan, Brno, Czech Republic) at 10 kV with ×5000.

I. Atomic force microscopy

Two additional samples were prepared for atomic force microscopy analysis (AFM, Alpha 300 RA, WITec, Ulm, Germany). The surface morphology was probed in "contact mode." Imaging was performed with an aluminum-coated cantilever with a 0.2 N/m force constant and operating point of

0.5 V. The scan rate was very slow in order to obtain details of the dentin structure without damaging the tip. The dimensions of the collected images were 30 μm × 30 μm, 256 × 256 pixels.

J. Statistical analysis

The collected data were organized into an Excel spreadsheet (Microsoft Office 2007) and analyzed using SPSS 13.0 (Statistical Package for the Social Sciences, Chicago, IL, USA) for Windows. Descriptive statistics were obtained and the Kruskal Wallis ($p = 0.01$) test was used to compare results between groups. In case of significant differences, the Mann Whitney test was used for pairwise comparison between groups ($p = 0.05$).

III. RESULTS

The results for the μSBS analysis are shown in Fig. 2. The maximum bond strength was recorded for the SD_{11} (16.42 MPa) and the minimum bond strength was recorded for the DD (8.89 MPa). The Kruskal Wallis test revealed significant differences between groups. The Mann Whitney test demonstrated differences between DD and all the other groups.

After that, the failure mode examination described the percentage of samples in each of the three assigned modes (Table I). A decrease in the number of adhesive fractures in the SD irradiated groups, when compared to the sound control group, was observed, as well as an increase in the number of mixed failures.

For a better understanding of the previous results, OCT, SEM, and AFM were used to evaluate the dentin surface morphology after laser irradiation and before the adhesive application. Among those, OCT has the advantage of being nondestructive, giving cross-sectional images of the ablated tissue without destructing or modifying the specimens. For this reason, it was applied to all irradiated samples, before the adhesion procedures. Representative cross-sectional OCT images of the four laser irradiated groups are shown in Fig. 3.

TABLE I. Percentage of samples (%) according to fracture mode for all experimental groups.

	Fracture pattern (μSBS)		
Group	Adhesive (%)	Cohesive (%)	Mixed (%)
SD	80	0	20
SD_{11}	60	0	40
SD_{18}	70	0	30
DD	40	10	50
DD_{11}	20	0	80
DD_{18}	20	10	10

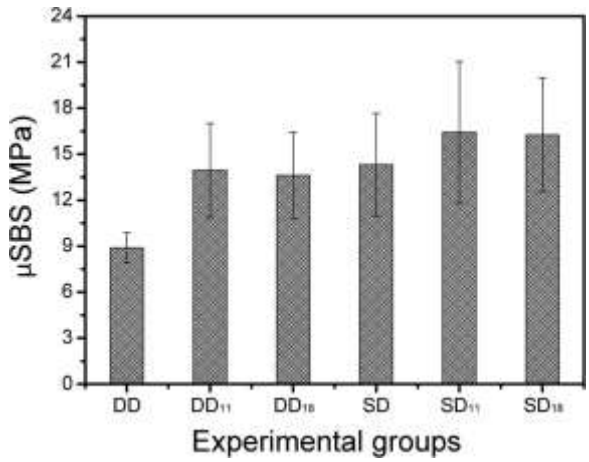

FIG. 2. Mean μSBS and standard deviation of the tested adhesive system.

The images show the ablation profiles generated on the samples by the incident laser, which are deeper and more homogeneous in the groups of demineralized dentins. Based on all collected images, it is possible to quantify the average tissue loss promoted in each irradiated group. These results are presented in Table II.

TABLE II. Mean tissue loss (μm) in all irradiated groups measured by OCT. Different superscript letters indicate statistical differences between groups ($p < 0.05$).

	Tissue loss (μm)
DD_{11}	22.20 ± 3.11^{A}
DD_{18}	22.80 ± 1.30^{A}
SD_{11}	11.80 ± 0.84^{B}
SD_{18}	13.20 ± 1.48^{B}

Figure 4(a) shows the representative SEM image of sound dentin before irradiation, with the dentin tubules completely covered by the smear layer. Figure 4(b) shows the dentin surface after the pH cycle. The total opening of the dentinal tubules, the

demineralized peritubular dentin, and rough intertubular dentin should be noticed. Figures 4(c)–4(f) show the morphology of the dentin surface after the femtosecond laser irradiation. The sound dentin irradiated groups presented an irregular and rougher appearance [Figs. 4(c) and 4(e)], with some dentinal tubules exposed and open [Fig. 4(c)]. SEM analysis revealed that the irradiated demineralized dentin showed a smoother surface. Also, morphological alterations, such as areas of melted and recrystalized hydroxyapatite [Figs. 4(d) and 4(f)] were observed.

Figure 5 shows the obtained AFM micrographs for all experimental groups. In Fig. 5(a), the SD group showed dentin surfaces with dentin tubules completely covered by the smear layer, and the ripples created by the action of abrasives were visible. However, in the DD group, the opening of dentin tubules is clearly evident, indicating that the smear layer was completely removed after the pH cycle [Fig. 5(b)]. In the irradiated groups [Figs. 5(c)–5(f)], the presence of peaks and valleys formed by the laser action was also visible. These AFM images led to conclusions similar to OCT and SEM images, corroborating previous finding, as discussed in Sec. IV.

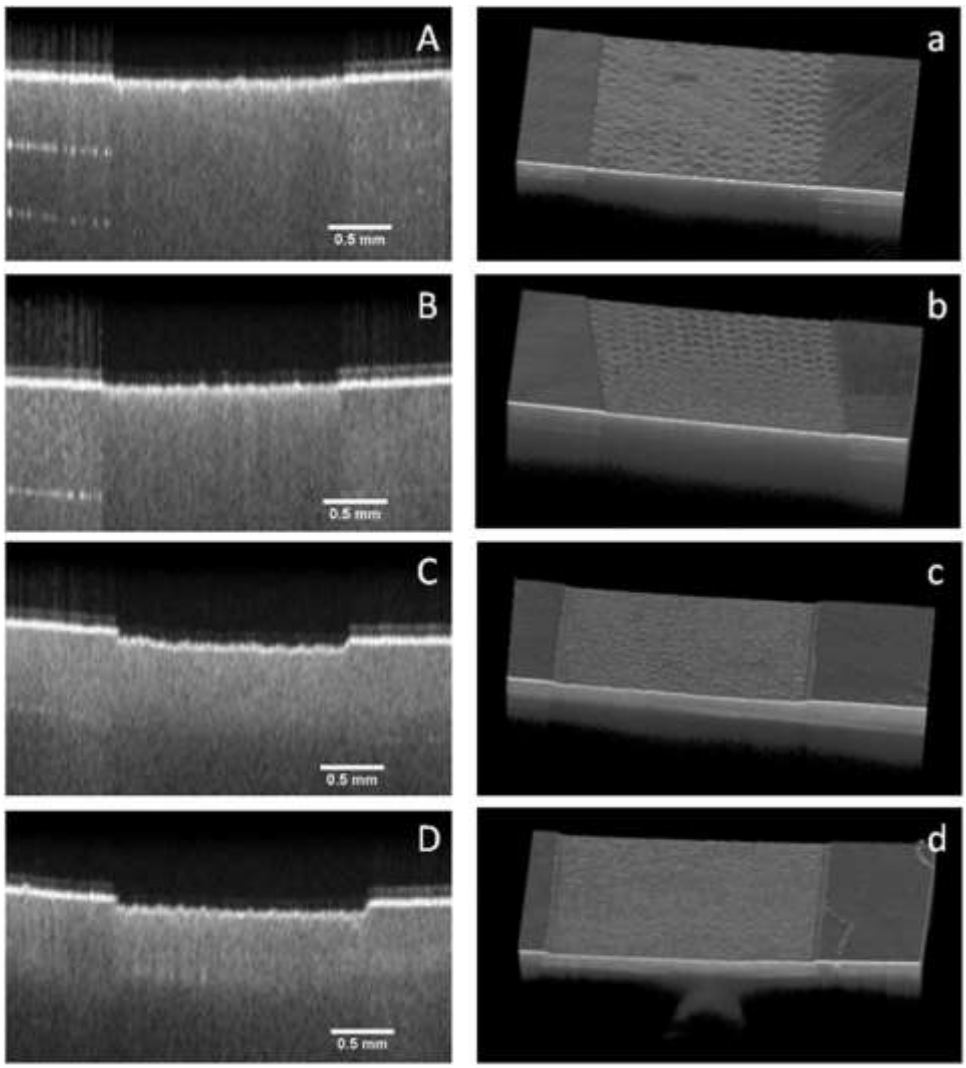

FIG. 3. Comparison of OCT images of the dentin surface reference and irradiated area. Images identified with lowercase represent 3D OCT and images by uppercase cross-sectional 2D OCT. (A) and (a): SD_{11}, (B) and (b): SD_{18}, (C) and (c): DD_{11}, (D) and (d): DD_{18}. Scale bar: 0.5 mm.

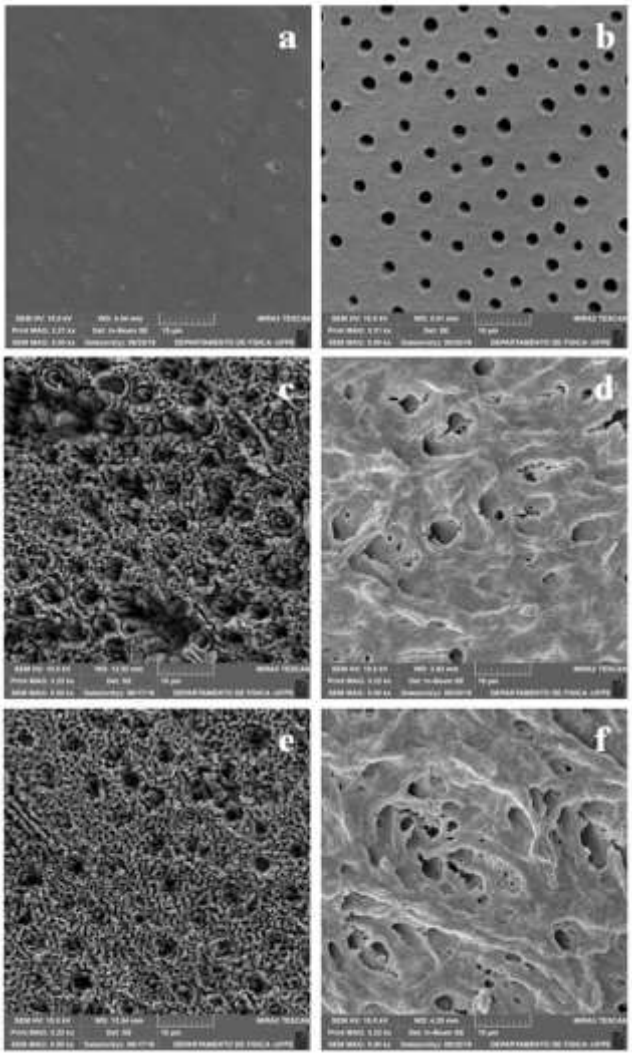

FIG. 4. Representative scanning electron microscope (SEM) images (5000×) of (a) sound dentin surface prepared with 400 and 600-grit water-cooled sandpaper only, (b) demineralized dentin, Ti:Sapphire laser irradiated areas (c) SD_{11}, (d) DD_{11}, (e) SD_{18}, and (f) DD_{18}.

IV. DISCUSSION

The in vitro pH cycling protocol used in this study was previously proposed by Ganss et al.[40] This process simulates the demineralization of dental hard tissues, removing the dentinal plugs and demineralizes the intertubular and peritubular dentin. It also increases the diameter of the tubules, exposing the organic matrix composed by a network of collagen fibrils, as described by Prati et al.[5] It has already been reported in the literature that demineralization can negatively affect the bond strength, since the presence of denatured collagen interferes with the bonding properties of adhesive materials.[41] This was evidenced in our results, when comparing the μSBS values of SD and DD control groups in Fig. 2.

In a deeply demineralized dentin, after the adhesive penetration, thicker and structurally imperfect hybrid layers are formed. Porosities and demineralized zones prevent resin reinforcement, since its monomers do not penetrate as deep as acid.[42] However, self-etch adhesive systems have an acid primer, which promotes demineralization and monomer infiltration simultaneously, promoting a more homogeneous hybrid layer. Zimmerli et al.[3] demonstrated that a self-etch adhesive system (Clearfil SE Bond) showed better results in demineralized dentin than an etch-and-rinse adhesive system. For this reason, we chose to use the self-etch type in our research.

Despite the large number of studies on dentin ablation by femtosecond lasers,[18,21,22,37,43–45] the ablation effects on demineralized dentin surfaces have only been explored using long-pulsed lasers.[46] To our knowledge, our experiment is the first to evaluate the adhesion on demineralized dentin after the pretreatment with femtosecond laser. In order to promote a superficial removal of the smear layer, and greater preservation of the underlying dentin characteristics, the fluences we used were lower than similar studies found in the literature. This condition was achieved by delivering the incident beam in a defocused way.

The loss of dentin tissue after laser irradiation was measured using OCT (Fig. 3 and Table II). The OCT is an imaging modality widely used in medical diagnosis and nonmedical areas, including dentistry.[47] A twofold increase in the mineral loss after laser irradiation could be observed in previously demineralized samples,

when compared to sound dentin, irrespective of the laser parameter used. Demineralized dentin has a lower ablation threshold than healthy dentin and, consequently, the same fluence as that applied in SD samples is expected to promote higher ablation rates in DD samples.[23,48,49]

3 and 5, respectively). Additionally, because the mean μSBS values on SD samples were always greater than their DD counterpart was, it can be concluded that laser-irradiated SD would be ideal to adhesion. The superior values in the bond strength found on femtosecond-treated dentin samples when compared to other results in the literature[9] using long-pulsed laser

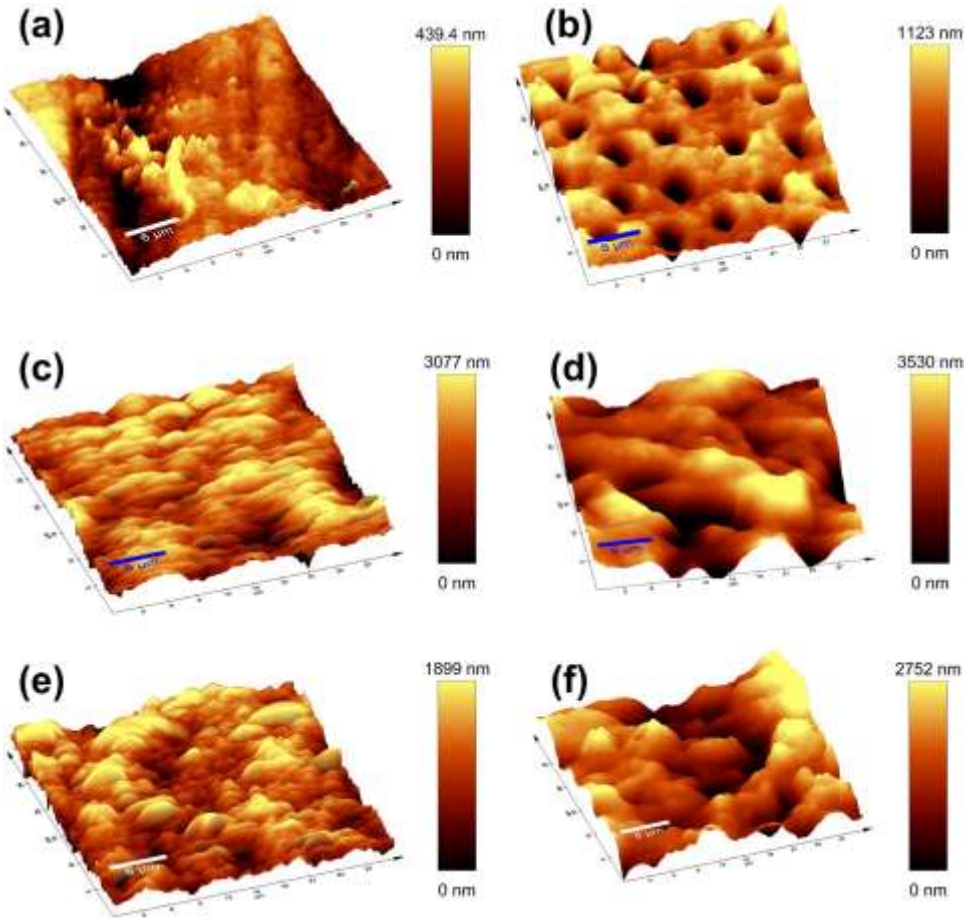

FIG. 5. AFM image of (a) sound dentin surface, (b) after erosive challenge, areas irradiated with Ti:Sapphire laser (c) SD_{11}, (d), DD_{11}, (e) SD_{18}, and (f) DD_{18}.

The laser-treated SD surface showed absence of smear layers, open dentinal tubules, and a rougher and more irregular appearance than demineralized dentin, as observed in Figs. 4(c) and 4(e). This was also confirmed in the 3D OCT images, as well as the AFM analysis (Figs.

sources should be highlighted. Using our irradiation parameters, an almost twofold increase in the μSBS was observed.

It is possible that an increase in the surface roughness, seen as consequence of the increase in the total

effective area available to adhesion, generated a greater adhesive force per unit area in the tubules. Together with the preservation of the collagen fibrils network, it contributed to the overall enhancement in the μSBS, compared to nonirradiated samples. Femtosecond lasers have already been used to increase the adhesion of bonding agents in sound dentin.[19,36,50] Dentin tissue is mainly formed by hydroxyapatite nanocrystals embedded in a collagen fibrils network and water. Although dentin is predominantly composed of hydroxyapatite, it is the continuity of the collagen fibrils network that ensures its integrity.[16] Studies have demonstrated that femtosecond laser ablation of sound dentin greatly preserves the collagen cohesive strength, essential to form hybrid layers and strong adhesive bonds during restorative procedures.[16,38] The consequence of such scenario would be a measurable improvement in the dentin/adhesive bond strength, confirmed by our results. Additionally, the bond strength evaluation revealed a deficient adhesion to the DD (nonirradiated) substrate (Fig. 2), but a statistically significant improvement of the μSBS in both irradiated groups (DD_{11} and DD_{18}). We believe this is caused by the partial exposure of the underlying sound dentin after fs ablation, unaffected by pH cycling protocol, positively affecting the formation of hybrid layers. These findings corroborate with other studies in the literature.[3,7,41,51]

Previous investigations[18,21,22,38,43,44,52] showed that sound dentin does not suffer thermal or mechanical damages when irradiated with femtosecond lasers. This is also expected when the laser is scanned over the sample, decreasing the delivered number of pulses in each point, as executed in our study. It should be highlighted that this is an important requirement because, even using femtosecond lasers, a large number of pulses delivered at the same point increase the thermal load and the plasma extent, generating microcracks, melting, and carbonization.[45]

In contrast, the groups of irradiated DD samples behaved differently. SEM images revealed morphological alterations within these groups, probably caused by melting and recrystallization of hydroxyapatite crystals [Figs. 4(d) and 4(f)]. Theoretically, this could hinder the adhesion to the tissue and is expected based on the chemical and morphological alterations caused by the pH cycling protocol.[53–56] The fusion point of the exposed organic matrix is extremely lower than hydroxyapatite, causing melting of the demineralized tissue more easily. In contrast, even with apparently unsatisfactory conditions for adhesion, irradiated demineralized samples had better μSBS values than demineralized/nonirradiated ones, with significant statistical difference. Moreover, the adhesion was not statistically different from the irradiated sound samples, regardless of the incident laser fluence. To explore the fundamental reasons for such behavior, further investigation is needed.

Regarding the observed fracture modes (Table I), we suggest that the opening of the dentinal tubules and the increased surface roughness caused by the laser irradiation would enhance the micromechanical retention. According to Guedes et al.,[57] the retention of part of the material seems to be positive, since complete debonding at the interface is related to an ineffective surface treatment or a failed infiltration of the adhesive system. No cohesive failure was observed in the groups of sound dentin. There was a 50% decrease in the number of adhesive failures in irradiated DD groups. Again, this can be explained by the removal of the softened outer dentin layer by the laser irradiation, exposing the deeper dentin tissue. Since it has not been demineralized, it would be more conducive to adhesion.

Finally, it is worth comparing our μSBS results with the microtensile bond strength measurements performed in fs laserirradiated dentin, reported by Portillo et al.[36] The authors employed the same Clearfil adhesive system and observed that femtosecond laser irradiation reduced the bonding effectiveness, contrary

to our results. This can be explained by the different laser parameters and the use of different bond strength measuring methods than our study. The microshear testing was chosen since it has been reported to provide more accurate

results than microtensile testing.[58,59]

V. CONCLUSION

In conclusion, the Ti:Sapphire femtosecond laser successfully ablated the smear layer of sound dentin samples, opened the dentinal tubules, and increased the surface roughness. These features enhanced the adhesion, seen by the higher microshear bond strength observed in sound irradiated dentin. The most significant improvement was observed in demineralized and irradiated dentin. The results suggest that femtosecond laser has the potential tool to be used to pretreat the dentin surface before the adhesion of resin composites. The fs laser also ablated the demineralized dentin tissue more efficiently, as observed via OCT, as well as promoted melting and recrystallization of hydroxyapatite, confirmed by SEM. The different outcomes indicate that optimal irradiation parameters for demineralized and sound dentin deserve further investigation.

ACKNOWLEDGMENTS

This study was carried out under the PRONEX program (Center of Excellence on Biophotonics and Nanophotonics APQ-0504-1.05/14) supported by FACEPE/CNPq (Foundation for Science and Technology of Pernambuco State and National Council of Technological and Scientific Development) and INCT-INFO (National Institutes of Science and Technology, Institute of Photonics - 465.763/2014-6), sponsored by CNPq/ MCT (National Council of Technological and Scientific Development and Ministry of Science and Technology). The authors report no conflict of interest related to this study. The research of F. G. Rego-Filho was supported by a postdoctoral fellowship from CAPES.

REFERENCES

1. F. M. Levy, A. C. Magalhães, M. F. Gomes, L. P. Comar, D. Rios, and M. A. Buzalaf, “The erosion and abrasion-inhibiting effect of TiF(4) and NaF varnishes and solutions on enamel in vitro,” Int. J. Paediatr. Dent. 22, 11–1 (2012).

2. A. Lussi, N. Schlueter, E. Rakhmatullina, and C. Ganss, “Dental erosion—An overview with emphasis on chemical and histopathological aspects,” Caries Res. 45, 2–12 (2011).

3. B. Zimmerli, J. De Munck, A. Lussi, P. Lambrechts, and B. Van Meerbeek,“Long-term bonding to eroded dentin requires superficial bur preparation,” Clin. Oral Invest. 16, 1451–1461 (2012).

4. T. Attin and F. J. Wegehaupt, “Impact of erosive conditions on toothcolored restorative materials,” Dent. Mater. 30, 43–49 (2014).

5. C. Prati, L. Montebugnoli, P. Suppa, G. Valdrè, and R. Mongiorgi, “Permeability and morphology of dentin after erosion induced by acidic drinks,” J. Periodontol. 74, 428–436 (2003).

6. C. Ganss, N. Schlueter, M. Hardt, J. von Hinckeldey, and J. Klimek, “Effects of toothbrushing on eroded dentine,” Eur. J. Oral Sci. 115, 390–396 (2007).

7. M. C. P. Cersosimo, A. B. Matos, R. S. D’Almeida Couto, M. M. Marques, and P. M. Freitas, “Short-pulse Er:YAG laser increases bond strength of composite resin to sound and eroded dentin,” J. Biomed. Opt. 21, 048001 (2016).

8. K. L. Mittal and T. Bahners, Laser Surface Modification and Adhesion (John Willey & Sons, Hoboken, NJ, USA, 2015).

9. A. P. S. Kuwana, L. M. Firoozmand, and M. A. M. de Araújo, “Evaluation of the shear bond strength of a composite resin in sound, demineralized and hypermineralized bovine dentin after irradiation with Er:YAG and Nd:YAG lasers, employing a self-etching adhesive system,” J. Laser Appl. 22, 99–105 (2010).

10. M. V. Cardoso, J. De Munck, E. Coutinho, R. B. Ermis, K. Van Landuyt, R. C. R. De Carvalho, and B. Van Meerbeek, “Influence of Er,Cr:YSGG laser treatment on microtensile bond strength of adhesives to enamel,” Oper. Dent. 33, 448–455 (2008).

11. M. Staninec, N. Meshkin, S. K. Manesh, R. O. Ritchie, and D. Fried, “Weakening of dentin from cracks resulting from laser irradiation,” Dent. Mater. 25, 520–525 (2009).

12. J. Serbin, T. Bauer, C. Fallnich, A. Kasenbacher, and W. H. Arnold, “Femtosecond lasers as novel tool in dental surgery,” Appl. Surf. Sci. 197, 737–740 (2002).

13. A. V. Rode, E. G. Gamaly, B. Luther-Davies, B. T. Taylor, J. Dawes, A. Chan, R. M. Lowe, and P. Hannaford, “Subpicosecond laser ablation of dental enamel,” J. Appl. Phys. 92, 2153–2158 (2002).

14. A. V. Rode, E. G. Gamaly, B. Luther-Davies, B. T. Taylor, M. Graessel, J. M. Dawes, A. Chan, R. M. Lowe, and P. Hannaford,

"Precision ablation of dental enamel using a subpicosecond pulsed laser," Aust. Dent. J. 48, 233–239 (2003).
15. Q.-T. Le, C. Bertrand, and R. Vilar, "Femtosecond laser ablation of enamel," J. Biomed. Opt. 21, 065005 (2016).
16. Q.-T. Le, C. Bertrand, and R. Vilar, "Structural modifications induced in dentin by femtosecond laser," J. Biomed. Opt. 21, 125007 (2016).
17. J. Neev, L. B. da Silva, M. D. Feit, M. D. Perry, A. M. Rubenchik, and B. C. Stuart, "Ultrashort pulse lasers for hard tissue ablation," IEEE J. Sel. Top. Quant. Electron. 2, 790–800 (1996).
18. H. Chen, H. Li, Y. C. Sun, Y. Wang, and P. J. Lü, "Femtosecond laser for cavity preparation in enamel and dentin: Ablation efficiency related factors," Sci. Rep. 6, 20950 (2016).
19. Gerhardt-Szep, K. Werelius, F. Weerth, D. Heidemann, and P. Weigl,"Influence of femtosecond laser treatment on shear bond strength of composite resin bonding to human dentin under simulated pulpal pressure," J. Biomed. Mater. Res. 100B, 77–184 (2012).
20. Petrov, E. Pecheva, A. D. Walmsley, and S. Dimov, "Femtosecond laser ablation of dentin and enamel for fast and more precise dental cavity preparation," Mater. Sci. Eng. C 90, 433–438 (2018).
21. M. P. Muñoz, M. C. L. Luengo, J. M. S. Llorente, M. P. Sánchez, A. Albaladejo, A. García, and P. M. Pedraz, "Morphological alterations in dentine after mechanical treatment and ultrashort pulse laser irradiation," Lasers Med. Sci. 27, 53–58 (2012).
22. H. Chen, J. Liu, H. Li, W. Ge, Y. Sun, Y. Wang, and P. Lü, "Femtosecond laser ablation of dentin and enamel: Relationship between laser fluence and ablation efficiency," J. Biomed. Opt. 20, 028004 (2015).
23. P. Weigl, A. Kasenbacher, and K. Werelius, "Dental applications," in Femtosecond Technology for Technical and Medical Applications, edited by F. Dausinger, H. Lubatschowski, and F. Lichtner (Springer, Berlin, 2004), pp. 167–185.
24. M. S. Bello-Silva, M. Wehner, C. P. Eduardo, F. Lampert, R. Poprawe, M. Hermans, and M. Esteves-Oliveira, "Precise ablation of dental hard tissues with ultra-short pulsed lasers. Preliminary exploratory investigation on adequate laser parameters," Lasers Med. Sci. 28, 171–184 (2013).
25. Q.-T. Le, R. Vilar, and C. Bertrand, "Influence of external cooling on the femtosecond laser ablation of dentin," Lasers Med. Sci. 32, 1943–1951 (2017).
26. T. Cloitre, I. V. Panayotov, H. Tassery, C. Gergely, B. Levallois, and F. J. G. Cuisinier, "Multiphoton imaging of the dentine-enamel junction," J. Biophotonics 6, 330–337 (2013).
27. M. C. Lorenzo, M. Portillo, A. Albaladejo, A. García, J. R. V. Aldana, and P. Moreno, "Effect of ultrashort laser microstructuring of enamel and dentin surfaces on bond strengths in orthodontics and conservative dentistry," Photon. Lasers Med. 1, 171–182 (2012).
28. M. C. Lorenzo, M. Portillo, P. Moreno, J. Montero, A. García, E. Santos-del Riego, and A. Albaladejo, "Ultrashort pulsed laser conditioning of human enamel: In vitro study of the influence of geometrical processing parameters on shear bond strength of orthodontic brackets," Lasers Med. Sci. 30, 891–900 (2015).
29. Yilmaz-Savas, N. Demir, A. N. Ozturk, and H. S. Kilic, "Effect of different surface treatments on the bond strength of lithium disilicate ceramic to the zirconia core," Photomed. Laser Surg. 34, 236–243 (2016).
30. M. V. Prieto, A. L. C. Gomes, J. M. Martín, A. A. Lorenzo, V. S. Mato, and A. A. Martínez, "The effect of femtosecond laser treatment on the effectiveness of resin-zirconia adhesive: An in vitro study," J. Lasers Med. Sci. 7, 214–219 (2016).
31. V. García-Sanz, V. Paredes-Gallardo, C. Bellot-Arcís, L. Martínez-León, R. Torres-Mendieta, J. Montero, and A. Albaladejo, "Femtosecond laser settings for optimal bracket bonding to zirconia," Lasers Med. Sci. (published online).
32. L. Hao, J. Lawrence, and K. S. Chian, "Osteoblast cell adhesion on a laser modified zirconia based bioceramic," J. Mater. Sci. Mater. Med. 16, 719–726 (2005).
33. A. Cunha, A.-M. Ellie, L. Plawinski, A. P. Serro, A. M. B. do Rego, A. Almeida, M. C. Urdaci, M.-C. Durrieu et al, "Femtosecond laser surface texturing of titanium as a method to reduce the adhesion of Staphylococcus aureus and biofilm formation," Appl. Surf. Sci. 360, 485–493 (2016).
34. A. Cunha, O. F. Zouani, L. Plawinski, A. M. B. do Rego, A. Almeida, R. Vilar, and M.-C. Durrieu, "Human mesenchymal stem cell behavior on femtosecond laser-textured Ti-6Al-4V surfaces," Nanomedicine 10, 725–739 (2015).
35. T. Cangueiro, R. Vilar, A. M. B. do Rego, and V. S. F. Muralha, "Femtosecond laser ablation of bovine cortical bone," J. Biomed. Opt. 17, 125005 (2012).
36. L. Portillo, M. C. Lorenzo, P. Moreno, A. García, J. Montero, L. Ceballos,M. V. Fuentes, and A. Albaladejo, "Influence of Er:YAG and Ti:sapphire laser irradiation on the microtensile bond strength of several adhesives to dentin," Lasers Med. Sci. 30, 483–492 (2015).
37. D. T. Zero, I. Rahbek, J. Fu, H. M. Proskin, and J. D. Featherstone, "Comparison of the iodide permeability test, the surface microhardness test, and mineral dissolution of bovine enamel following acid challenge," Caries Res. 24, 181–188 (1990).
38. S. Alves, V. Oliveira, and R. Vilar, "Femtosecond laser ablation of dentin," J. Phys. D Appl. Phys. 45, 245401 (2012).
39. J. Krüger, W. Kautek, and H. Newesely, "Femtosecond-pulse laser ablation of dental hydroxyapatite and single-crystalline fluorapatite," Appl. Phys. A 69, S403–S407 (1999).
40. C. Ganss, J. Klimek, U. Schäffer, and T. Spall, "Effectiveness of two fluoridation measures on erosion progression in human enamel and dentine in vitro," Caries Res. 35, 325–330 (2001).

41. J. Perdigão, “Dentin bonding-variables related to the clinical situation and the substrate treatment,” Dent. Mater. 26, e24–e37 (2010).
42. J. B. Cruz, G. Bonini, T. L. Lenzi, J. C. P. Imparato, and D. P. Raggio, “Bonding stability of adhesive systems to eroded dentin,” Braz. Oral Res. 29, 1–6 (2015).
43. R. F. Lizarelli, M. M. Costa, E. Carvalho-Filho, F. D. Nunes, and V. S. Bagnato, “Selective ablation of dental enamel and dentin using femtosecond laser pulses,” Laser Phys. Lett. 5, 63–69 (2008).
44. L. Ji, L. Li, H. Devlin, Z. Liu, J. Jiao, and D. Whitehead, “Ti:sapphire femtosecond laser ablation of dental enamel, dentine, and cementum,” Lasers Med. Sci. 27, 197–204 (2012).
45. F. A. M. G. Rego-Filho, M. Dutra-Corrêa, G. Nicolodelli, V. S. Bagnato, and M. T. de Araujo, “Influence of the hydration state on the ultrashort laser ablation of dental hard tissues,” Lasers Med. Sci. 28, 215–222 (2013).
46. S. K. Moura, C. C. Lopes, L. T. Trevelin, A. B. Matos, I. V. L. Martinez, M. Estevam, and S. K. Bussadori, “Effects of different treatments on chemical and morphological features of eroded dentin,” Lasers Med. Sci. 33(7), 1441–1446 (2018).
47. M. E. Brezinski, Optical Coherence Tomography: Principles and Applications (Elsevier, Burlington, 2006).
48. C. Engelbach, C. Dehn, C. Bourauel, J. Meister, and M. Frentzen, “Ablation of carious dental tissue using an ultrashort pulsed laser (USPL) system,” Lasers Med. Sci. 30, 1427–1434 (2015).
49. P. Kohns, P. Zhou, and R. Störmann, “Effective laser ablation of enamel and dentine without thermal side effects,” J. Laser Appl. 9, 171–174 (1997).
50. A. Vorobyev and C. Guo, “Making superwetting human enamel and dentin surfaces for enhanced adhesion,” Appl. Phys. Lett. 99, 193703 (2011).
51. L. F. Francisconi-dos-Rios, L. C. Casas-Apayco, M. P. Calabria, P. A. Francisconi, A. S. F. Borges, and L. Wang, “Role of chlorhexidine in bond strength to artificially eroded dentin over time,” J. Adhes. Dent. 17, 133–139 (2015).
52. A. Daskalova, S. Bashir, and W. Husinsky, “Morphology of ablation craters generated by ultra-short laser pulses in dentin surfaces: AFM and ESEM evaluation,” Appl. Surf. Sci. 257, 1119–1124 (2010).
53. L. Breschi, P. Gobbi, G. Mazzotti, M. Falconni, T. H. Ellis, and I. Stangel, “High resolution SEM evaluation of dentin etched with maleic and citric acid,” Dent. Mater. 18, 26–35 (2002).
54. A. T. Hara, M. Ando, J. A. Cury, M. C. Serra, C. González-Cabezas, and D. T. Zero, “Influence of the organic matrix on root dentine erosion by citric acid,” Caries Res. 39, 134–138 (2005).
55. L. E. S. Soares, L. R. Lima, L. S. Vieira, A. M. E. Santo, and A. A. Martin, “Erosion effects on chemical composition and morphology of dental materials and root dentin,” Microsc. Res. Tech. 75, 703–710 (2012).
56. C. Ganss, A. Lussi, and N. Schlueter, “The histological features and physical properties of eroded dental hard tissues,” in Erosive Tooth Wear, Monographs in Oral Science 25, edited by A. Lussi and C. Ganss (Karger, Basel, 2014), pp. 99–107.
57. S. F. F. Guedes, M. A. S. Melo, J. P. M. Lima, C. Ely, A. J. S. Rôla, E. Piva, L. and K. A. Rodrigues, “Acid etching concentration as a strategy to improve the adhesive performance on Er:YAG laser and bur-prepared demineralized enamel,” Photomed. Laser Surg. 32, 379–385 (2014).
58. M. Beloica, C. Goracci, C. A. Carvalho, I. Radovic, M. Margvelashvili, Z. R. Vulicevic, and M. Ferrari, “Microtensile vs microshear bond strength of all-in-one adhesives to unground enamel,” J. Adhes. Dent. 12, 427–33 (2010).
59. A. A. El Zohairy, M. H. Saber, A. I. Abdalla, and A. J. Feilzer, “Efficacy of microtensile versus microshear bond testing for evaluation of bond strength of dental adhesive systems to enamel,” Dent. Mater. 26, 848–854 (2010).